DESIGN OF DUAL POLARIZED ANTENNA ARRAY FOR X BAND OFF-THE-GRID CASA OTG RADAR

by

Pallavi Sharma

A thesis submitted in partial fulfillment of the requirements for the degree of

MASTER OF SCIENCE
in
ELECTRICAL ENGINEERING

UNIVERSITY OF PUERTO RICO
MAYAGÜEZ CAMPUS
2012

Approved by:

_____	_____
José Colom Ustariz, PhD Member, Graduate Committee	Date
_____	_____
Henrick-Mario Ierkic, PhD Member, Graduate Committee	Date
_____	_____
Rafael A. Rodríguez Solís, PhD President, Graduate Committee	Date
_____	_____
Mario Rivera Borrero, PhD Representative of Graduate Studies	Date
_____	_____
Pedro I. Rivera, PhD Chairperson of the Department	Date

ABSTRACT

The design of a dual polarized antenna array operating at the center frequency of 9.4 GHz is presented in this thesis. A 2X2 dual polarized antenna sub array is designed on a multilayered structure for operation at 9.4GHz. A series-fed linear array is created using 2X2 sub array structures as elements. Two different layered structures are presented for the sub array structure. For the first structure, the patch radiators and the feed network are designed using a substrate (RT Duroid 5870) with permittivity of 2.33 and a thickness of 0.787 mm. For the second structure, the patch radiators are placed on a substrate (RT Duroid 5870) with height 0.787 mm while the feed network is placed on a different material (TSM DS3) having permittivity of 3 and thickness 0.254 mm. The multilayered sub array was fabricated at Prototron Circuits and the measurements were taken at the Radiation Laboratory at UPRM. For the linear array several amplitude distributions including uniform, Taylor 1-P and Taylor $\bar{n}$ was considered. The design of the sub array and linear array including results of simulation and experimental results are presented and discussed in the thesis.

RESUMEN

Esta tesis presenta el diseño de un arreglo de antenas polarizadas duales operando en un centro de frecuencia de 9.4 GHz. Un subarreglo de antenas polarizadas duales 2X2 está diseñado en una estructura de múltiples capas para operar a 9.4 GHz. Un arreglo lineal de "series-fed" es creado usando estructuras de subarreglos 2X2 como elementos. Dos estructuras en capas son presentadas para la estructura del subarreglo. Para la primera estructura, la antena y la red de alimentación son diseñadas usando un sustrato (RT Duroid 5870) con permisividad de 2.33 y espesor de 0.787 mm. Para la segunda estructura, las antenas están colocadas en un sustrato (RT Duroid 5870) con altura 0.787 mm mientras que la red de alimentación se encuentra en un material diferente (TSM DS3) teniendo permisividad de 3 y espesor de 0.254 mm. El subarreglo de multiples capas fue fabricado por "Prototron Circuits" y las medidas fueron tomadas en el Laboratorio de Radiación de la UPRM. Para el arreglo lineal fueron consideradas múltiples distribuciones de amplitud, incluyendo "Taylor" y "Taylor 1-P". El diseño de un subarreglo y un arreglo lineal de microcintas, incluyendo resultados de simulaciones y experimentos realizados, son presentados y discutidos en esta tesis.

मेरो परिवारलाई।

For my family.

ACKNOWLEDGEMENTS

During the period of my graduate studies and research work at the University of Puerto Rico, I met and collaborated with several people and institutions without whose support it would have been impossible for me to complete my studies. I wish to dedicate this section to acknowledge their support.

First and foremost, I would like to express my sincere gratitude to my advisor, Dr. Rafael A. Rodriguez Solis for providing me with the opportunity to work with, the lessons in microwave antenna engineering, allowing me to freely explore ideas during my research while constantly providing me with the support and guidance that I required, being patient with me, encouraging me to persevere and for inculcating the highest academic standards and ethics. I hold the highest regards for you both as an academician and as a person. I could not have asked for a better advisor, thank you for everything.

I will always remain indebted to Dr. Sandra Cruz Pol and Dr. José Colom Ustariz for providing me with the opportunity to do research work for CASA. The research grant from CASA provided the funding for carrying out my research. Right from having the perfect platform for research to making some very good friends, my experience of working for CASA has enriched me by all means. I would like to thank you both for providing support and guidance and also for encouraging and facilitating team work among students. On the personal front, I would like to thank both of you for opening your hearts out to me and always making me feel comfortable. I have grown fonder of both of you over the period of two years that I have spent at Puerto Rico.

I would also like to thank my friends, Melisa Acosta, Estefany Lancheros, Wilson Castellano, Jose Cordero, Juan Perez and Jonathan Toro for all the help that I received from them.

I would like to thank Sandra Montalvo at the Department of Electrical and Computer Engineering at UPRM for all the advice and encouragement that she provided me with during my graduate study.

I would like to express my gratitude towards Dr. Miguel Velez Reyes for allowing me to use the research facility at CID. I would like to thank Victor Asencio at CID for the technical support that I received.

I am grateful to Dr. Anand Sharma at the Graduate School both on academic and personal fronts. I am grateful to him for providing me with necessary advice and guidance.

TABLE OF CONTENTS

TABLE LIST

Tables **Page**

FIGURE LIST

Figures **Page**

1 INTRODUCTION

1.1 Motivation

Atmospheric phenomenon is currently studied with the help of satellite imagery or ground based radars. Although weather satellites provide information regarding storm clouds, they cannot provide information about precipitation beyond cloud tops. On the other hand ground based radars such as WSR-88D (referred to as NEXRAD) measure precipitation intensity with the help of reflections of radar signals from precipitation The maximum range of the radar is 143 miles (230 km) from the radar location. In cases where the echoes are further away and in cases where the precipitation lies higher or below the radars beam, such ground based radars are ineffective. The radar also suffers from terrain blockage from obstacles such as mountain ranges that block the radar beam preventing observation of events beyond the obstacle. A network of radars located at closer range (~25 Km) addresses the issues mentioned above.

CASA Student Led Test Bed (STB) Off-The-Grid (OTG) radar node is the first prototype of low infrastructure X-band weather radar network to aid forecasts in the western region of Puerto Rico [1]. The main objective of the Student Led Test-bed (STB) is to establish a Quantitative Precipitation Estimation (QPE) sensing network to cover the western region of Puerto Rico and to fill the coverage gap in regions not covered by NEXRAD located in the northeast section of the island. QPE provides an estimation of rainfall and is a key tool in the construction of flash flooding forecasts.

Present day polarimetric weather radars demand high efficiency and lightweight antennas capable of differential phase measurements. Due to the advantages offered by differential phase measurements by polarimetric radars, such as accuracy of rainfall estimates, discrimination among different

precipitation types (rain, hail and snow) and mitigation of calibration error problems and mitigation of attenuation and ground clutter problems, there has been increasing interest in the development of dual-polarized antenna arrays for polarimetric radar applications [2]. In such polarimetric applications, it is advantageous to use shorter wavelengths for measurements in light and moderate rainfall. Not only does using shorter wavelengths allow easy detection of propagation differential phase shift, which is proportional to the reciprocal of the wavelength, but also increases the sensitivity of detecting weak targets. Most X-band radars offer good spatial resolution and less problematic ground clutter with relatively small size, which makes them a preferable tool for polarimetric radar applications compared to large S-band radars [3].

Currently, CASA OTG radar network uses modified marine radars with parabolic reflectors at each node. The main goal of this project is to design and build a light weight dual polarized antenna array with good spatial resolution and low cross polarization level to meet the requirements for the CASA OTG radar node [1].

1.2 Objective

1.2.1 General Objective

- To design, simulate, fabricate and characterize a dual polarized antenna array for X band solid state radar for one of the nodes of the CASA OTG radar network.

1.2.2 Specific Objectives

- To design a sub-array with orthogonal arrangement of patch element for dual polarization operation at 9.4 GHz in the X band.
- To simulate the sub-array design and demonstrate low cross polarization levels and high isolation between the ports for dual polarization operation.
- To fabricate the sub-array and validate the simulation results by performing tests on the sub-array in the Anechoic chamber at UPRM
- To design an antenna array (the sub-array acting as individual element of the array) for operation with one of the solid state radars of the OTG network.

1.3 Thesis Organization

This thesis consists of five chapters. Chapter 1 provides the justification for the thesis and the objectives of the project. The theory of microstrip antenna technology, dual polarized antennas, linear antenna arrays and feed mechanism is discussed in Chapter 2. Chapter 3 discusses the methods used to design the antenna array. Chapter 4 contains the results of simulation as well as the results obtained from testing the fabricated antenna at the Radiation Laboratory. Conclusions are presented in Chapter 5.

2 THEORETICAL BACKGROUND

2.1 Introduction to Microstrip Antennas

The origin of microstrip antennas (MSAs) can be traced back to 1950s when they were first proposed in 1953 by Deschamps [4] in the USA and patented in 1955 by Gutton and Bassinot [5] in France. However it was only in the 1970s that radiation from half wavelength and several wavelengths wide conducting strip placed on a dielectric substrate above a ground plane was reported in literature by Byron [6], and Munson [7] received a patent for the microstrip radiator. Mathematical modeling of the microstrip antennas based on the transmission line model was reported in [8], [9], followed by modal expansion techniques for analyzing rectangular, circular and triangular patches [10]. Since then, much research has been conducted in the field of microstrip antennas and practical antennas have been developed for use from 400 MHz up to 60 GHz and beyond.

In its basic configuration, MSAs comprise of a rectangular, square, circular or triangular (and other shapes) conducting strip of metal radiator placed over a dielectric substrate of height h, as shown in Figure 2-1. The radiator and the ground plane are on either sides of the dielectric substrate.

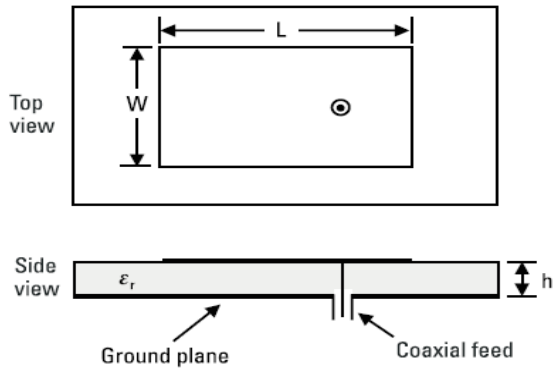

Figure 2-1: MSA configuration

Since their inception, MSAs have become a popular choice in communication systems due to their advantages, which include low cost, low profile and low weight configurations, dual and triple frequency operations, conformability, easy integration into arrays and MMICs and polarization agility, etc. Disadvantages of MSAs include low gain, low bandwidth, spurious feed radiation, poor polarization purity and limited power capability among others.

2.2 MSA Basics

Radiation from MSAs takes place due to fringing fields between the periphery of the patch radiator and the ground plane as shown in Figure 2.1. In the dominant TM_{10} mode of operation, L is nearly equal to λ_g /2 where λ_g is the wavelength in the dielectric medium. This wavelength λ_g is related to free space wavelength λ_0 by equation (1):

$$\lambda_g = \frac{\lambda_0}{\sqrt{\epsilon_{eff}}} \tag{1}$$

Here, ε_{eff} is the effective dielectric constant of the medium [11]. The electric field lines in the patch are not confined to the dielectric substrate. They also form fringing fields in the air from the edges of the patch. The empirical formula for calculating ε_{eff} is given by

$$\epsilon_{eff} = \frac{\epsilon_r + 1}{2} + \frac{\epsilon_r - 1}{2}\left[1 + \frac{10h}{W}\right]^{1/2} \tag{2}$$

where ϵ_r is the relative permittivity of the dielectric material.

In the fundamental TM_{10} mode, the field varies half-wavelength cycle along the length but does not vary along the width. The voltage is maximum at the edges and minimum at the center of the patch

while the current is minimum. For simplicity in analysis, the RMSA can be thought to be consisting of two parallel plates of length L and W placed over a substrate of height h and having capacitance C given[11] by:

$$C = \epsilon_0 \epsilon_r \frac{\mathrm{WL}}{\mathrm{h}} \tag{3}$$

Due to fringing fields, the effective capacitance increases. This can be accounted for by increase in the dimensions of the microstrip antenna. Hence at resonance the effective length can be written as [11]

$$L_e = \mathrm{L} + 2\Delta\mathrm{L} = \frac{\lambda_0}{2\sqrt{\epsilon_{\mathrm{eff}}}} = \frac{\mathrm{c}}{2\mathrm{f}_0\sqrt{\epsilon_{\mathrm{eff}}}} \tag{4}$$

where c is the velocity of light in free space and f_0 is the resonant frequency.

For efficient radiation, the width is taken as being half wavelength corresponding to the average of the two dielectric mediums (air and substrate). Hence, the value of W becomes

$$\mathrm{W} = \frac{\mathrm{c}}{2\mathrm{f}_0\sqrt{\frac{\epsilon_r + 1}{2}}} \tag{5}$$

The radiation from a rectangular MSA can be calculated by combining the radiation patterns from two slots of length W_e and placed L_e apart on an infinite ground plane [12]. The field components can be expressed as follows:

$$E_\theta = \frac{sin\left(\frac{k_0 \Delta \mathrm{L} \sin\theta}{2}\right)}{\frac{k_0 \Delta \mathrm{L} \sin\theta}{2}} cos\left(\frac{k_0(\mathrm{L} + \Delta\mathrm{L})}{2} \sin\theta\right) \tag{6}$$

$$E_{\varphi} = \frac{sin\left(\frac{k_0 W_e}{2}\sin\theta\right)}{\frac{k_0 W_e}{2}\sin\theta} cos\theta \tag{7}$$

2.3 Definition of Dual Polarized Antennas

Dual polarization is the superposition of two linearly polarized modes. When the physical dimensions of the MSA are adjusted so as to produce two degenerate orthogonal modes within the cavity region [12], it results in the radiation of two orthogonally polarized waves near broadside direction. Such MSAs are called dual (linearly) polarized antennas. Dual polarization is obtained when two orthogonal modes are excited with equal amplitude and phase.

A square or rectangular microstrip antenna with two orthogonal feed points can be used to achieve orthogonal polarizations. An orthogonal dual-fed square patch yields dual polarizations at the same frequency while a rectangular patch yields dual polarization at two separate frequencies corresponding to the length and width of the patch [11].

2.4 Dual Polarization Realization

Although early realization of dual polarization was reported using waveguide slot array [11], the square microstrip antenna (SMSA) has been the dominant structure in most of the dual polarization antenna applications. Two orthogonal modes can be excited in the SMSA when two feeds are placed in both X-axis and Y-axis respectively as shown in Figure 2-2.

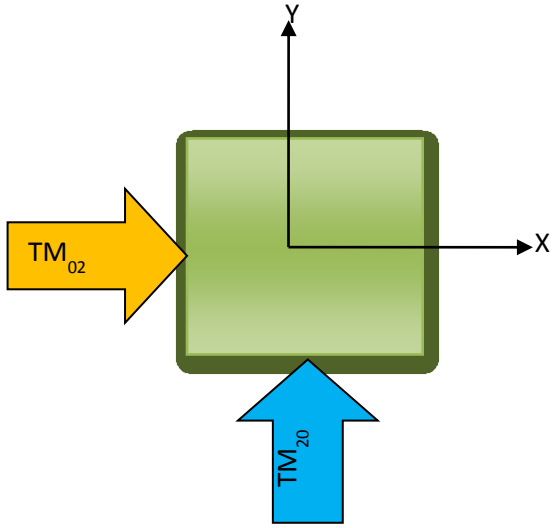

Figure 2-2: Square Microstrip Antenna with two orthogonal feeds

The two desired linear polarizations are generated by two separate feeds and the coupling between the two (S_{21}) is an indicator of quality in such antennas. Feed geometry is another critical part of dual linear polarized antennas.

Although several novel techniques have been developed [13], the realization of dual polarized antennas can be achieved in broadly the following three different ways:

i. Use stacked structures of the radiating elements

ii. Use special feeding techniques

iii. Make an orthogonal arrangement of the radiation elements for two polarizations [23-25]

One of the ways to realize dual polarization in microstrip antennas is by stacking radiating elements to form multilayer structures [14-16]. A dual band dual polarized array of dipoles and square patches for operation in the S and X bands respectively has been presented in [15]. For operation in the X-band, the proposed antenna array comprises of square patches stacked in five different substrate

layers as shown in Figure 2-3. The VSWR bandwidth is reported to be 17% for the X band and 8.9% for S band while the cross-polarization levels are of the order of - 26 dB for the S-band and -31 dB for the X-band.

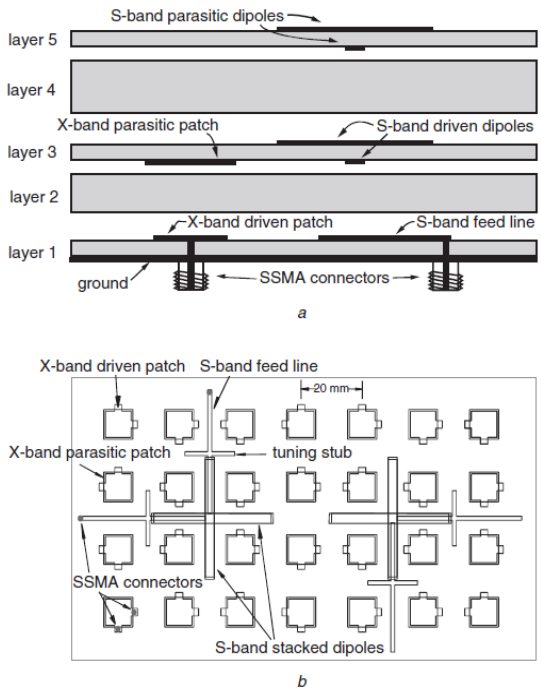

Figure 2-3: Geometry of antenna array proposed in [15] a) side view b) top view

Another design of planar multilayered microstrip antenna array using aperture-coupled stacked patch radiating elements with dual polarization capability is presented in [16] Figure 2-4. The proposed antenna array has been designed for operation in the frequency bands ranging from 0.8 to 15 GHz. The antenna array is designed with a combination of stacked patch elements fed by symmetrically positioned slots with separate strip feed network for better port isolation and low cross polarization levels. The authors have reported frequency bandwidth of up to 26% (VSWR < 2), cross polar radiation level better than -30 dB and isolation between orthogonally polarized channels >30 dB. Several multilayer techniques that have been used to realize dual polarization can be found in [17, 18]

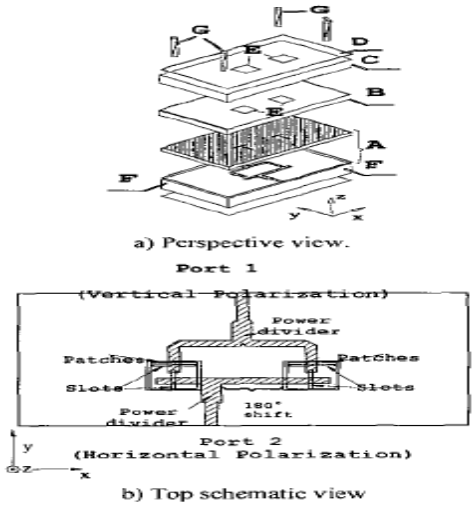

Figure 2-4: Geometry of antenna array proposed in [16]

Another method of improving the performance of dual polarized antennas and arrays in terms of polarization purity and isolation between ports is by making use of different feed mechanisms [19-20]. Use of a square patch with two triangular slots as a compact dual linearly-polarized antenna has been reported in [20]. The antenna is excited by electromagnetically coupling from two 50 O feed lines as shown in Figure 2-5. A high degree of isolation between the ports (better than 35 dB) with cross-polarization levels lower than 25 dB in both ports was reported.

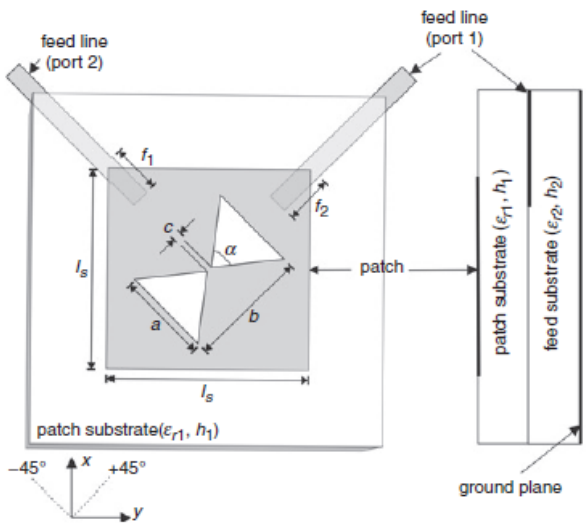

Figure 2-5: Geometry of the antenna proposed in [20]

A slot fed dual-polarized patch antenna using a square ring slot and a single layer laminate for the feeding network has been presented in [21], geometry for which is shown in Figure 2-6. Another aperture coupled microstrip patch antenna for X band series-fed array is presented in [22], geometry for which is shown in Figure 2-7. For both the designs, high cross polarization levels (greater than 20 dB) and high port isolation has been reported.

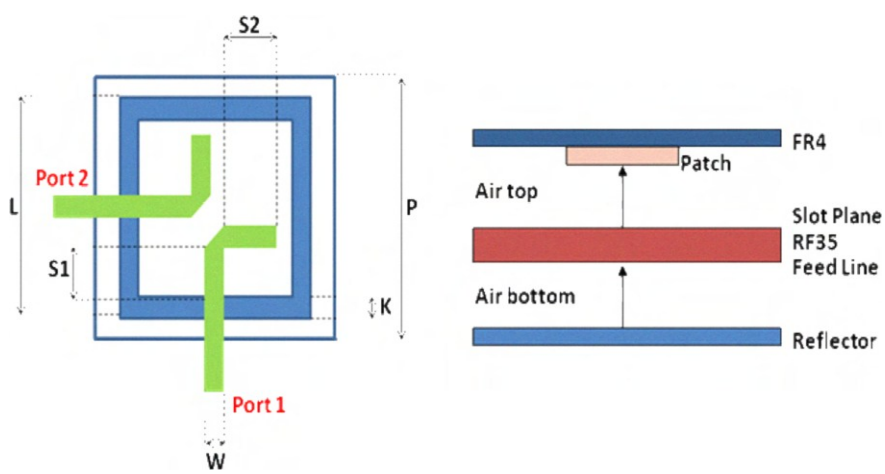

Figure 2-6: Geometry of the antenna proposed in [21]

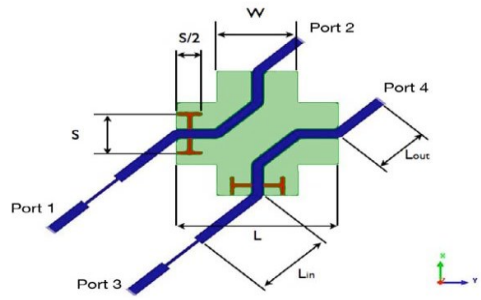

Figure 2-7: Geometry of the antenna proposed in [26]

A widely popular technique of realizing dual polarization is by making orthogonal arrangements of radiating elements [23-25]. A dual-corner-fed patch antenna array is presented in [23]. Several configurations have been proposed for the antenna array for operating frequency of 6 GHz and 12 GHz as shown in Figure 2-8. For all the different array configurations in [23], port isolation of the order of 27 dB have been reported .However, the various proposed array configurations suffer from low impedance bandwidth and low cross polarization levels (-17 dB).

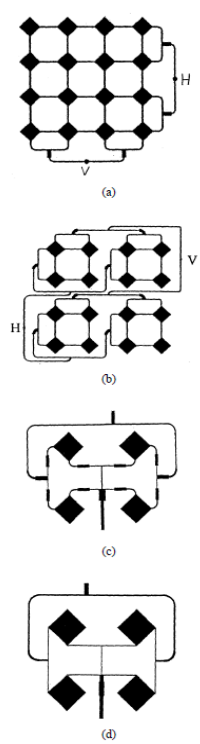

Figure 2-8: Geometry of the antenna proposed in [23]

Similar to [23], a 2 X 2 microstrip antenna for dual polarization is presented in [24]. It consists of a square patch with two ports located at the two corners as shown in Figure 2-9. Serial corner feeding mechanism has been used in the design for a single patch to achieve dual polarization at operating frequency of 6.07 GHz. The 2 X 2 array formed by using such a patch is fed through a coplanar feed network. It has been shown that isolation of -41.43 dB can be achieved with the design.

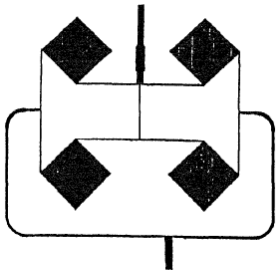

Figure 2-9: Geometry of the antenna proposed in [24]

One of the simplest designs for dual polarization operation in radars using orthogonal arrangement of square patches has been presented in [25].A 2 x 2 microstrip array utilizing the technique of using a single feed on each patch of paired elements with opposite feed locations and phases to suppress the undesirable higher-order modes has been presented. The geometry of the 2 x 2 microstrip array along with microstrip-transmission-line feeds presented in [25] is shown in Figure 2-10. Both the V-port (vertical polarization) and the H-port (horizontal polarization) feed locations are offset from the centers of the feed lines, to achieve the required 180° phase difference. The 2 X 2 microstrip array has been reported to have port isolation of -40 dB, over a bandwidth of at least 5%. The worst cross-polarization level, measured in the broadside direction of the array for both ports is -28 dB from the co-polarization peak, and is -25 dB or all other- angles for operating frequency of 5.3 GHz. Additional literature regarding dual polarized antennas can be found in [26-29].

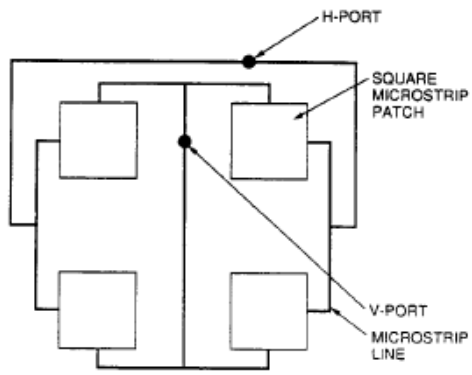

Figure 2-10: Geometry of the 2 X 2 antenna array proposed in [25]

Compared to a single square patch, the 2 X 2 sub array of orthogonally placed square patches offers higher directivity and polarization performance. Also, the feed network design is simple which makes it easy to integrate such sub arrays in a large array of such elements. Due to the advantages offered by the design over other methods of dual polarization realization, the 2 X 2 sub array of orthogonally located square patches is chosen as the basis for building a dual polarized antenna array discussed in Chapter 4.

2.5 Design Parameters for Dual Polarized Antennas/Arrays

Although literature regarding design considerations for basic radiating elements is available [30]-[32], there is limited literature reported specifically for dual polarized elements. However, the general characteristics of basic elements still hold true for dual polarized elements. Several factors [11] such as width, substrate height, substrate permittivity, etc. affect the resonant frequency and bandwidth of MSA. Some of the design parameters for dual polarized antennas are as discussed below:

- *patch dielectric constant:*

Affects the bandwidth and radiation efficiency of the antenna. Lower substrate permittivity substrates are used for increased impedance bandwidth. The gain of the antenna increases with decrease in substrate permittivity.

- *patch substrate thickness*

With an increase in height h, the resonant frequency decreases, the bandwidth increases and the directivity increases marginally. However, care should be observed so as to avoid surface wave excitation since the excitation of surface waves is a function of height h and ϵ_r. Surface waves cause an increase in cross polarization levels and decrease in gain of the antenna. Thickness up to 0.11λ is generally used for patch antennas.

- *patch length l*

The resonant frequency of MSA depends upon the length of the antenna. When the length L is increased, the resonant frequency decreases.

- *Patch width w*

Affects the input impedance. As the width is increased, the input impedance at resonance decreases, the aperture area increases leading to increase in directivity and hence gain. Square patches with equal length and width are used for most dual polarization applications.

- *feed substrate dielectric constant*

Affects the performance of the feed network. A high dielectric constant is preferred for microwave circuitry and it typically selected with values between 2 and 10.

- *feed substrate thickness*

  Affects the performance of the feed circuitry. A thin substrate is preferred for microwave circuitry in order to avoid spurious radiation. Thickness of the order of 0.01λ to 0.02 λ is generally used for feed substrates.

- *microstrip feed line width*

  Affects the impedance of the feed lines. Thinner feed lines have higher impedance values and result in higher losses from feed lines.

- *via hole diameter D*

  Via holes connect the patch antennas to the backside of the board where the feed network is located. Via holes add inductance to the circuitry. Generally, the inductance decreases as the via diameter to substrate height ratio (D/H) increases. However, greater values of D/H mean bigger pads. Generally D/H ratio is between 0.5 and 2.

- *ground plane size*

  Affects the radiation pattern. Smaller ground plane size results in back lobes in the radiation pattern. A rule of thumb is that the distance between the ground plane edge and the edge of the radiating patch should not be less than a quarter wavelength.

- *feed geometry*

  Increasing the feed geometry (feed port size) increases coupling between the ports and also causes the beamwidth to be unequal in two principal planes for dual polarized elements.

- *spacing between sub array/array elements*

Controls the occurrence of grating lobes in the visible region of the array.

- *spacing between radiating elements and feed lines*

  Affects the coupling between the radiating element and feed line located in close proximity of each other and affects isolation.

2.6 Antenna Arrays

2.6.1 Microstrip Arrays

Microstrip antennas have long been popular as single elements. The ease with which it can be integrated into coplanar linear and planar geometries make it most suitable for frequency scanning, polarization agile, series-fed and corporate-fed array applications. Due to their popularity as elements and conformability, microstrip antennas were fast integrated into monolithic arrays. First generation fixed beam arrays were developed using basic array configuration used in circularly polarized arrays and series arrays with linear and dual linear or circular polarization. Soon phased array antennas arrays were developed with beam steering capabilities used for scanning in aircraft and satellites [33].

Although extremely popular, microstrip arrays are narrow band and the feed circuitry operate at low power levels as compared to waveguide and coaxial feed. Microstrip feed circuitry provides the power distribution to the array. Additionally, it is also used for phase control in arrays. A monolithic array contains the radiating elements and the feed network in the same side of the substrate. The feed network can also be placed in layers below the patch layer resulting in multilayer structure. In either case, the feed network is generally series, corporate or a hybrid of the two mechanisms.

Corporate feed configuration employs a 1: n power divider network having identical length from feed point to each element. It is simple to design, easy to integrate with other devices such as amplifiers

and phase shifters and offers flexibility in element spacing. However, there are losses associated with corporate feed, as reported in [34], which can be summarized as follows:

- Radiation losses are higher in end-fed lines than in center-fed lines whereas surface wave losses are the similar for both.

- The losses are proportional to $1/Z_0$ where Z_0 is the characteristic impedance of the feed line. Hence, in order to minimize surface wave loss and radiation from feed lines high characteristic impedances should be chosen.

- For given length and characteristic impedance of a microstrip line, the loss due to surface wave increases with $\left(\frac{h\sqrt{\epsilon_r}}{\lambda_0}\right)^3$ while the radiation loss increases with $\left(\frac{h\sqrt{\epsilon_r}}{\lambda_0}\right)^2$. Thus, in order to lower the values of radiation and surface wave losses due to the feed circuitry, lower values of $\left(\frac{h\sqrt{\epsilon_r}}{\lambda_0}\right)$ must be selected.

- For given length and characteristic impedance of a microstrip line, the radiation loss from the feed network depends on the line length while the surface wave loss dependence on the line length is oscillatory. For the range of $0<L<\lambda_0$, radiation loss increases as $\left(\frac{L}{\lambda_0}\right)^2$ increases. For $L \geq 3\lambda_0$, radiation loss is not sensitive to variations in length.

From the discussion above it can be concluded that typical losses in microstrip transmission lines are directly proportional to the square of the thickness of the substrate, inversely proportional to the characteristic impedance and fairly insensitive to the length of the lines.

Although a one-sided board offers simple microstrip fabrication, it suffers inherent disadvantages due to the feed circuitry. For instance, in large arrays, the feed circuitry has shown to exhibit high losses.

Also, in cases of array design with space restrictions, the feed network cannot be accommodated on the same side as the radiating elements. In such cases, the feed network is placed on a separate layer.

Spurious radiation from series or corporate feed networks is unavoidable and sets a lower limit on the side lobe levels and cross polarization levels in a dual polarized antenna array. Better cross polarization levels have been achieved by placing the feed network in a separate layer below the ground plane and connecting the two layers by vias or by aperture coupling.

2.6.2 Linear Array Theory

Most modern day communication applications (such as that in radars) require highly directive and narrow beam antennas. Increasing the gain of the antenna leads to increase in directivity and hence narrow beamwidth [35]. In order to suffice such requirement for high gain, either the radiating element size should be increased or the assembled to form arrays. Increasing the physical size of a single radiating element is not always a viable option due to increase in fabrication, installation and maintenance costs and reliability issues. Arrays of antennas are a convenient way of increasing the directivity without having to increase the physical size of radiating elements and offer more degrees of freedom.

The total field radiated by the array is a vector sum of the fields radiated by individual elements. For an array of identical radiating elements, the overall radiation pattern of the array can be controlled by the following variables [35]:

- geometrical configuration of the array
- the relative displacement between individual elements
- the excitation amplitude of individual elements

- the excitation phase of individual elements
- the relative pattern of individual elements

The beam radiated by the array can be controlled or varied by changing the excitation amplitude of the radiating elements and by varying the phase of individual elements, arrays can be used to shift the location of the main beam to a particular angle allowing electronic scanning [35-36]. The following section outlines basic aspects of array theory. For further details the reader is expected to refer to [35] and [36].

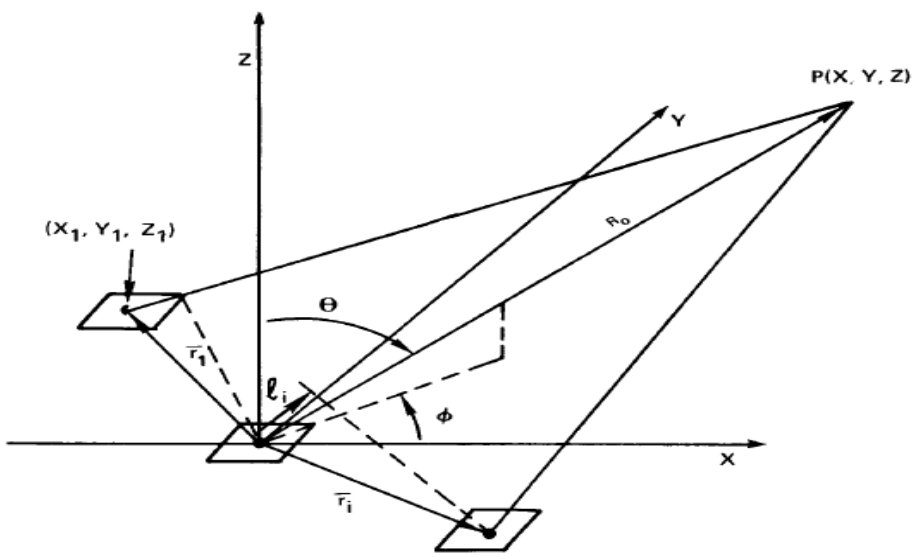

Figure 2-11: Generalized Array Configuration [36]

Figure 2.11 shows the generalized configuration for an antenna array. Each individual element (represented by a square) radiates a field that has both radial and angle dependence around the vicinity of the element. For large distances away from the radiator assembly, the field is a product of $\left[\frac{e^{-jkR}}{R}\right]$ spherical wave and vector function of angle $f_i(\theta, \phi)$ called the element pattern.

The far field due to the ith element can be written as follows:

$$E_i(R,\theta,\varphi) = f_i(\theta,\phi) * \frac{e^{-jkR_i}}{R_i} \tag{8}$$

for

$$R_i = \sqrt{(x-x_i)^2 + (y-y_i)^2 + (z-z_i)^2} \tag{9}$$

where $f_i(\theta,\phi)$ is the field due to each element and $k = \frac{2\pi}{\lambda}$ is the free space wave number.

At very large distance away from the radiating sources, the radial vector R_i can be approximated as:

$$R_i \cong R - \hat{r}.\vec{r_i} \tag{10}$$

Then,

$$\frac{e^{-jk\,R_i}}{R_i} = \frac{e^{-jk\,R}}{R} e^{-jk(\hat{r}.\vec{r_i})} \tag{11}$$

In the above equation, $\vec{r_i}$ is the position vector of the ith element relative to the center of the coordinate system given by:

$$\vec{r_i} = \hat{x}x_i + \hat{y}y_i + \hat{z}z_i \tag{12}$$

and $\hat{r}$ is the unit vector in the direction of any point in space (r,θ,ϕ) expressed in terms of direction cosines u and v as follows

$$\hat{r} = \hat{x}u + \hat{y}v + \hat{z}\cos\theta$$

$$u = \sin\theta\cos\phi \qquad (13)$$

$$v = \sin\theta\sin\phi$$

A good approximation used to represent far field distances [35] is given by

$$R = \frac{2D^2}{\lambda} \qquad (14)$$

where D is the largest dimension of the array and λ is the wavelength. However, in several cases where deep null regions exist and for extremely low side lobe regions, a modification of the above equation i.e. $R = \frac{10D^2}{\lambda}$ may be used.

The general expression for the electric field for an arbitrary array may be written as follows:

$$\vec{E}(r) = \frac{e^{-jk\,R}}{R}\sum_{i} a_i f_i(\theta,\phi)\, e^{-jk(\hat{r}.\vec{r_i})} \qquad (15)$$

Now let us consider two horizontal dipoles positioned along the z-axis as shown in Figure 2-12. Assuming that there is no coupling between the two radiators, the total field radiated by the two elements is given as follows [35]:

$$\vec{E}_T = \vec{E}_1 + \vec{E}_2 = \hat{a}_\theta j\eta\frac{kI_0 l}{4\pi}\left\{\frac{e^{-j\left|kr_1-\frac{\beta}{2}\right|}}{r_1}\cos\theta_1 + \frac{e^{-j\left|kr_2-\frac{\beta}{2}\right|}}{r_2}\cos\theta_2\right\} \qquad (16)$$

where β is the difference in phase excitation between the two dipoles and assuming that the magnitudes of excitation for both the radiators are the same.

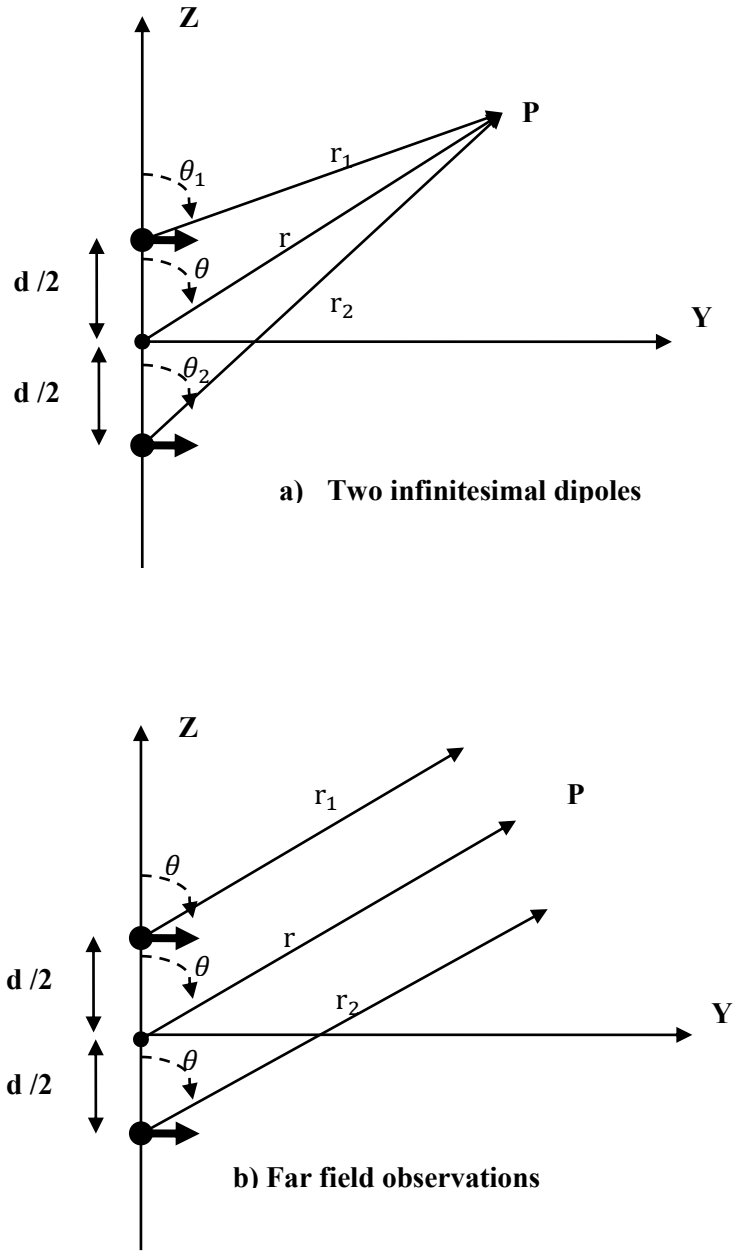

Figure 2-12: Geometry of two dipole array placed along Z-axis [36]

Assuming far field observations, as shown in Figure 2-12(b), we can use the following approximations:

$$\left.\begin{aligned} &\theta_1 \cong \theta_1 \cong \theta \\ &r_1 \cong r - \frac{d}{2}\cos\theta \\ &r_2 \cong r + \frac{d}{2}\cos\theta \end{aligned}\right\} \text{ for phase variations} \tag{17}$$

$$r_1 \cong r_2 \cong r \qquad \text{for amplitude variations} \tag{18}$$

Then, the total electric field reduces to

$$\vec{E}_T = \hat{a}_\theta j\eta \frac{kI_0 l e^{-jkr}}{4\pi r}\cos\theta \left\{ e^{+j\frac{kd\cos\theta+\beta}{2}} + e^{-j\frac{kd\cos\theta+\beta}{2}} \right\} \tag{19}$$

$$\vec{E}_T = \hat{a}_\theta j\eta \frac{kI_0 l e^{-jkr}}{4\pi r}\cos\theta * 2\cos\left(\frac{kd\cos\theta+\beta}{2}\right) \tag{20}$$

Thus the total field of the array is the product of the field of individual element and the array factor where the array factor is expressed as

$$AF = 2\,cos\left(\frac{kd\,cos\,\theta + \beta}{2}\right) \tag{21}$$

For an array of N elements having uniform amplitude excitation, progressive phase β and each spaced d distance apart, the array factor is

$$AF = \sum_{n=1}^{N} e^{j(n-1)\,\psi} \tag{22}$$

where

$$\psi = kd\,cos\,\theta + \beta \tag{23}$$

This array factor can also be written as

$$AF = \frac{e^{jN\psi} - 1}{e^{j\psi} - 1} = e^{j\left(\frac{N-1}{2}\right)\psi}\left[\frac{\sin\left(\frac{N\psi}{2}\right)}{\sin\left(\frac{\psi}{2}\right)}\right] \tag{24}$$

When the reference point is the physical center of the array, the array factor can be expressed as

$$AF = \left[\frac{\sin\left(\frac{N\psi}{2}\right)}{\sin\left(\frac{\psi}{2}\right)}\right] \tag{25}$$

In normalized form equation (25) can be written as

$$(AF)_n = \frac{1}{N}\left[\frac{\sin\left(\frac{N\psi}{2}\right)}{\sin\left(\frac{\psi}{2}\right)}\right] \tag{26}$$

And for small values of ψ,

$$(AF)_n \cong \left[\frac{\sin\left(\frac{N\psi}{2}\right)}{\frac{N}{2}\psi}\right] \tag{27}$$

The nulls of equation (27) are obtained when $\sin\left(\frac{N\psi}{2}\right) = 0$ i.e.

$$\Theta_{null} = \cos^{-1}\left[\frac{\lambda}{2\pi d}\left(-\beta \pm \frac{2n\pi}{N}\right)\right] \tag{28}$$

$$n = 1,2,3 \ldots \ldots.$$

$$n \neq N, 2N, \ldots \ldots$$

Similarly, the maximum occurs when

$$\Theta_{max} = \cos^{-1}\left[\frac{\lambda}{2\pi d}(-\beta \pm 2m\pi)\right] \tag{29}$$

$$m = 0,1,2,3 \ldots \ldots$$

The 3-dB point for the array factor given by eq (27) occurs when

$$\frac{N\psi}{2} = \frac{N}{2}(kd\cos\theta + \beta)|_{\theta=\theta_h} = \pm 1.391$$

$$\theta_h = \cos^{-1}\left[\frac{\lambda}{2\pi d}\left(-\beta \pm \frac{2.782}{N}\right)\right] \tag{30}$$

For $d \gg \lambda$ equation (30) reduces to

$$\theta_h \cong \left[\frac{\pi}{2} - \frac{\lambda}{2\pi d}\left(-\beta \pm \frac{2.782}{N}\right)\right] \tag{31}$$

The half-power beamwidth of the array can then be expressed as

$$\theta_{HPBW} = 2|\theta_{max} - \theta_h| \tag{32}$$

For a uniformly illuminated array at broadside the 3-dB beamwidth is given by

$$\theta_{HPBW} = 0.886\frac{\lambda_0}{D} \tag{33}$$

However when tapering is used, a more general form of the 3-dB beamwidth used for the radiation pattern of a linear array is

$$\theta_{HPBW} = 0.886\frac{B_b\lambda_0}{D} \tag{34}$$

where B_b is the beam broadening factor [33]

The directivity of an antenna is defined as the ratio of the radiation intensity in a given direction from the antenna to the average radiation intensity around the antenna and is expressed in terms of far-field pattern $f(\theta, \phi)$ as:

$$\mathrm{D}(\theta, \phi) = 4\pi \frac{f(\theta, \phi)}{\int_0^{2\pi} \int_0^{\pi} f(\theta, \phi)\, d\theta\, d\phi} \tag{35}$$

When linear arrays are used for scanning along either θ or ϕ there is scan loss which depends on the directive gain in the plane orthogonal to the plane in which the array scans. However, for a linear array of isotropic elements placed at distances equal to integer number of half wavelength is independent of the scan angle and given by

$$\mathrm{D}_0 = \frac{|\sum {a_n}^2|}{\sum |a_n|^2} \tag{36}$$

2.6.3 Series-fed Arrays

Modern communication links such as aircraft-to-satellite, satellite-to-satellite and radar communication systems require high gain beams capable of being steered to wide angles over a full hemisphere. Scanning losses in phased arrays increase rapidly beyond 60°. [34-35]

A modular approach of designing array antennas by forming building blocks or sub-arrays of radiating elements and using such sub arrays to form large arrays has been presented in [36-38]. The effect of sub arraying on scan blindness in a large array has been studied in [38] and the results show that sub arrying can greatly reduce scan blindness in large arrays but at the expense of introduction of grating lobes at certain scan angles. Amplitude tapering is an effective way to reduce grating lobes in a sub array environment. Sub array amplitude tapering applied on a 70 element linear array with a 30

dB, $\bar{n} = 4$ Taylor amplitude distribution with 10 subarrays has been reported in [39] which has been shown to produce effective trade-off by maintaining the advantages of having identical subarrays in addition to reducing grating lobes.

2.6.4 Multilayer Dual Polarized Antenna Arrays with Orthogonally placed elements

Arrays having proximity coupled elements have improved bandwidth and reduced radiation from feed networks. However, the feed line radiation is high enough making it hard to realize cross-polarization levels lower than -25 dB. As an alternative, aperture coupled elements can be used in dual polarized arrays. Although aperture coupling is a viable alternative to proximity coupling, it is generally suitable for multilayer antennas with small patch substrate thickness.

For dual polarization applications using multilayer technology with relatively thick patch substrate, higher order modes can be cancelled by using a single feed per element. This can be achieved by having each pair of adjacent elements use oppositely located feeds with opposite phases. As a consequence, in the far field region, the co-polarization feeds reinforce each other while the cross polarized fields cancel in both E and H planes. Using the geometry of orthogonally placed patches such as that in the 2 X 2 sub array in [25], cross polarization levels as high as -40 dB can be achieved. Also the phase difference of 180° between the ports allows cancellation of energy coupled in through the patches' cavities from its orthogonal port at the port itself. This results in better isolation between the ports, typically of the order of -30dB throughout the bandwidth.

3 METHODOLOGY

3.1 Problem Statement

CASA Student Led Test Bed (STB) Off-The-Grid (OTG) X band radar node [1], is the first prototype of a low infrastructure X-band weather radar network to aid forecasts in the western region of Puerto Rico. An antenna array needs to be developed for use with the OTG nodes for polarimetric studies of the lower atmosphere and related weather events. Based on the requirements for the OTG radar node [1], a light weight dual polarized antenna array having good spatial resolution and low cross polarization level needs to be built.

The main objective of this project is to design and develop an antenna array suitable for integration at one of the nodes of the OTG Radar network and having the following specifications:

- Half Power Beam Width (HPBW) of 6°
- Bandwidth of around 250 MHz
- Side Lobe Level (SLL) < -20 dB
- Cross Polarization levels < -30 dB
- Front –to-Back Ratio (FBR) < -13 dB

As discussed in Chapter 2, dual polarized antennas can be constructed either by using stacked structures, orthogonal arrangement of elements or by using complex feed structures. While stacked structures would result in bulky structures, complex feed structures tend to increase the overall antenna area. Hence, for the requirements of the OTG radar, orthogonal arrangement of the radiating elements is the apt choice. Subsequent sections of this chapter discuss the design of a microstrip fed

orthogonal arrangement of 2 X 2 antenna subarray to be used in a series-fed microstrip antenna array for the X band OTG radar.

3.1.1 Modular Array Design Procedure

As shown in the work flow diagram in Figure 3-1 a modular approach is followed while designing the array antenna. The following sections describe in detail the sequential design procedure. Ansoft Designer® (version 5) is chosen as the simulation software for the project. Based on Method of Moments, Designer® uses full wave electromagnetic functions for planar analysis based on Maxwell's equations.

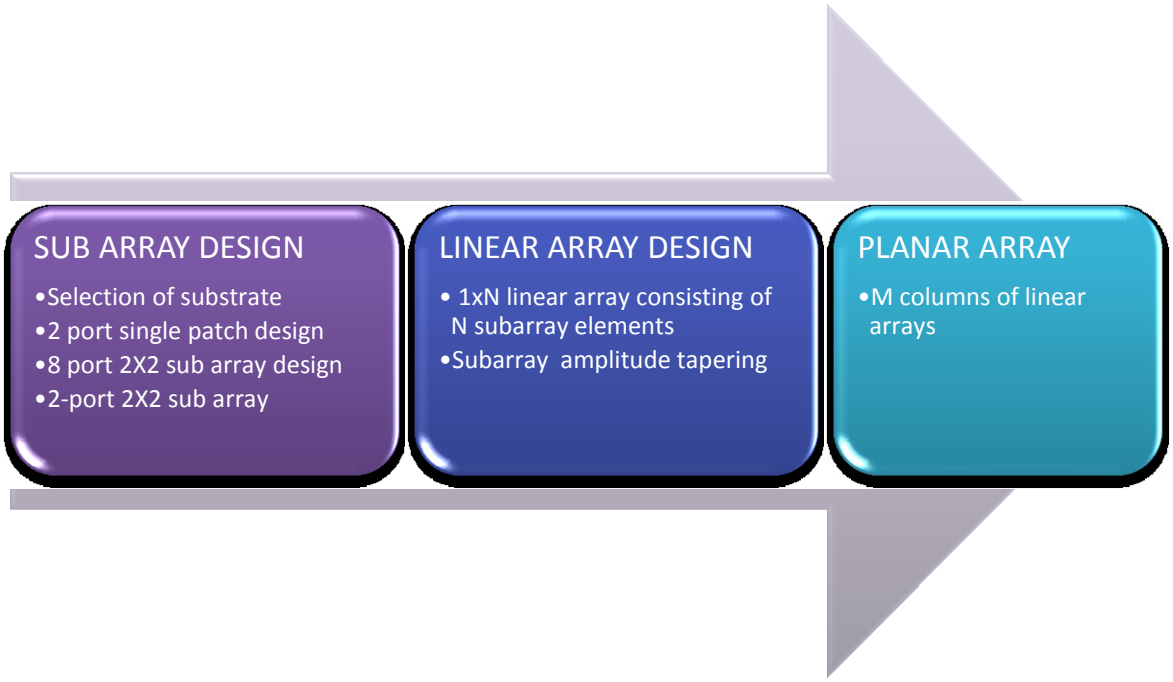

Figure 3-1: Work Flow Diagram

3.1.1.1 Sub-Array Design

First, a single patch is designed for dual polarization and resonated at 9.4 GHz. Then a 2x2 sub array is designed for the same frequency. The sequential procedure is explained in the sections below:

3.1.1.1.1 Selection of Substrate

The foremost aspect of the antenna array design is choosing the appropriate substrate. First, the permittivity of the substrate is chosen to be used for calculation of permissible substrate height in (37).

$$\frac{h}{\lambda} \leq \frac{0.3}{2\pi\sqrt{\epsilon_r}} \tag{37}$$

For $h > 0$ and $\epsilon_r > 0$, this inequality can be further simplified as

$$0 < \epsilon_r \leq \frac{2.33204 * 10^{-6}}{h^2} \tag{38}$$

Also, the cut off frequency of propagation of the second higher order surface wave is given by

$$f_{sw} \leq \frac{c}{4h\sqrt{\epsilon_r - 1}} \tag{39}$$

Based on the inequalities in (38) and (39) a number of solutions exist for both h and ϵ_r . There are several substrates available commercially as shown in the Table 3-1(a) and Table 3-1 (b).

Table 3-1: (a) List of Commercial Microwave Laminates

Dk@10GHz	Supplier	Name	Type	D.F.	CTE-X	CTE-Y	CTE-Z	MIL REF	IPC
2.08 +/ -0.02	Nelco	NY9208	P,W	0.0006	25	35	260	-	-
2.1	Polyflon	CuFlon	P	0.00045	12.90	12.90	12.90	-	-
2.17-2.20 +/- 0.02	Arlon	CuClad 217LX	P,W,CP	0.0009	29	28	246	GY	4103/05
2.17-2.20 +/- 0.02	Arlon	DiClad 880	P,W	0.0009	25	34	252	GY	4103/05
2.17+/-0.04	Arlon	IsoClad 917	P,R	0.0013	46	47	236	GP,GR	4103/03
2.17 +/- 0.02	Arlon	Intermod/-165dbc	P,W	0.0009	25	34	252	-	125/05
2.17 +/- 0.02	Nelco	NY9217	P,W	0.0008	25	35	260	-	-
2.17	Taconic	TLY-5A	P,W	0.0009	20	20	280	GY	125/05
2.20 +/- 0.02	Nelco	NY9220	P,W	0.0009	25	35	260	-	-
2.20 +/- 0.02	Rogers	RT/Duroid 5880	P,R	0.0009	31	48	237	GP,GR	125/04
2.20	Taconic	TLY-5	P,W	0.0009	20	20	280	GY	125/05
2.32 +/- 0.005	Polyflon	Polyguide	P,W	0.0002	108	108	108	-	-
2.33 +/- 0.02	Arlon	CuClad 233LX	P,W,CP	0.0013	23	24	194	GY	4103/05
2.33 +/- 0.02	Arlon	DiClad 870	P,W	0.0013	17	29	217	GY	4103/05
2.33 +/- 0.04	Arlon	IsoClad 933	P,R	0.0016	31	35	203	GP,GR	4103/03
2.33 +/- 0.02	Nelco	NY9233	P,W	0.0011	25	35	260	-	-
2.33 +/- 0.02	Rogers	RT/Duroid 5870	P,R	0.0012	22	28	173	GP,GR	125/04
2.33	Taconic	TLY-3	P,W	0.0012	20	20	280	GY	125/05
2.4-2.6 +/- 0.02	Arlon	CuClad 250GT	P,W,CP	0.0010	18	19	177	GT	4103/01
2.4-2.6 +/- 0.02	Arlon	CuClad 250GX	P,W,CP	0.0022	18	19	177	GX	4103/02
2.4-2.6 +/- 0.02	Arlon	DiClad 522	P,W	0.0018	14	21	173	GT	4103/01
2.4-2.6 +/- 0.02	Arlon	DiClad 527	P,W	0.0018	14	21	173	GX	4103/02
2.4-2.6 +/- 0.04	Rogers	Ultralam 2000	P,W	0.0019	15	15	200	GX	125/02
2.40 +/- 0.04	Nelco	NX9240	P,W	0.0016	12	18	150	-	-
2.45 +/- 0.04	Nelco	NX9245	P,W	0.0016	12	18	150	-	-
2.45	Taconic	TLX-0	P,W	0.0019	9	12	140	GX	125/02
2.50	Arlon	AD250	P,W	0.0018	12	15	95	-	4103/02

Table 3-1: (b) List of Commercial Microwave Laminates Continued

2.50 +/- 0.04	Nelco	NX9250	P,W	0.0017	12	18	150	GX	125/02
2.50	Taconic	TLX-9	P,W	0.0019	9	12	140	GX	125/02
2.55	Arlon	AD255	P,W	0.0018	12	15	95	-	4103/02
2.55	Polyflon	NorClad	P,W	.0007@1Mhz	53	53	53	-	125/02
2.55 +/- 0.04	Nelco	NX9255	P,W	0.0018	12	18	150	GX	125/02
2.55 +/- 0.04	Taconic	TLX-8	P,W	0.0019	9	12	140	GX	125/02
2..6	Sheldahl	ComClad HF	T	0.0025	59	59	59	Copper Clad Norel	-
2.60	Arlon	AD260A	P,W	0.0017	12	15	95	-	N/A
2.60 +/- 0.04	Nelco	NX9260	P,W	0.0019	12	18	150	GX	125/02
2.60	Taconic	TLX-7	P,W	0.0019	9	12	140	GX	125/02
2.65	Taconic	TLX-6	P,W	0.0019	9	12	140	GX	125/02
2.70	Arlon	AD 270	P,W	0.0030	12	15	95	-	4103/09
2.70 +/- 0.04	Nelco	NX9270	P,W	0.0022	25	35	260	GX	125/02
2.75	Taconic	TLC-27	P,W	0.0030	9	12	70	-	-
2.92 +/- 0.04	Rogers	RT/Duroid 6002	P,C	0.0012	16	16	24	-	-
2.94	Arlon	CLTE-XT	P,C,W	0.0012	8	8	20	-	4103/06
2.94	Arlon	LC-CLTE	P,C,W	0.0025	10	12	35	-	4103/06
2.94 +/- 0.04	Nelco	NX9294	P,W	0.0022	25	35	260	GX	125/02
2.94 +/- 0.07	Nelco	NH9294	P,W	0.0022	9	12	71	-	-
2.94 +/- 0.04	Rogers	RT/Duroid 6202	P,C,W	0.0015	15	15	30	-	-
2.95	Taconic	TLE-95	P,W	0.0030	9	12	70	-	-
2.96	Arlon	CLTE	P,C,W	0.0025	10	12	35	-	4103/06
3.00	Arlon	AD300A	P,W	0.0020	12	12	125	-	4103/09
3.00 +/- 0.04	Nelco	NX9300	P,W	0.0023	25	35	260	GX	125/02
3.00 +/- 0.07	Nelco	NH9300	P,W	0.0023	9	12	71	-	-
3.80	Nelco	N9300-13 RF	ME	0.0040	13-20	-	67	-	-
3.00 +/- 0.04	Rogers	RO3003	P,C	0.0013	17	17	24	GX	125/02
3.00	Taconic	TLC-30	P,W	0.0030	9	12	70	-	-
3.00	Taconic	TacLam TLG-30	P,C,W	0.0026	8	12	61	-	-
3.00 @ 1.9 GHz	Taconic	Rf-30	P,C,W	0.0014	11	21	125	-	-
3.00	Taconic	TSM-30	P,C,W	0.0015	23	28	78	-	-
3.02 +/- 0.05	Rogers	RO3203	P,C,W	0.0016	13	13	58	-	-
3.05 +/- 0.05	GIL	GML 1000	polyester	0.004	40	34	80	-	-

Higher permittivity substrates yield lower bandwidths. Hence, as a starting value of $\epsilon_r = 2.2$ is selected. RT Duroid® 5880 is a commercial microwave laminate which comes in a variety of thicknesses as shown in the table below.

Table 3-2: RT Duroid® 5880 standard thickness values

Permittivity ϵ_r	**Standard Thickness(mm)**
2.2	0.127
	0.254
	0.381
	0.508
	0.787
	1.575
	3.175

For the selected Duroid® 5880 substrate, the thicknesses that can be used for antenna design at 9.4 GHz, according to (38), is as obtained below:

$$0 < h \leq 1.0297mm \tag{40}$$

In order to increase the substrate options for the antenna design $h = 1.575\,mm$ is tested for occurrence of surface wave at the vicinity of the desired frequency of operation (9.4 GHz). For $h = 1.575\,mm$, the cutoff frequency for the substrate with $\epsilon_r = 2.2$ as according to inequality (39) is $f_{sw} \leq 43.47\,GHz$. Hence, $h = 1.575\,mm$ can be used to design the antenna. Also, for microstrip antennas, thicker substrates are preferred for higher bandwidth. Hence, thickness values less than 0.5mm is not taken into consideration. Therefore, the first set of substrate properties for antenna design is listed in Table 3.3.

Table 3-3: First set of substrate parameters for design

Permittivity ϵ_r	Thickness(mm)
2.2	0.508
	0.787
	1.575
	3.175

Similar calculations are performed to obtain other permittivity-height combinations suitable for both the patch design and for feed network layer as preliminary step towards design and as starting points for simulations.

3.1.1.1.2 Two-port Single Element Design

After selecting several permittivity-height combinations suitable for the design, a single square element is designed and simulations are performed in Ansoft Designer®. The "Estimate" Module in Ansoft Designer® offers a wide variety of parameter estimates for microstrip line, quarter-wave transformer, tuning stub, rectangular and square antennas Although Designer® only has estimates for a circularly polarized nearly-square patch, the estimated vertical or horizontal length can be used as the starting parameter values for a dual polarized square patch antenna.

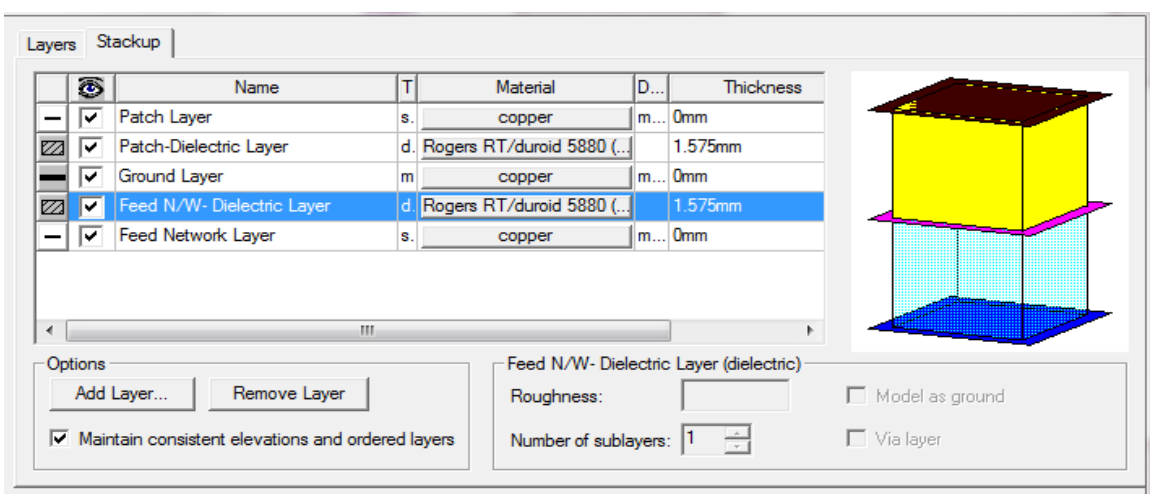

Figure 3-2 and Figure 3-3 show the dielectric stack and the estimate for length of a square patch. Also, since a square patch has high impedance values (~ 220 Ω) along its edges, the port impedance is chosen appropriately as shown in Figure 3-4.

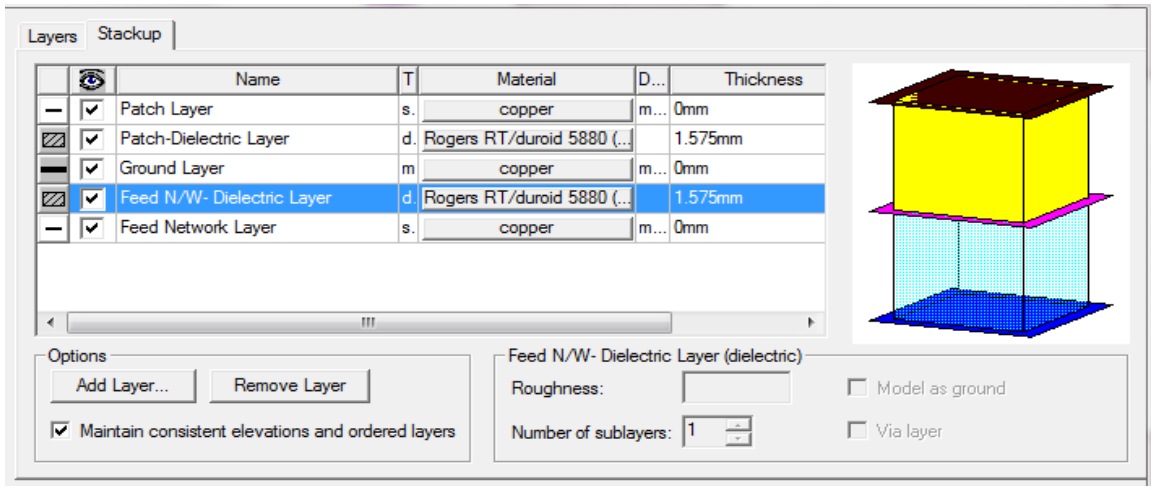

Figure 3-2: Dielectric Layer Stack

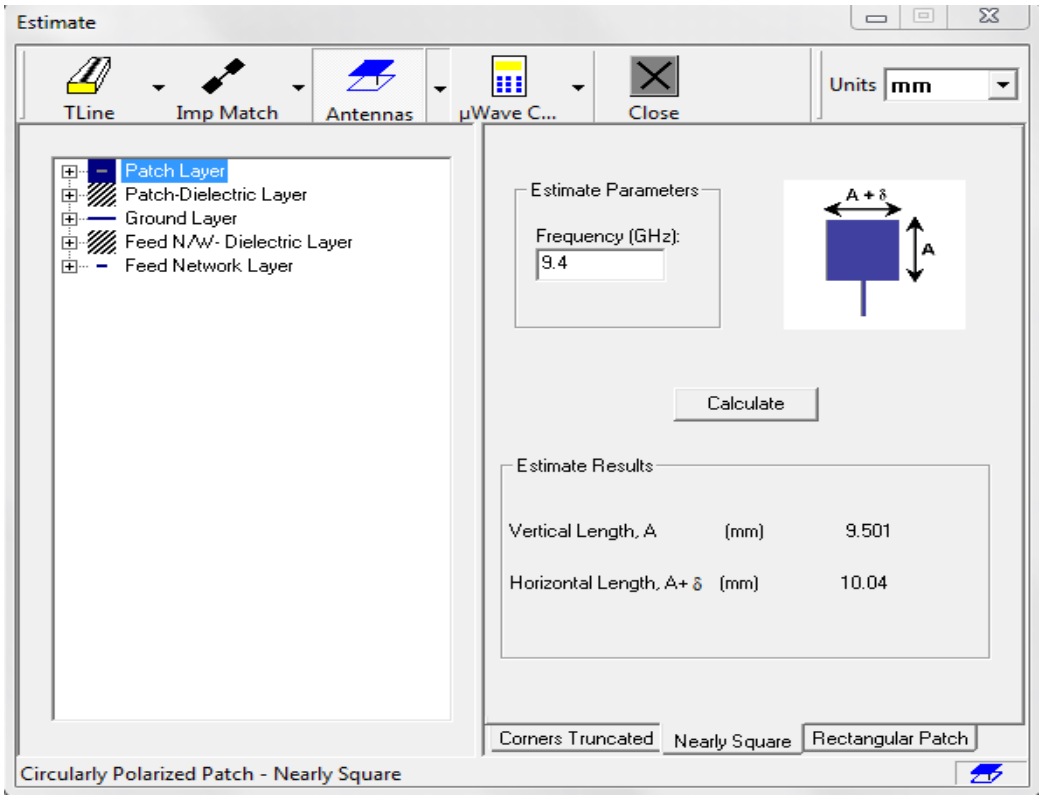

Figure 3-3: Estimate of length for square patch

Name	Value	Unit	Evaluated Value
Port	Port1		
PortSolver	☑		
Phase	0	deg	0deg
Magnitude	1	V	1V
PostProcess	☑		
Renormalize	200 + 0i	ohm	200ohm + 0i ohm
Deembed	10	mm	10mm
RefToGround	☐		
Type	Single Strip Gap Source		

Figure 3-4: Port Impedance Value

Using the estimated value for the length “L”, a single square patch is designed as shown in Figure 3-5.

The first simulation is performed and results are recorded as shown in Figure 3-6and Figure 3-7.

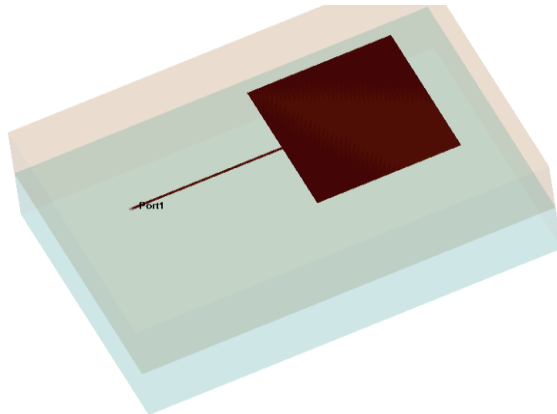

Figure 3-5: Single polarized square patch

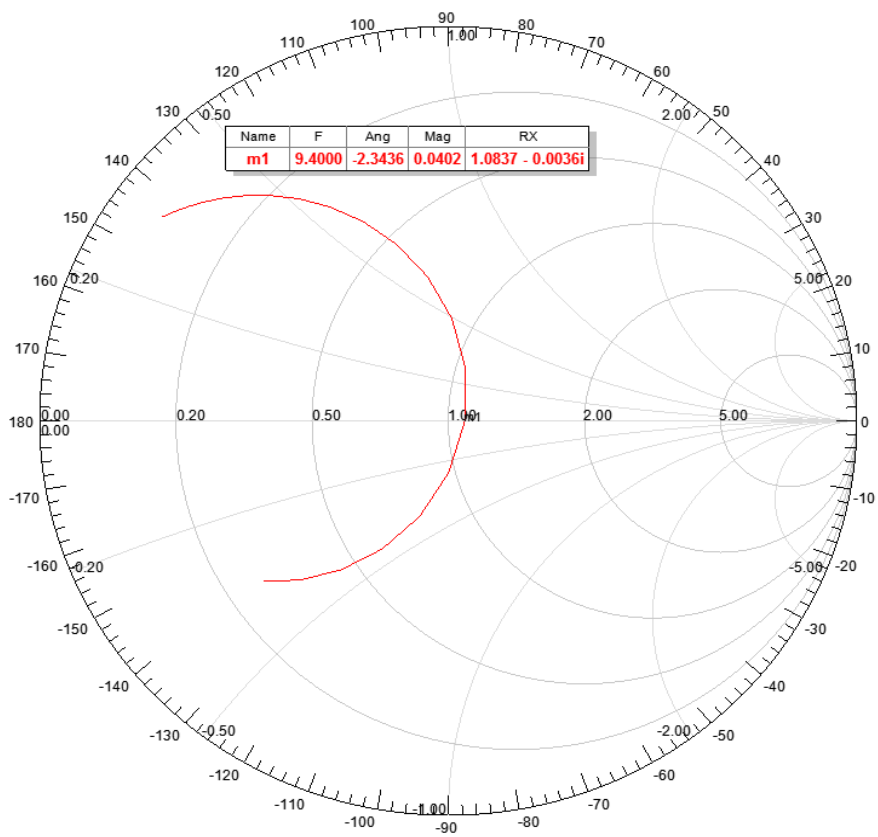

Figure 3-6: Smith Chart plot for first simulation

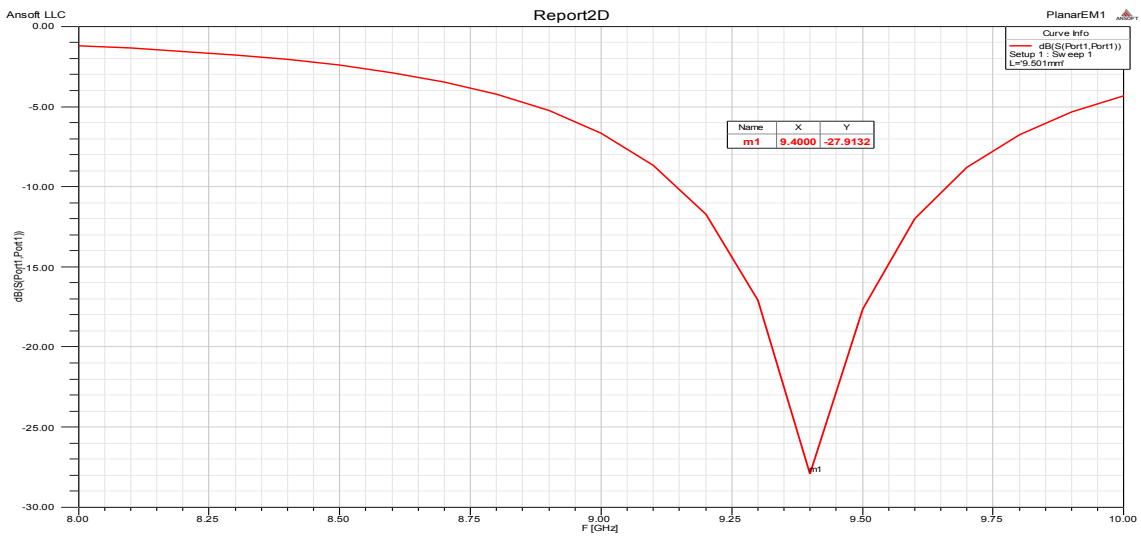

Figure 3-7: Plot of Return Loss for first simulation

Similar simulation is performed next but with an additional port making the element dual polarized as shown in Figure 3-8. The port impedance values are shown in Figure 3-9. The results for dual polarized elements are shown in

Figure 3-10 and Figure 3-11.

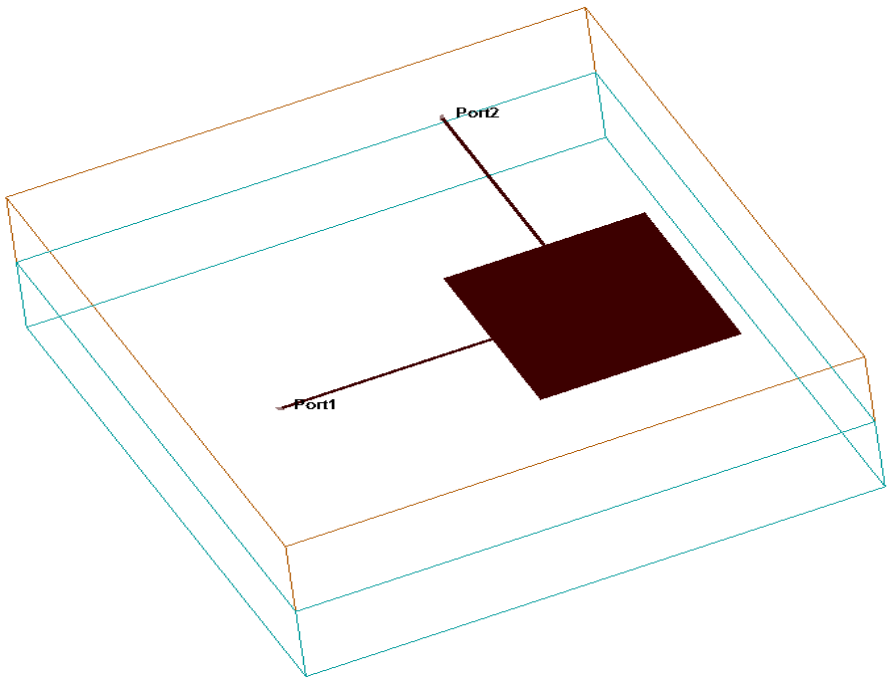

Figure 3-8: Dual polarized square patch

Name	Value	Unit
Port	Port1	
PortSolver	☑	
Phase	0	deg
Magnitude	1	V
PostProcess	☑	
Renormalize	200 + 0i	ohm
Deembed	10	mm
RefToGround	☐	
Type	Single Strip Gap Source	

Name	Value	Unit
Port	Port2	
PortSolver	☑	
Phase	0	deg
Magnitude	1	V
PostProcess	☑	
Renormalize	200 + 0i	ohm
Deembed	10	mm
RefToGround	☐	
Type	Single Strip Gap Source	

Figure 3-9: Port impedance values for dual polarized patch

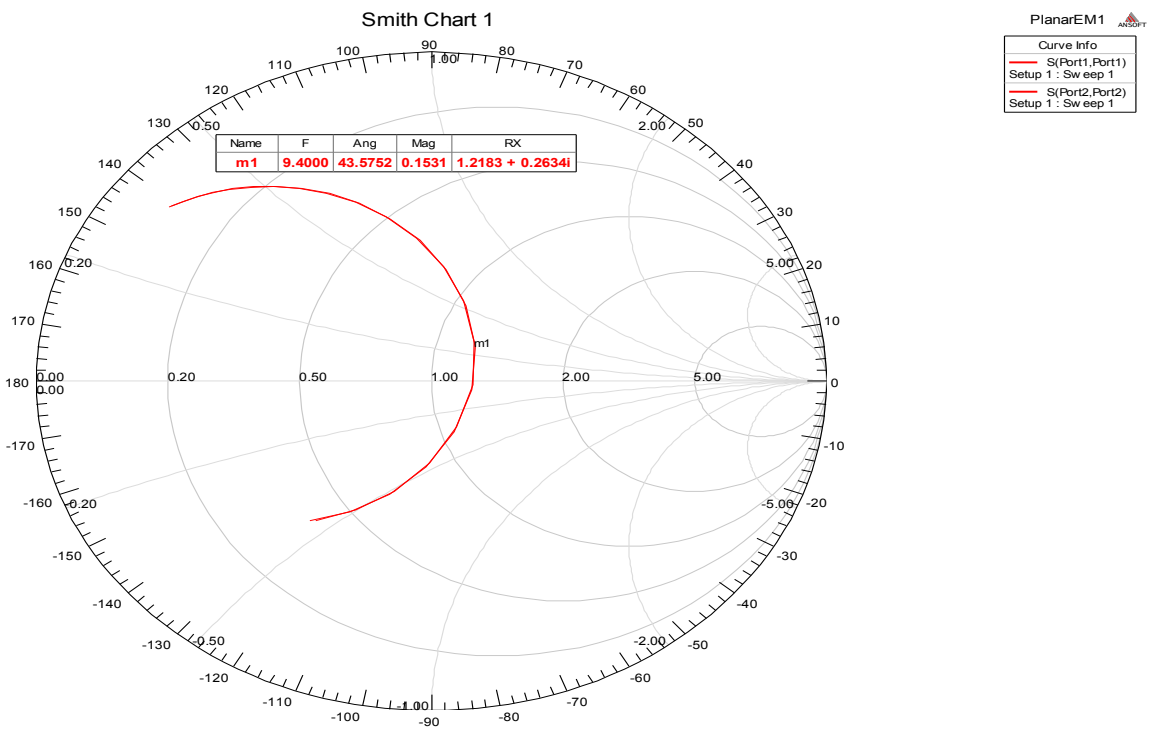

Figure 3-10: Smith Chart plot for dual polarized square patch

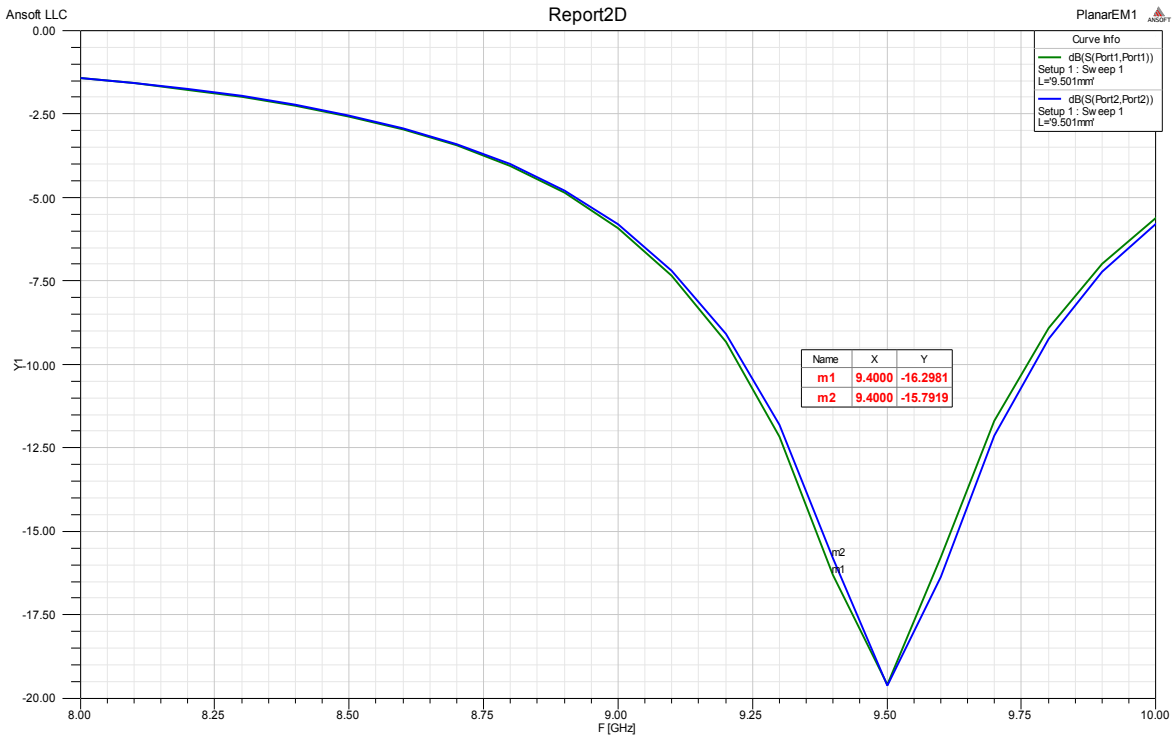

Figure 3-11: Plot of Return Loss for dual polarized square patch

As evident from Figure 3-11, after the addition of another port shifts the resonant frequency. The length of the patch is adjusted in order to bring the resonance back to the desired frequency.

3.1.1.1.3 Eight-port 2 X 2 Sub-Array Design

After tuning the length of a single patch having two ports for scaling the resonant frequency, three similar patches are added. The resulting the assembly is a 2 X 2 sub array of square patches each of length L as shown in Figure 3-12. At this stage, all of the radiators are fed with two ports in each patch making a total of eight ports in the sub array. The initial value of the separation between the patches is chosen as half-wavelength. The assembly is then simulated with the same excitation at all the feed ports. The simulation results for the sub array are shown in Figure 3-13 and Figure 3-14. As seen from Figure 3-13 and Figure 3-14, the impedance values and hence the resonant frequency shifts

changes due to mutual coupling between the patches. In order to make the entire assembly resonate at 9.4 GHz, the spacing between the patches dx and dy are changed until an optimum value is obtained. In order to have the same aperture for all the ports, dx and dy are made equal.

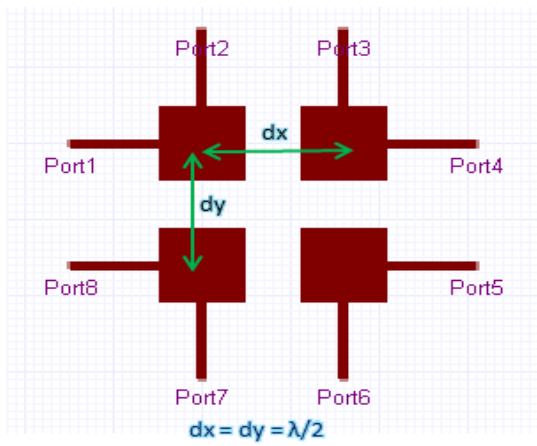

Figure 3-12: 2 X 2 radiator assembly with 8 ports spaced λ/2 apart

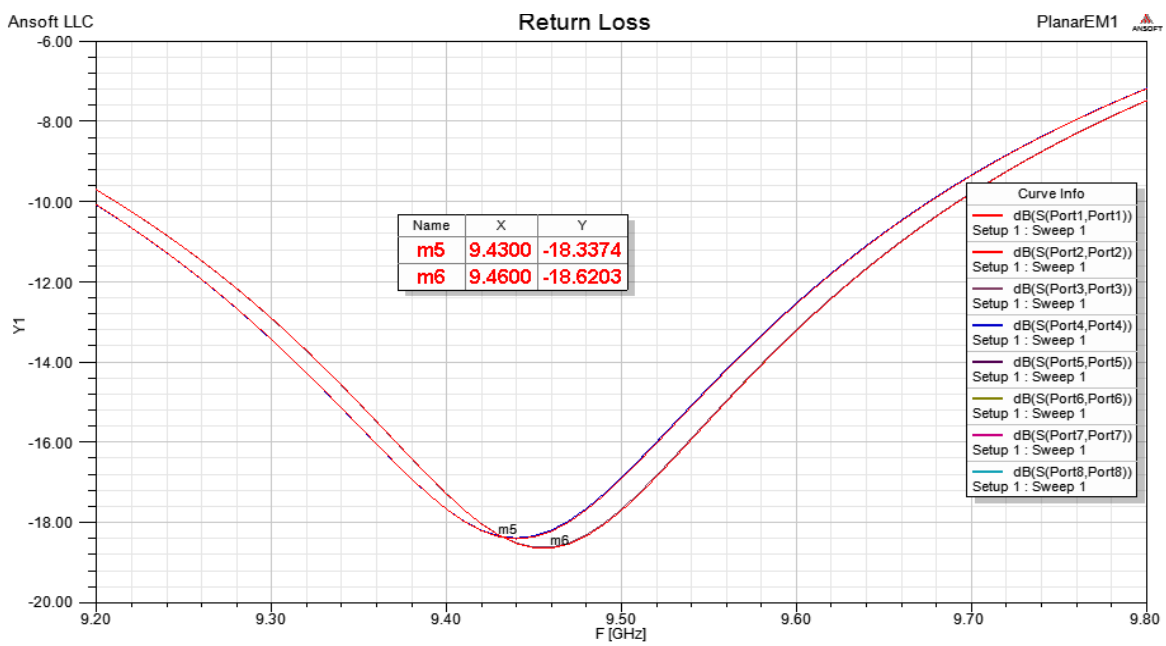

Figure 3-13: Return Loss plot of the 2X2 radiator assembly with 8 ports

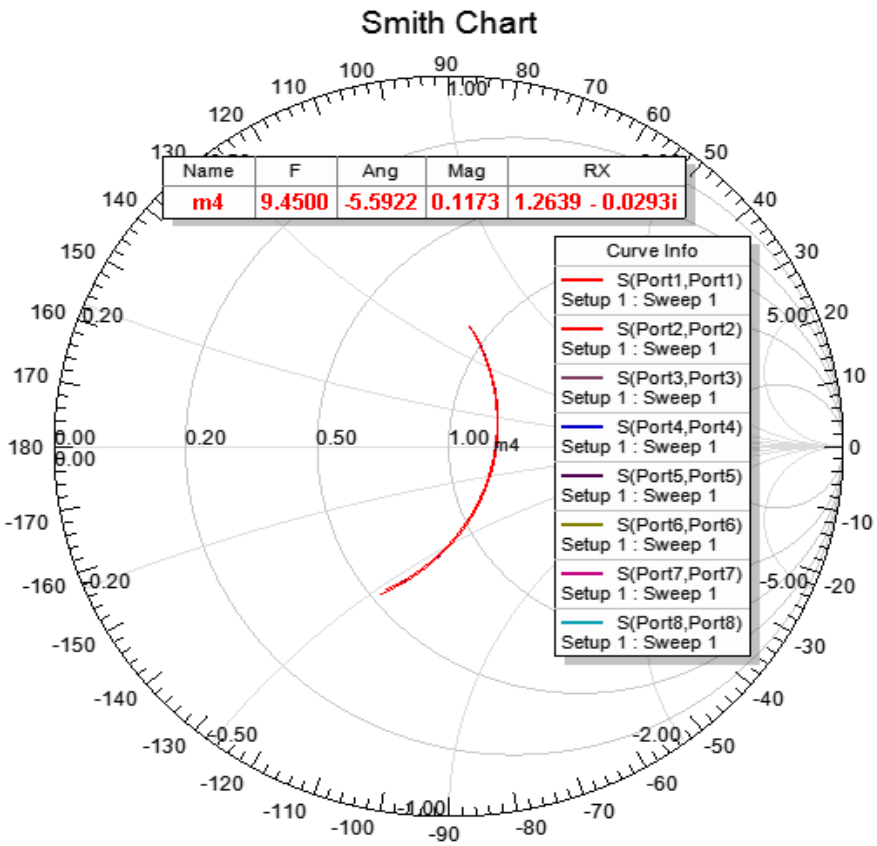

Figure 3-14: Smith chart plot of the 2 X 2 radiator assembly with 8 ports

Since all the patches and the feed line are of the same dimension, it is assumed that input impedances at all the ports are identical. In order to ballpark on the value of dx necessary for making the patch assembly resonate at 9.4 GHz, a parametric analysis of the effect of dx on the resonance is performed. The results of the parametric analysis for different values of dx and resulting S_{11} values are shown in Figure 3-15. From Figure 3-15, it can be seen that the value of dx lies between 25 mm and 30 mm. In order to zero in on the appropriate value of dx, another parametric analysis in conducted but with smaller increment in the values for dx.

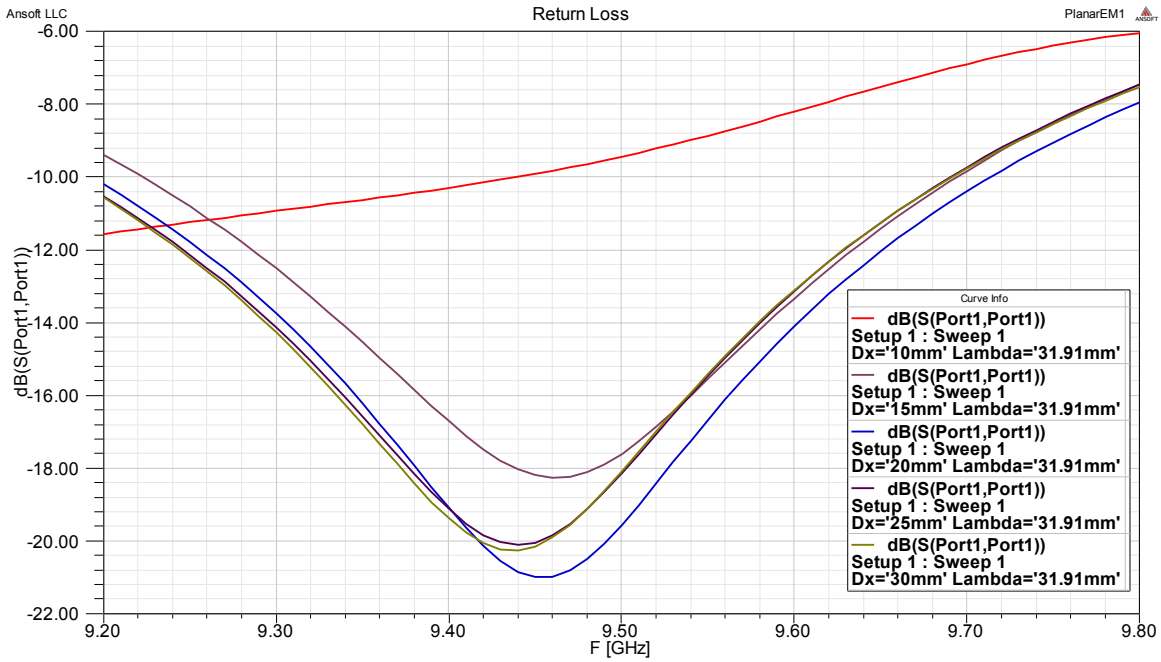

Figure 3-15: Return Loss (S11) for parameterized values of separation dx from 10 mm to 30 mm

If there is no significant change in the return loss values with changes in the values of the chosen parameter, its value is fixed and a parametric analysis of another variable is performed. As seen from Figure 3-16 there is no significant change in the return loss values for changes in separation between the patches within this interval. Hence, by inspection a value is chosen and dx is set at that value.

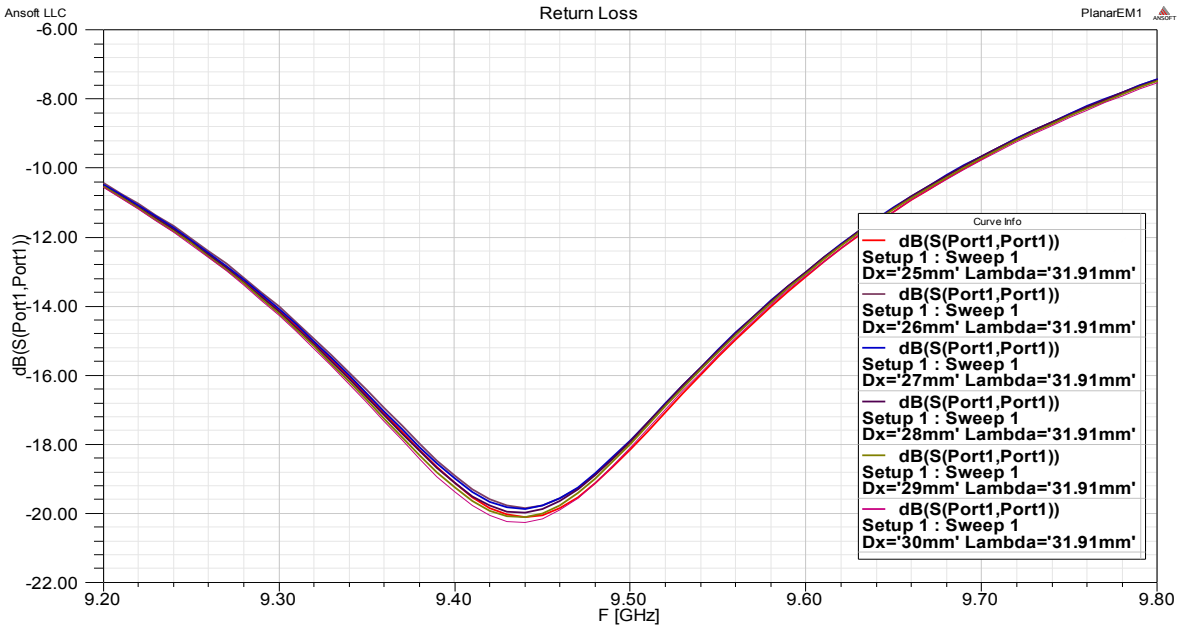

Figure 3-16: Return Loss (S11) for parameterized values of separation dx from 25 mm to 30 mm

After fixing the value for dx, another parametric analysis is performed by varying values of length L with large variations as shown in Figure 3-17. This helps to estimate the range of values for L which brings the resonance closer to the desired frequency. As was done earlier for dx, a suitable range of values is chosen by inspection of the results and the parametric analysis is performed again to select a suitable value of L as shown in Figure 3-18. This process is iterative and is continued several number of times before the values of both L and dx can be fixed to yield less than -20 dB for the return loss at the operating frequency.

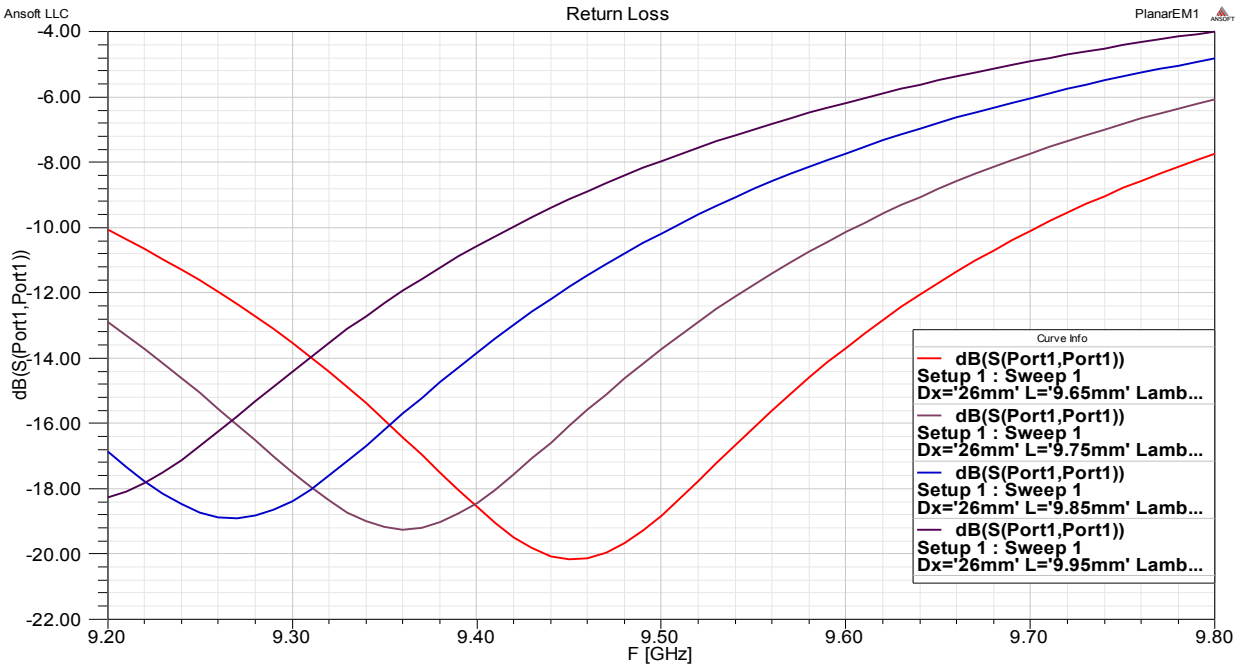

Figure 3-17: Return Loss (S11) for parameterized values of length L with large intervals

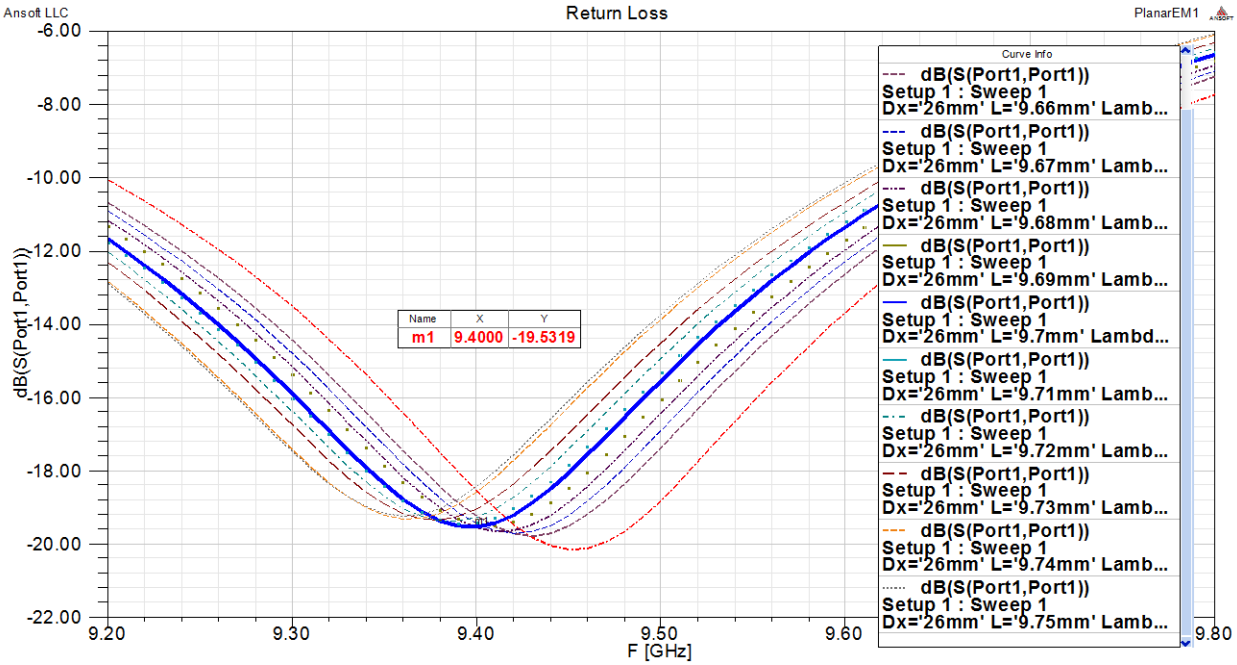

Figure 3-18: Return Loss (S11) for parameterized values of length L with smaller intervals within the estimated range

3.1.1.1.4 Two-port 2 X 2 Sub-Array Design

3.1.1.1.4.1 Monolithic structure

Once the values of L and dx are chosen so that the return loss at the operating frequency is the least (preferably < -20 dB), the matching network is designed. The impedance at each port is calculated from the Smith Chart as shown in Figure 3-19.

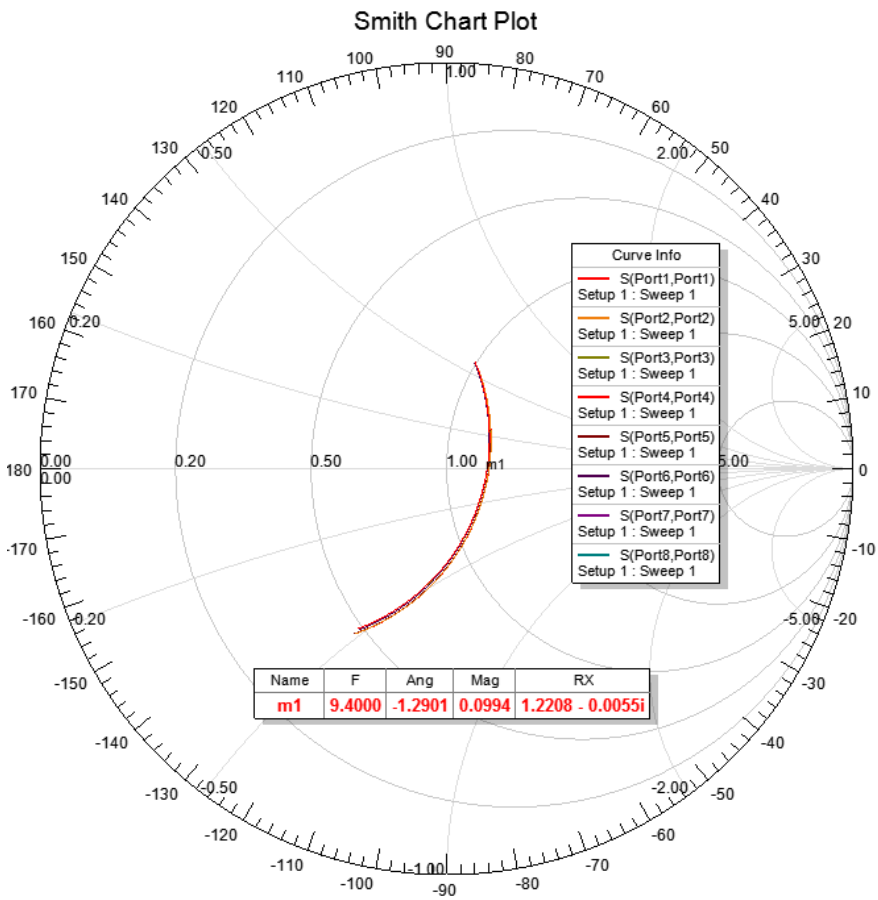

Figure 3-19: Smith Chart Plot for calculation of input impedance at each port

The input impedance Z^{in} at each port is identical and is calculated using the following equation:

$$Z_{Port\ n}^{in} = \frac{1 + S_{nn}}{1 - S_{nn}} \tag{41}$$

for n=1, 2, 3, 4….

After calculating the input impedance, the impedance, width and length of quarter wave transformers are calculated. The Estimate Tool of Ansoft Designer® can be used to get the estimates of the parameters at the desired frequency as shown in Figure 3-20. Although the Estimate tool only allows transformation of real values, the inductive/reactive part of the input impedance is taken care of by adjusting the lengths of the quarter wave transformers at each junction.

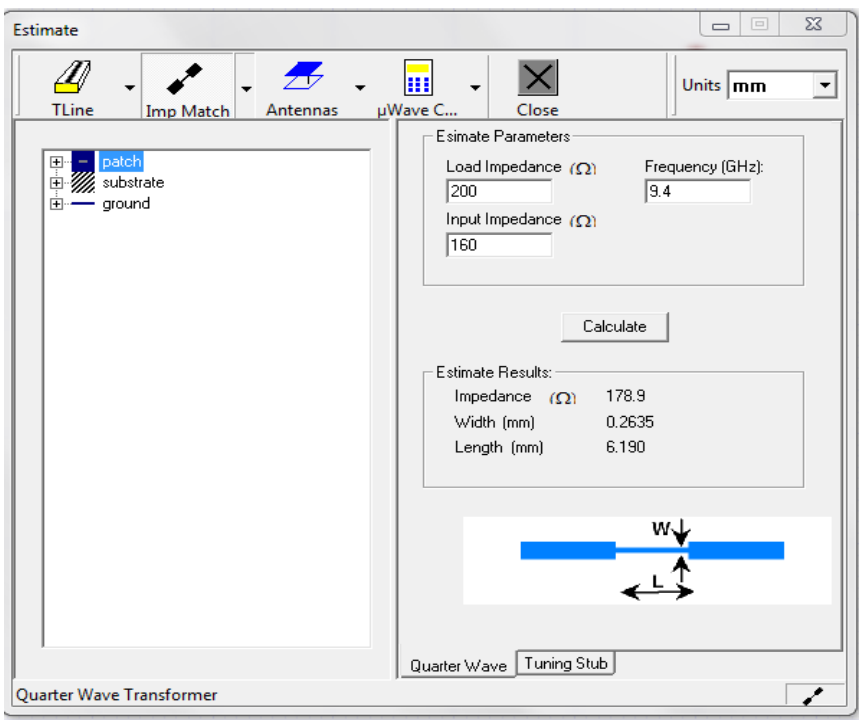

Figure 3-20: Approximating dimensions of quarter wave transformer sections using the Estimate Tool

After addition of the quarter wave sections at each port, the radiator assembly is simulated to for the new values of port impedances. Once the input impedance at each port is close to the desired value, the opposite ports are connected to each other using transmission lines. For initial analysis, the feed

ports are placed in the same plane as the radiator assembly resulting in the geometry as shown in Figure 3-21.

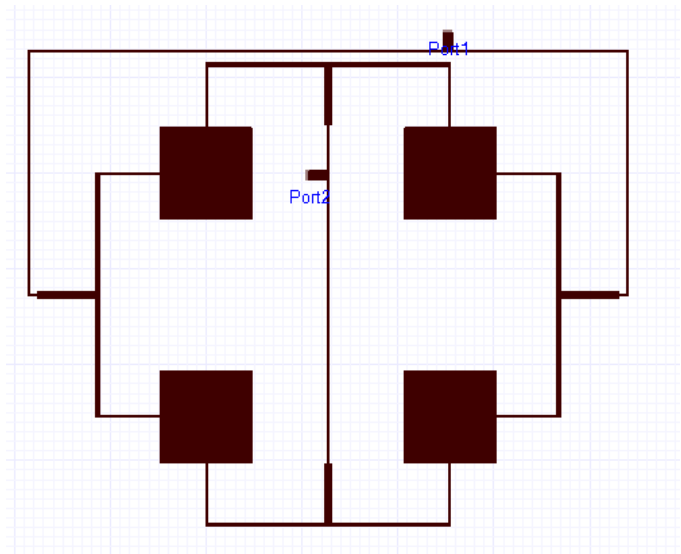

Figure 3-21: Sub array geometry with matching network

The next step is to add the feed ports for dual polarization. Initially, the feed ports are added using microstrip lines on the same plane as the radiator assembly as shown in Figure 3-21. The resulting geometry is similar to that presented in [25] and forms the building block of the linear array to be designed.

3.1.1.1.4.2 Multilayer structure

Since the structure of Figure 3-21 contains both feed ports in the same plane, it would be impossible to use the geometry in a linear array without the feed lines crossing one another. To avoid such a situation, the feed lines are moved into another layer below the ground plane. The feed network and the patch layer are connected with the help of vias. The resulting stack up of the layers and resulting structure are shown in Figure 3-22 , Figure 3-23 and Figure 3-24 . The results of simulation for the multilayer structure are shown in Figure 3-25 and Figure 3-26.

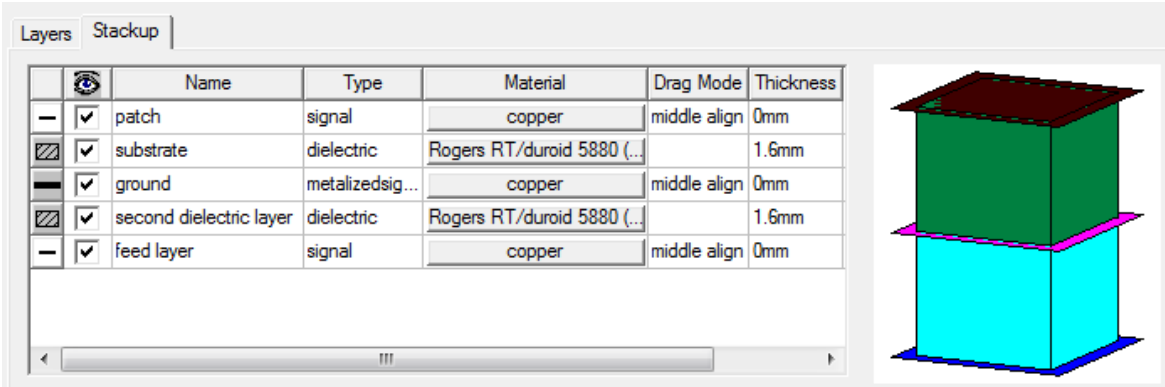

Layers | Stackup

	Name	Type	Material	Drag Mode	Thickness
✓	patch	signal	copper	middle align	0mm
✓	substrate	dielectric	Rogers RT/duroid 5880 (...		1.6mm
✓	ground	metalizedsig...	copper	middle align	0mm
✓	second dielectric layer	dielectric	Rogers RT/duroid 5880 (...		1.6mm
✓	feed layer	signal	copper	middle align	0mm

Figure 3-22: Multilayer stack up including additional layer for feed network

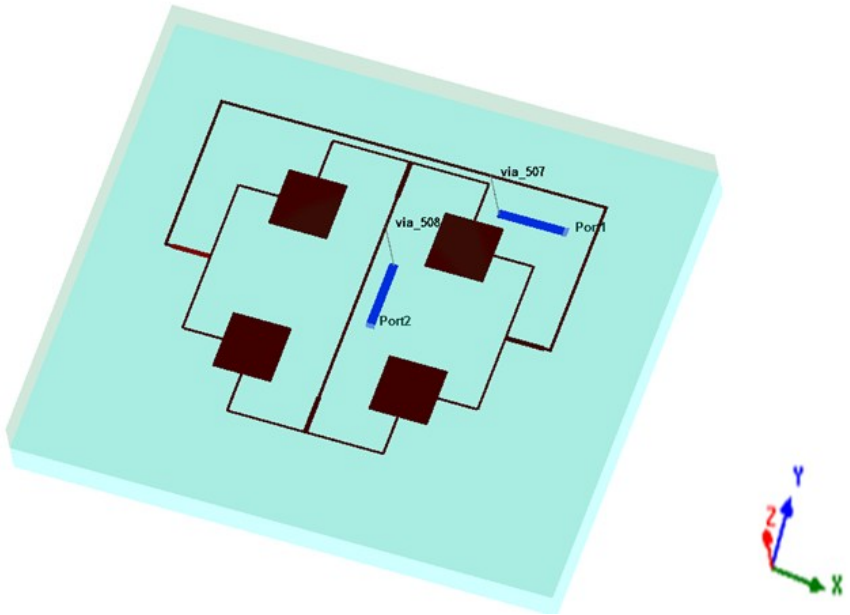

Figure 3-23: Top view of the multilayer sub array with separate patch and feed layers

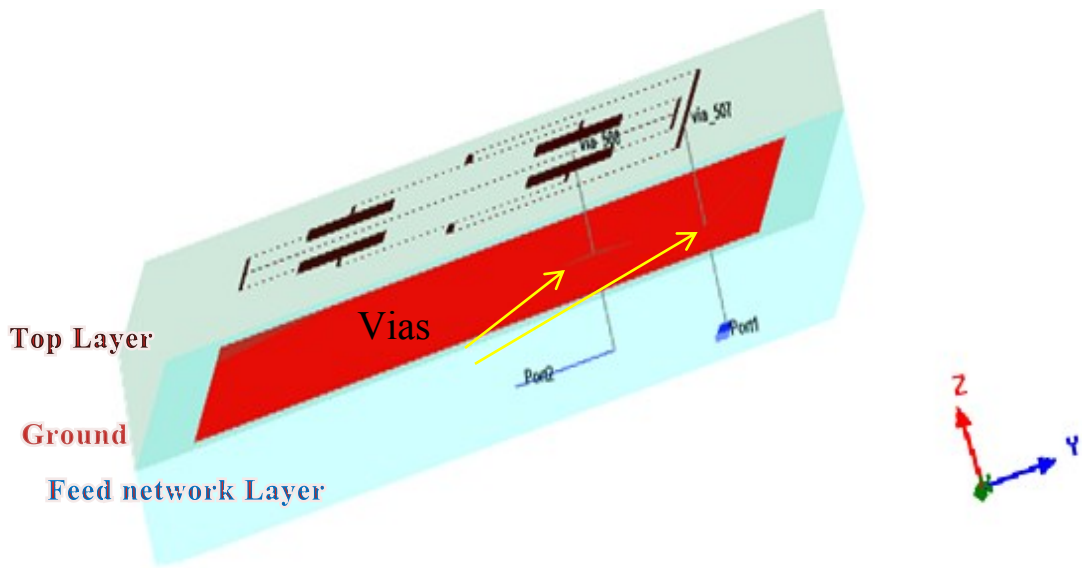

Figure 3-24: Cross section view of the multilayer sub array showing different layers and vias

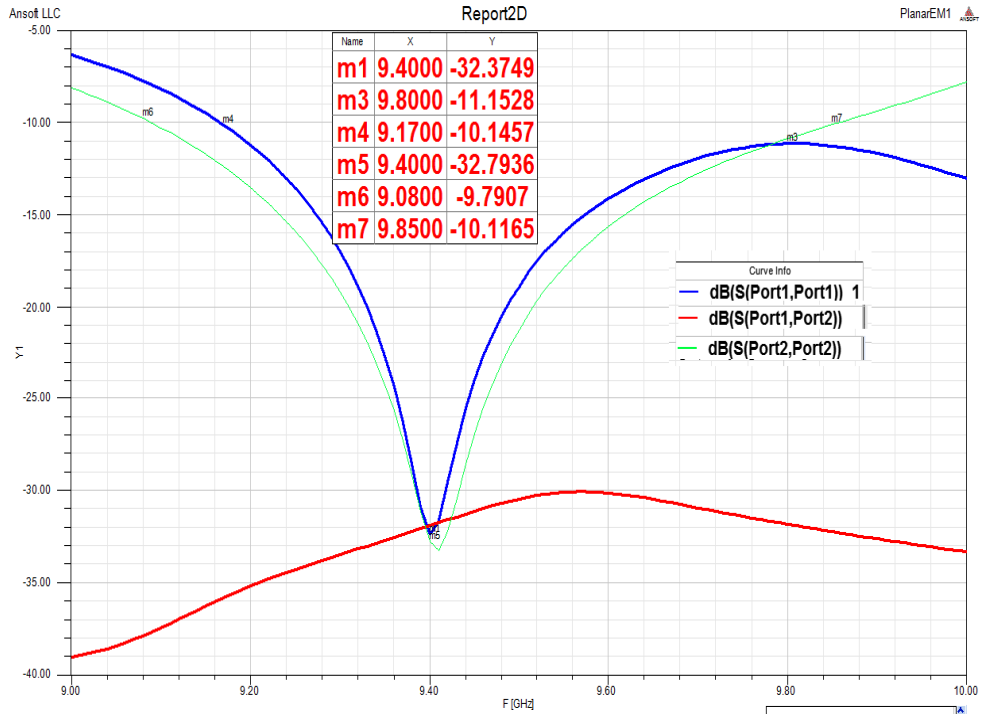

Figure 3-25 : Return Loss of 2X2 multilayer sub array

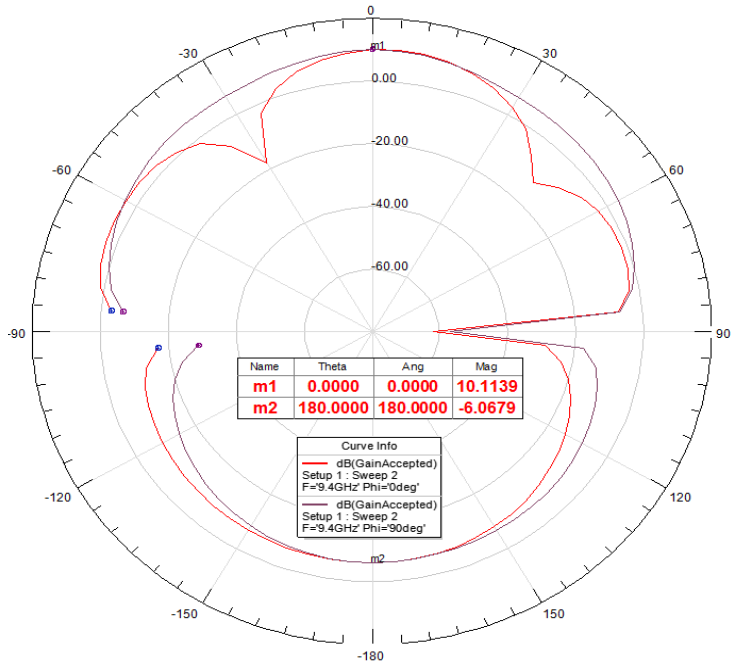

Figure 3-26: Radiation Pattern for 2X2 multilayer sub array

Once the multilayer structure has been designed, the structure is simulated in Designer® and results are analyzed. Due to addition of another layer for the feed network and addition of vias, there is a change in the impedance and resonant frequency of the sub array. Rigorous changes are then made to design parameters such as the separation between the patches, the length of the square patches, the via diameter and the widths of the transmission lines to make the sub array resonate at the desired frequency as discussed in the following paragraphs.

First the stack up of the different layers of the multilayer antenna is created with suitable values of permittivity and height. In order to provide better isolation between the two ports, a three layer structure having two separate dielectric layers (as shown in Figure 3-27) is designed and simulated. Then a 2 X 2 sub array of square patches is created with values of L obtained from the design of Figure 3-21. A parametric study of the length and separation between the patches is performed, as

shown in Figure 3-28 and Figure 3-29 , to ascertain the best values for the variables that result in resonance of the assembly at the desired frequency.

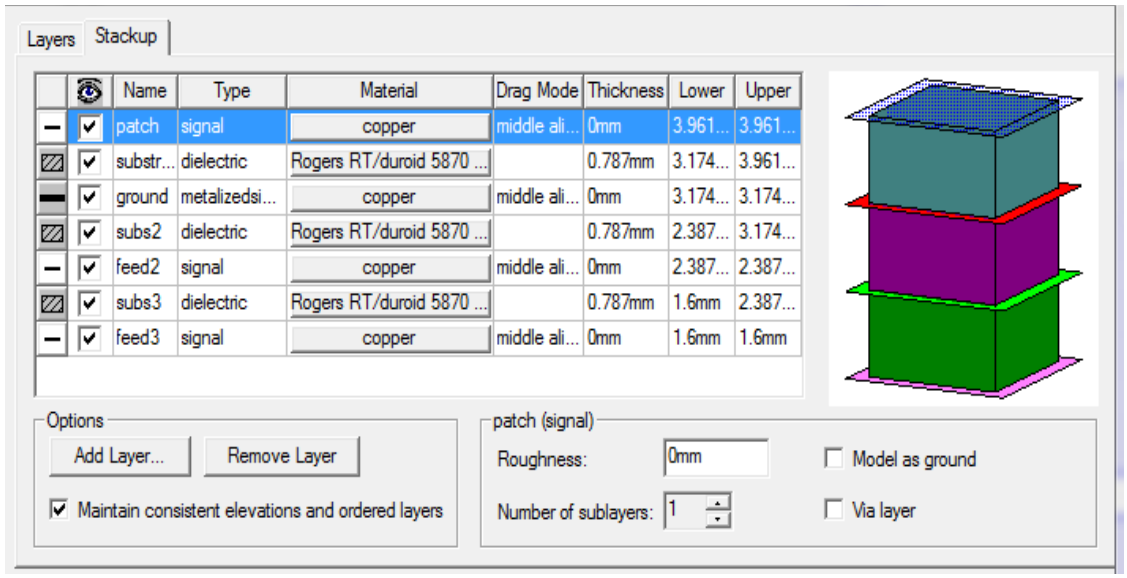

Figure 3-27: Stack up of three layered structure

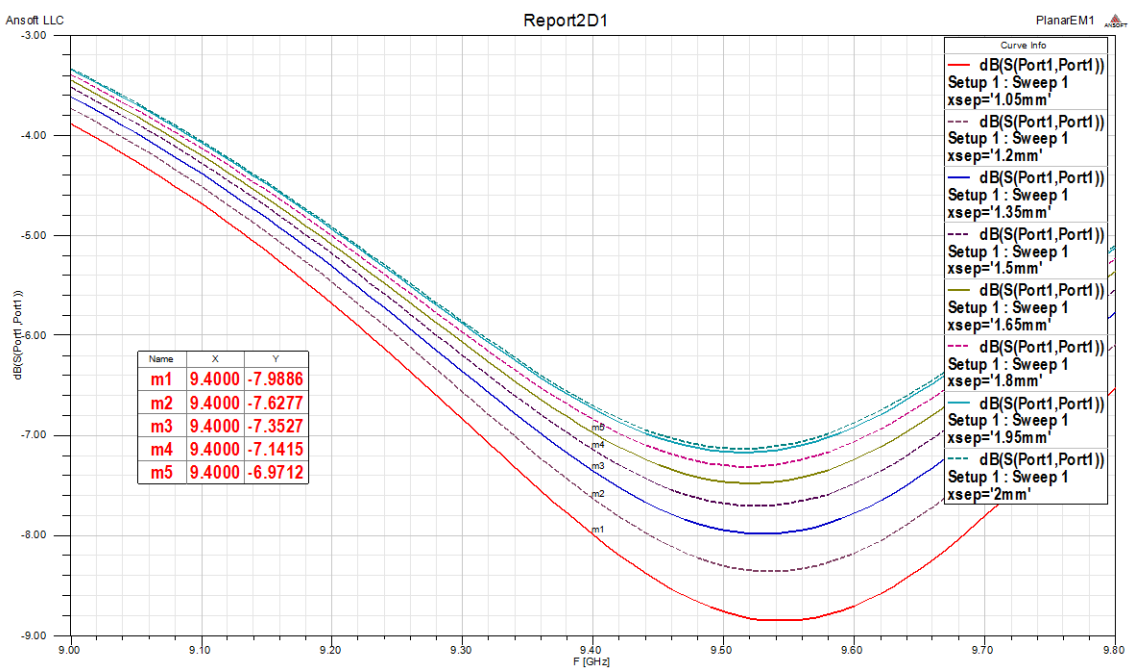

Figure 3-28: Return Loss for parameterized values of separation between the patches (xsep)

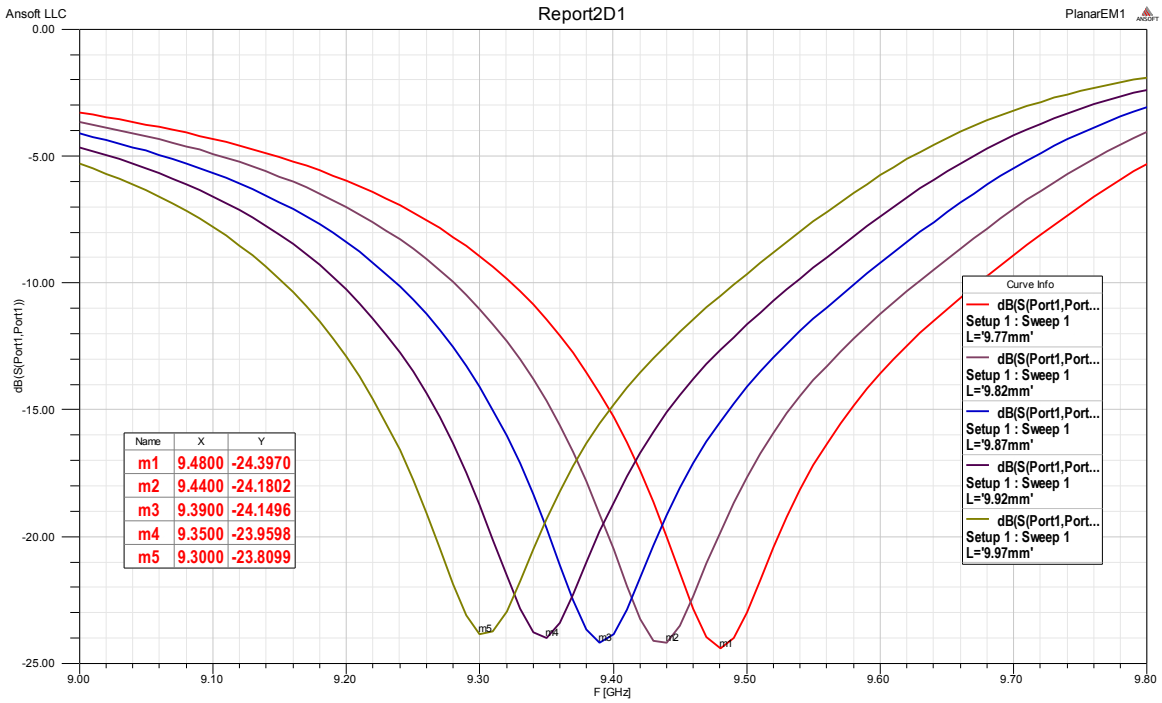

Figure 3-29: Return Loss for parameterized values of patch length (L)

Once the optimum values of length L and separation between the patches is determined, a feed network of transmission lines is designed for the sub array as shown in Figure 3-30. The simulation results for such geometry are as shown in Figure 3-31 and Figure 3-32.

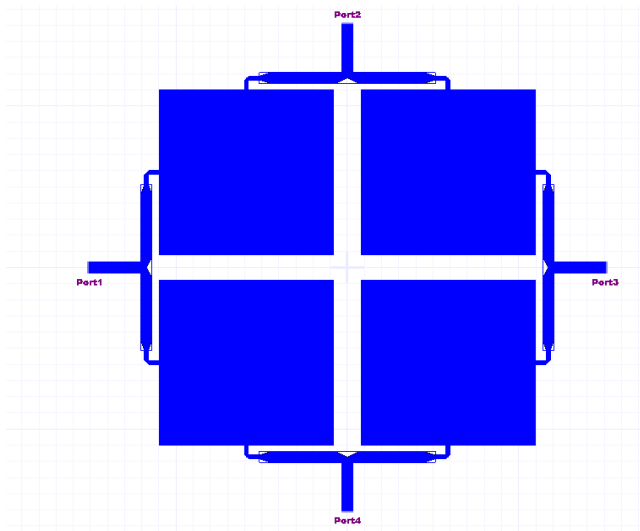

Figure 3-30: 2 X 2 patch assembly with matching network with 4 ports

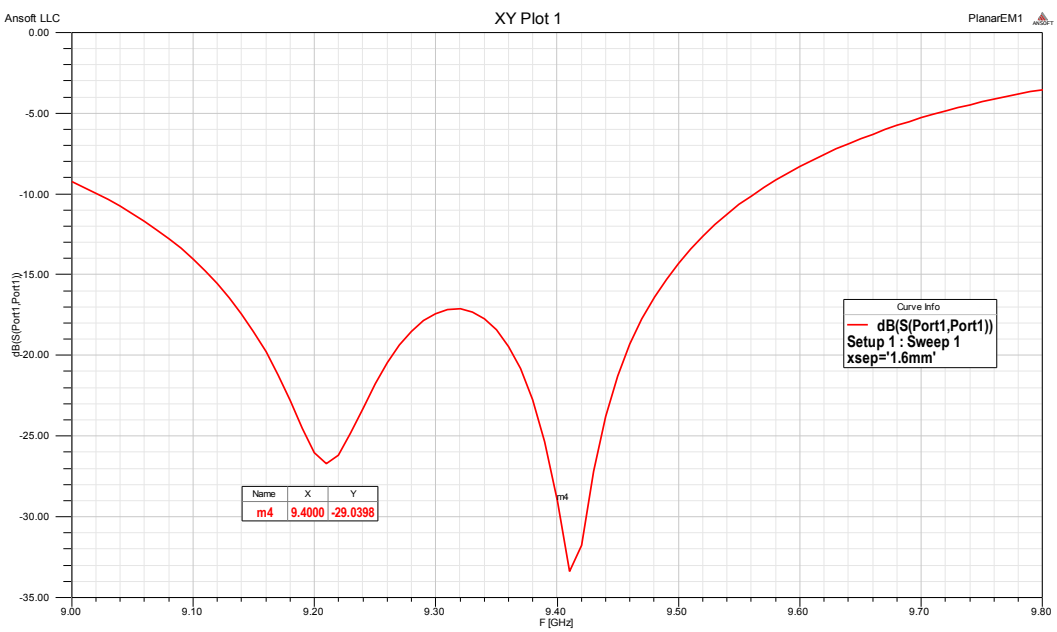

Figure 3-31: Return Loss plot for the three layer sub array in Figure 3-30

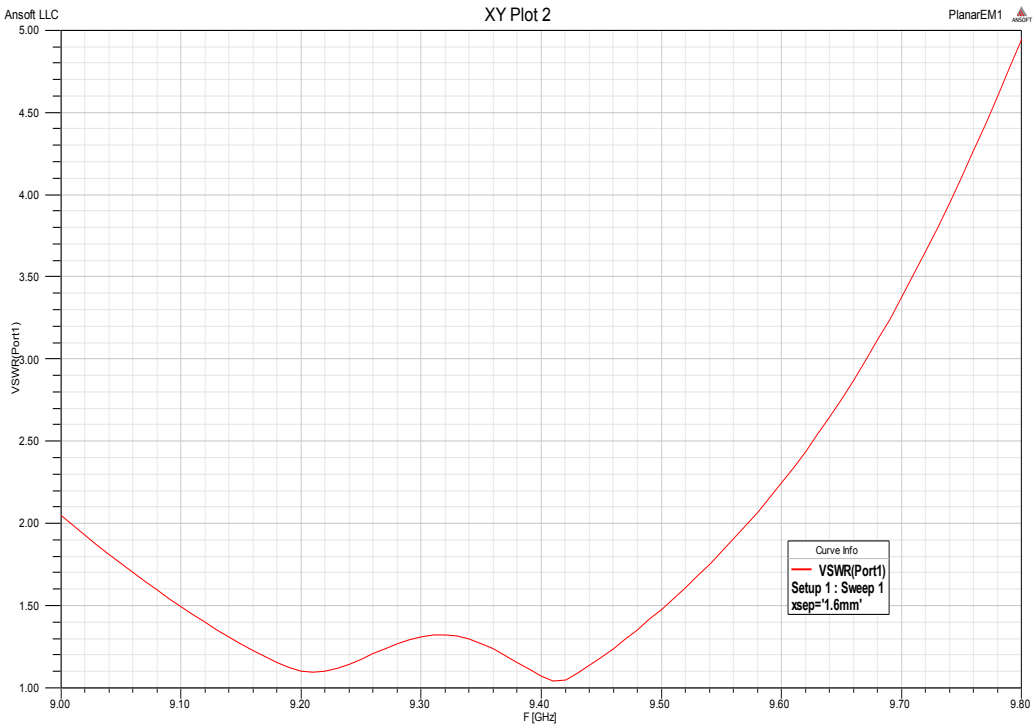

Figure 3-32: VSWR plot for three layer sub array in Figure 3-30

Next two ports on opposite sides are connected to each other. In order to avoid crossing of the lines one of the transmission lines connecting opposite pair of patches is placed in the layer below the ground in the second dielectric layer, as shown in

Figure 3-33, as a preliminary step. The feed network in the layer is connected to the patch layer by vias. The simulation result for such a structure is shown in Figure 3-34.

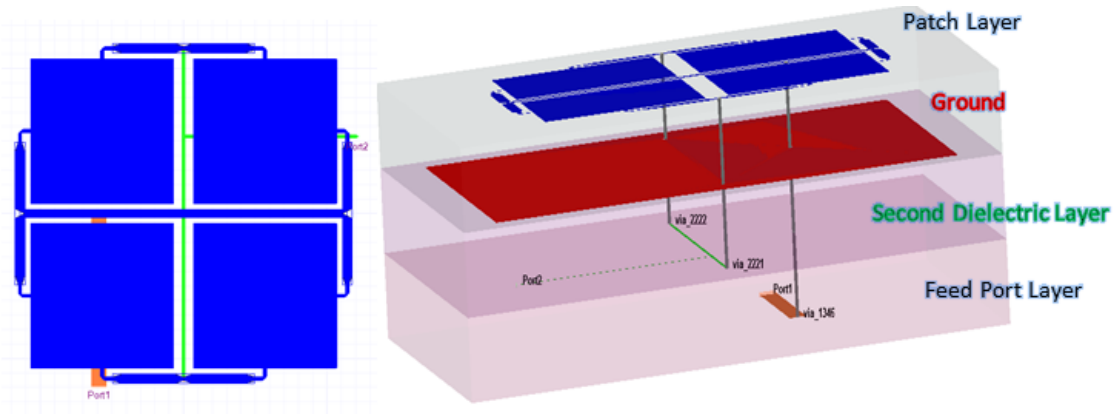

Figure 3-33: Modified structure for Figure 3-30 with transmission line below the ground plane

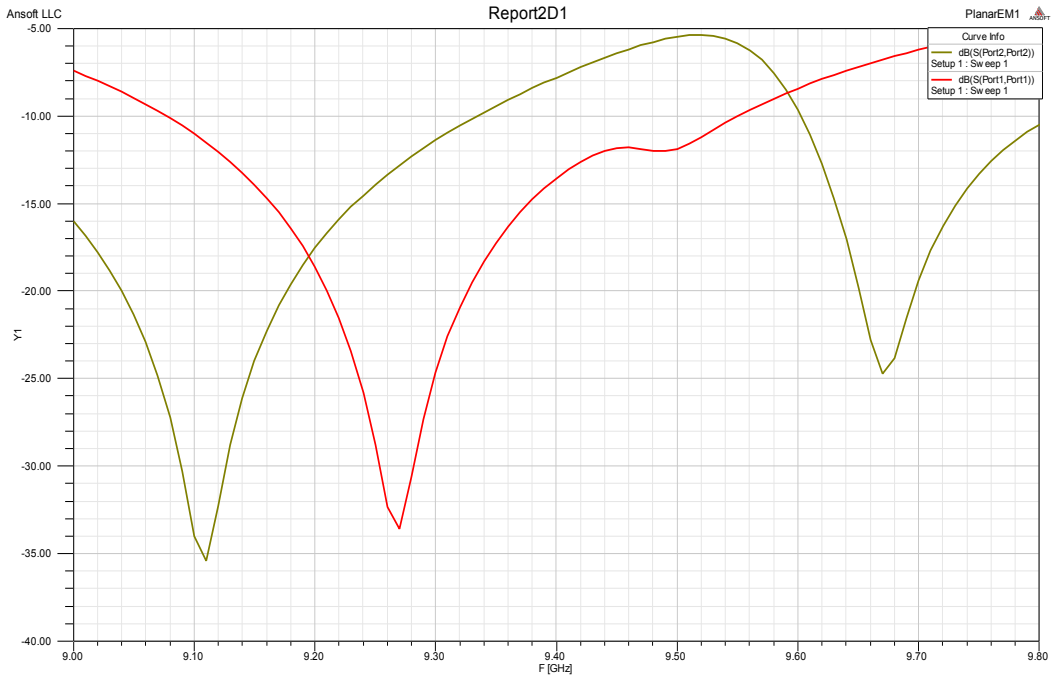

Figure 3-34: Simulation result for structure of Figure 3-33

As seen from Figure 3-34, the return loss plots are not identical for both ports. The structure is then modified again by placing Port 2 in the feed layer and connecting the transmission line in the second

dielectric layer by the help of vias as shown in

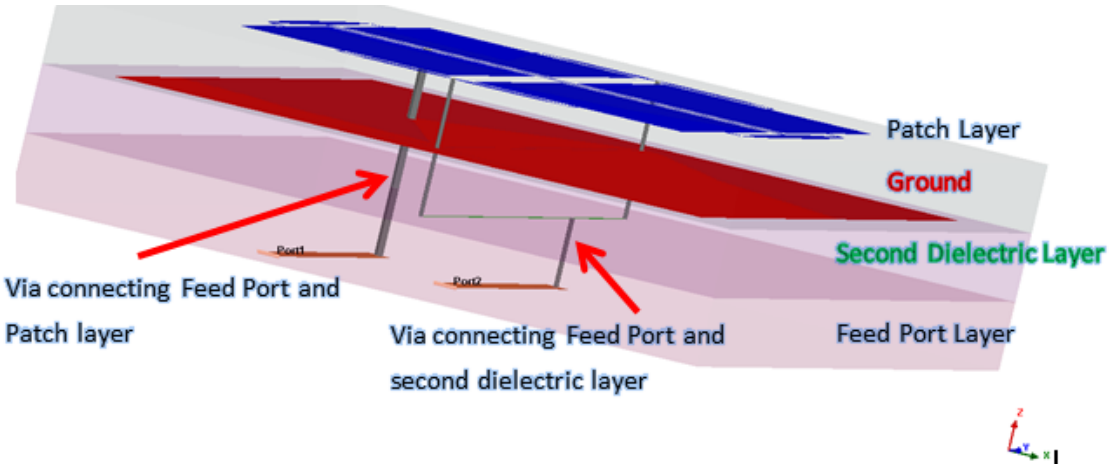

Figure 3-35 and the result as shown in Figure 3-36 is obtained. Matching QWT sections are then added to each port as shown in

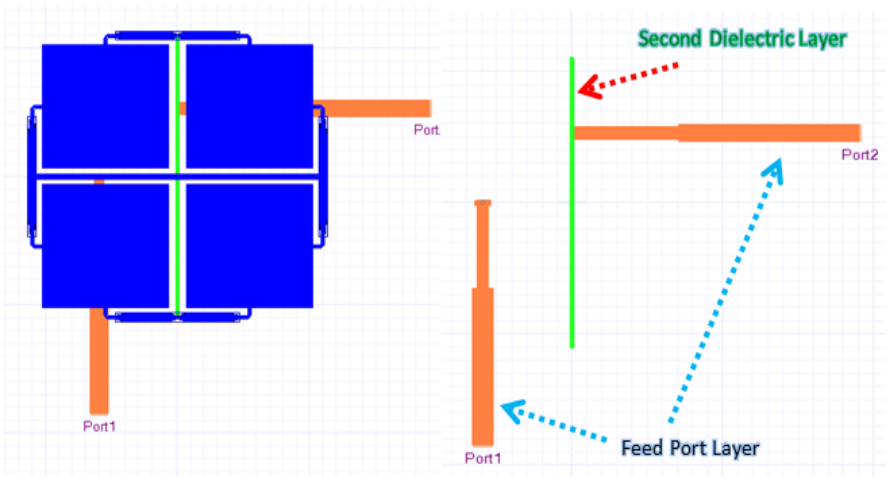

Figure 3-37 and the results are checked for resonance at the desired frequency as shown in Figure 3-38.

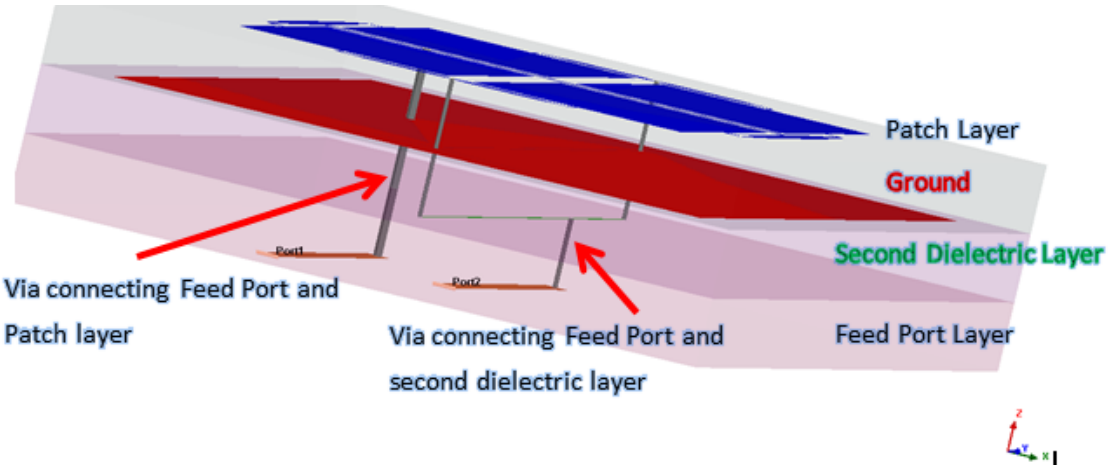

Figure 3-35: Modification to structure of Figure 3-33

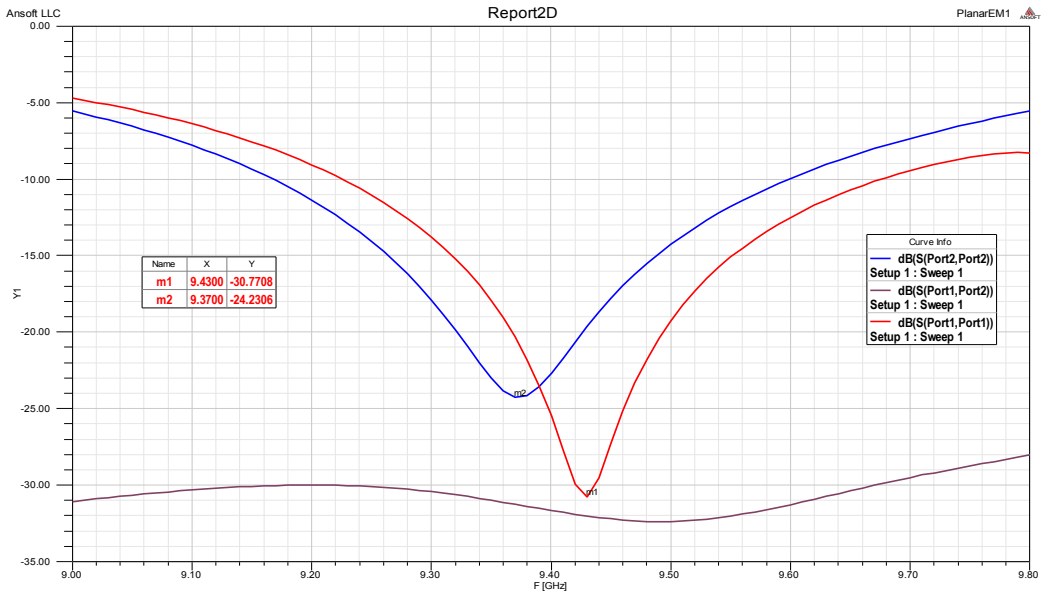

Figure 3-36: Return Loss plot for structure of Figure 3-35

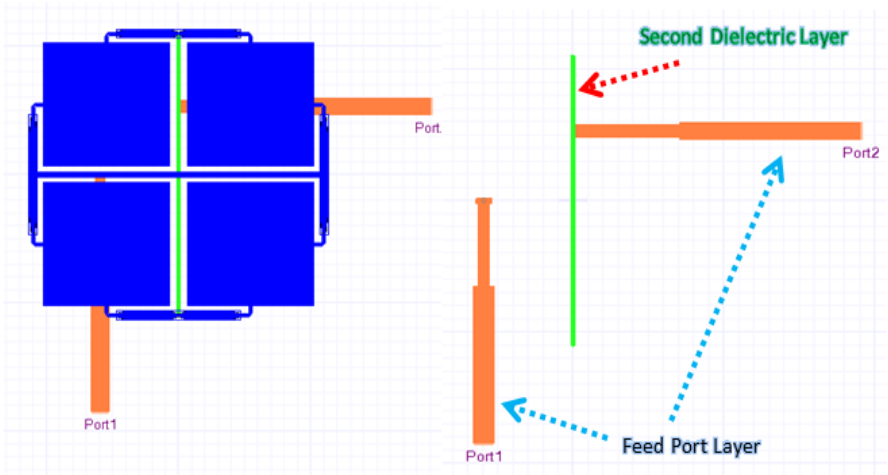

Figure 3-37: Addition of QWT sections to structure of Figure 3-35 a) Top View b) View or Second Dielectric Layer and Feed Port Layer

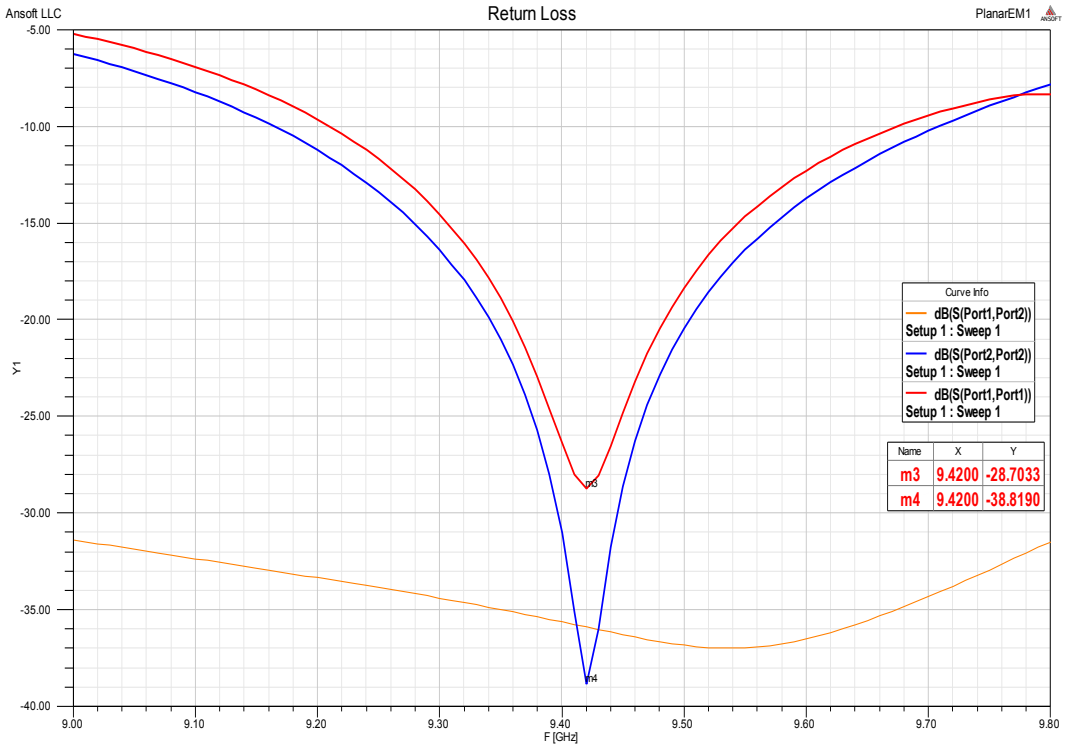

Figure 3-38: Return Loss for the three layer antenna of Figure 3-37

Once the appropriate QWT sections are added and the antenna is resonating at the desired frequency (9.4 GHz), the radiation pattern is plotted as shown in Figure 3-39. The values for the accepted again and Front to Back Ratio are determined from the plot.

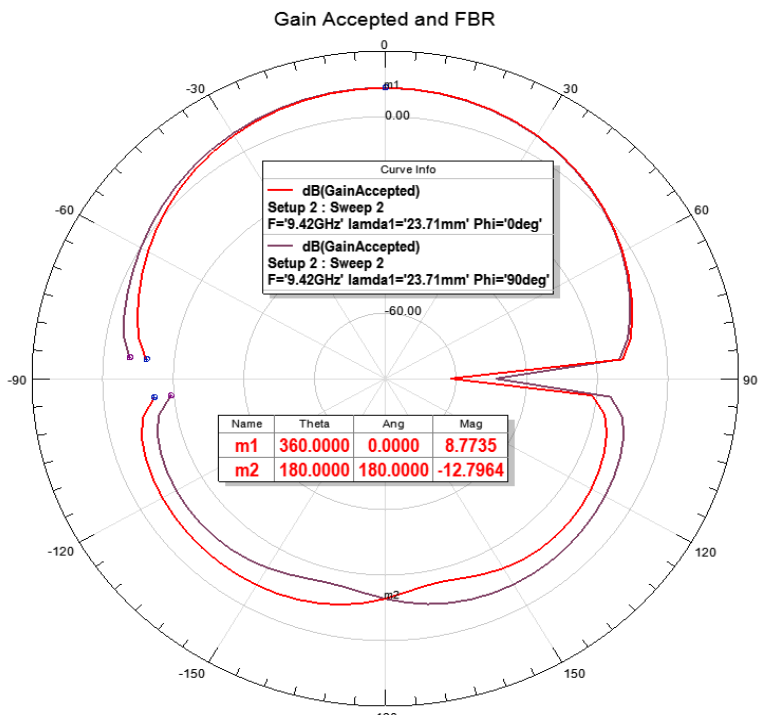

Figure 3-39: Gain and Front to back ratio for antenna structure of Figure 3-37

Then, the co-polarization levels and cross polarization levels are determined when either of the ports are driven and the other is matched as shown in Figure 3-40 and Figure 3-41. For a dual polarized antenna, a good design should yield cross polarization levels lower than -30 dB.

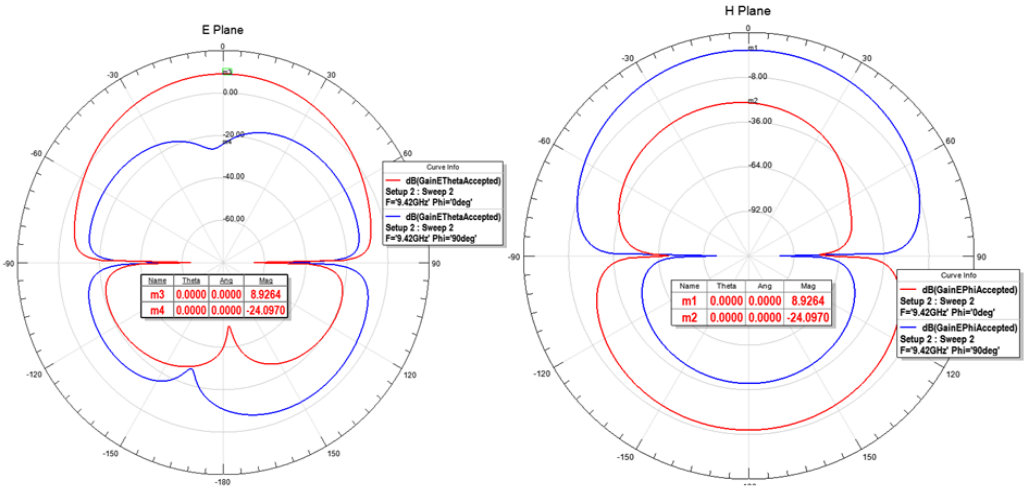

Figure 3-40: Co and cross polarization levels for the antenna of Figure 3-37 when only Port 1 is driven

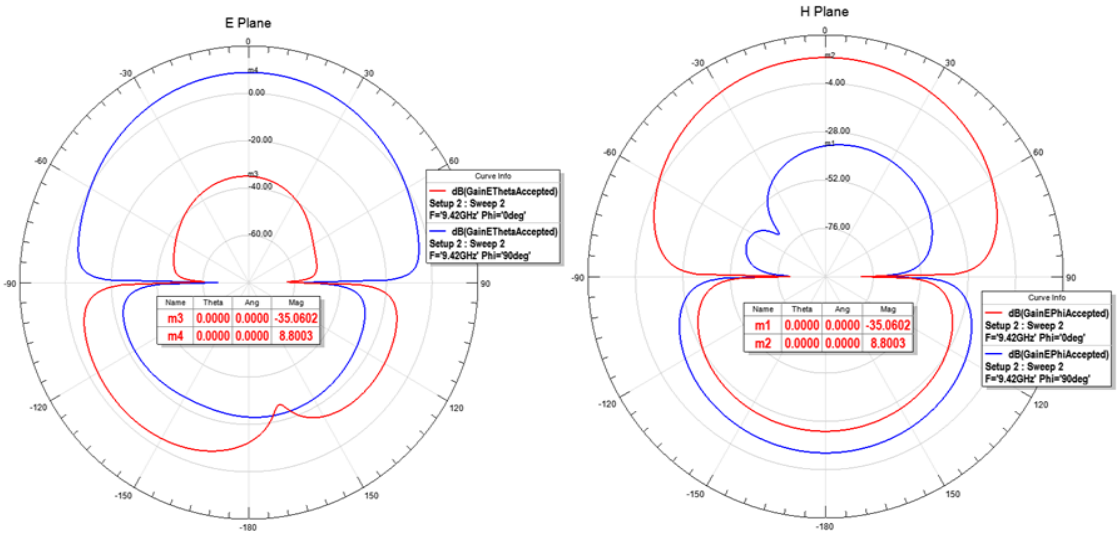

Figure 3-41: Figure 3 40: Co and cross polarization levels for the three layer antenna when Port 2 is driven

Once the preliminary steps as mentioned in the sections above have been followed, desired range for port isolation and cross polarization levels have been obtained for the dual polarized antenna sub array, the dimensions of the antenna structure (lengths and widths of transmission lines, bends in

transmission lines, etc.) are tuned to improve the isolation and cross polarization levels. Once this has been achieved, the final dimensions of the sub array are calculated and final results are recorded and a prototype is fabricated. Measurements of return loss and radiation pattern are taken and the data is compared to simulation results.

3.1.1.2 Linear Array Design

Once the sub array has been made to resonate at the desired frequency, a linear array is designed using the sub array as a building block for the construction of a linear array. The following subsections present the step wise procedure of designing the linear array.

3.1.1.2.1 Defining the linear array aperture

The first step in the design of linear array is to identify a "ball-park" value for the element spacing which is the spacing between sub arrays. Since spacing equal to and above 0.8λ gives rise to grating lobes, the element spacing is kept below 0.8λ. The sub array dimensions are measured as shown. Once the sub array dimensions have been measured the maximum spacing between elements in order to avoid grating lobes in the linear array is determined. As shown in Figure 3-42, the largest dimension of the sub array is 0.71λ, hence to avoid grating lobes the sub array spacing is kept below 0.75λ. For preliminary analysis the spacing is set to 0.74λ.

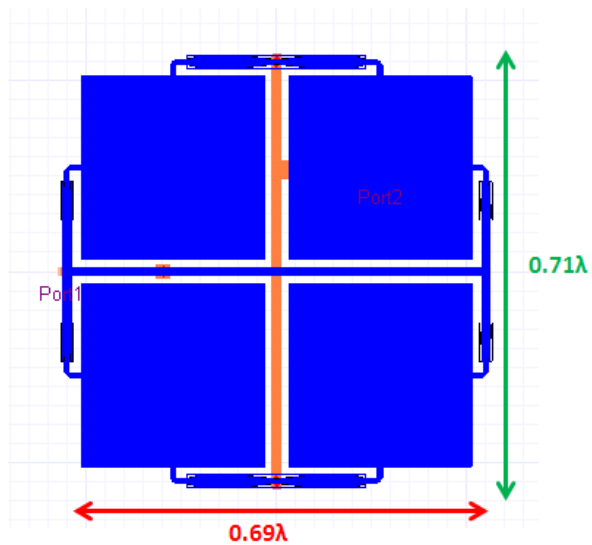

Figure 3-42: Sub array dimensions in terms of wavelength

Next, the aperture size is calculated. For preliminary analysis, uniformly illuminated aperture is considered. For a uniformly illuminated aperture L_{ap} meters long (in either X or Y dimension) operating at wavelength λ, the 3 dB beamwidth, scan angle off bore sight and directivity are given by the following set of equations:

$$\theta_{3dB}(\text{broadside}) = \frac{0.886\lambda}{L_{ap}} * \frac{180}{\pi} \tag{41}$$

$$\theta_{3\,dB} = \frac{\theta_{3dB}(\text{broadside})}{\cos\theta_0} \tag{42}$$

where $\cos\theta_0$ is the scan angle off bore sight

$$D = 10\ \log_{10}\left(\frac{32400\cos\theta_0}{\theta_{x3db} * \theta_{y3db}}\right) \tag{43}$$

Where D is in dBi and θ_{x3db} and θ_{y3db} are the x and y 3 dB beamwidths in degrees.

As a preliminary analysis to determine the correct aperture size necessary, 11 sub arrays are spaced 0.75λ apart and simulated. For a maximum spacing of 0.75λ between sub arrays, the aperture size is limited to the multiples of 0.75λ on both X and Y dimensions.

From Equation (41) and (43) we get the following:

X dimension (0.7λ) 3dB beamwidth 72.52°

Y dimension (8.25λ) 3dB beamwidth 2.57°

Directivity (dBi) is 22.7 dBi

The obtained values from theoretical analysis is tested by simulating a linear array model consisting of 11 sub arrays arranged in the Y axis with 0.74λ separation between sub arrays as shown in Figure 3-43 . The results of preliminary analysis are recorded and analyzed (details presented in Chapter 4). Using the above set of equations, the aperture is adjusted until the beamwidth and directivity required for the array is achieved.

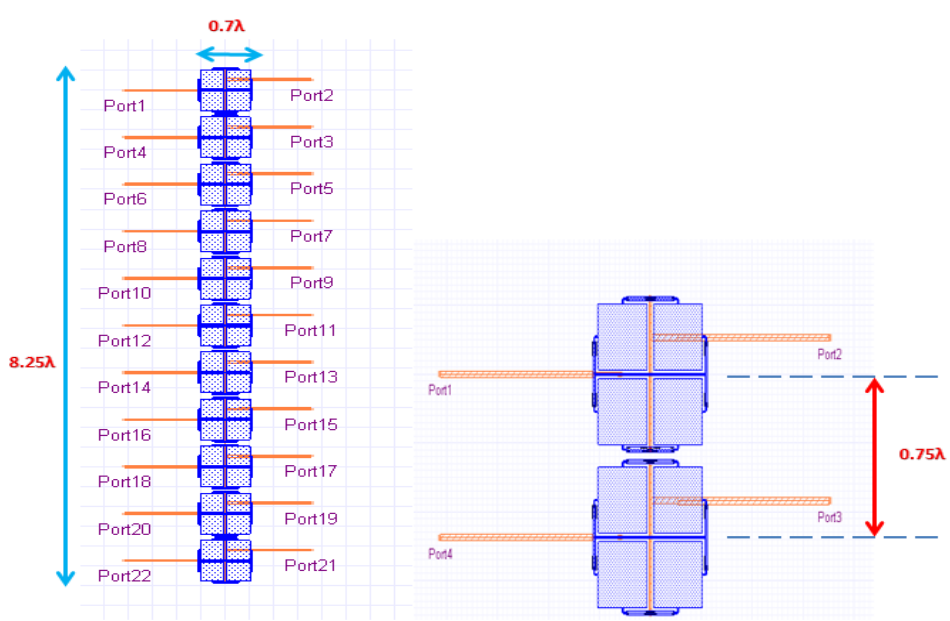

Figure 3-43: a) linear array showing aperture size b) element spacing

3.1.1.2.2 Initial modeling

Once the aperture size and the number of elements have been decided, a basic configuration of the linear array is modeled. Preliminary analysis is done by placing the required number of sub arrays, 0.75λ spacing and uniformly excited over a ground plane. The linear array is analyzed using Ansoft Designer® and the results are inspected for occurrence of grating lobes for 0.75λ spacing and also the required beamwidth in broadside. If there are no grating lobes present, some of the elements (i.e. sub arrays) are removed and the resulting geometry analyzed again. However, if grating lobes are present in the preliminary analysis itself, the spacing between the elements is reduced until the grating lobe(s) have been eliminated. Detailed analysis is presented in the next chapter.

3.1.1.2.3 Amplitude Taper

Once the aperture size (number of elements) and spacing has been fixed so that no grating lobes are present in the far field pattern in the initial model for uniformly excited elements, side lobe levels are dealt with. Unwanted side lobe levels are reduced using amplitude taper. Although several distributions can be applied, two of the most commonly used distributions are used in the linear array design. The Dolph Tschebycheff and modified Taylor distributions are used to produce amplitude taper.

Dolph Tschebycheff Distribution

This distribution is based on the Tschebycheff polynomial and gives a uniform side lobe reduction ratio for all the side lobes. This distribution also gives the minimum beamwidth for a given aperture size and side lobe level. The coefficients of the Dolph Tschebycheff distribution for the linear array are calculated based on the theory in Chapter 2. The values are calculated by Matlab® code which gives the values of array weights and half power beamwidth for specified values of separation

between elements, beam angle, number of array elements and relative side lobe level. The amplitude distribution is applied to the linear array and results are analyzed for the required side lobe level and beamwidth.

For a linear array of 22 elements spaced 0.75λ with the main beam at broadside and 30dB relative side lobe level, the Dolph Tschebycheff array weights are as given in Table 3-4.

Table 3-4: Dolph Tschebycheff array weights for 22 element linear array spaced 0.75λ with 30dB SLL

Dolph Tschebycheff Array Weights			
Calculated weights a_m	Maximum value $\max(a_m)$	Normalized weights $a_{mnorm} = a_m / \max(a_m)$	Calculated HPBW Degrees
1.0000	2.9045	0.344	3.8201
0.7980		0.274	
1.0709		0.368	
1.3658		0.470	
1.6703		0.575	
1.9702		0.678	
2.2505		0.774	
2.4964		0.859	
2.6943		0.927	
2.8330		0.975	
2.9045		1	
2.9045		1	
2.8330		0.975	
2.6943		0.927	
2.4964		0.859	
2.2505		0.774	
1.9702		0.678	
1.6703		0.575	
1.3658		0.470	
1.0709		0.368	
0.7980		0.274	
1.0000		0.344	

Although Dolph Tschebycheff distribution gives the smallest beamwidth for a given number of elements and spacing in an array it is not the ideal choice for all array applications. This is due to the fact that Dolph Tschebycheff distribution maintains a uniform side lobe level and manufacturing tolerances, mutual coupling and electrical beam tilt tends to have a greater effect on side lobes away from the main beam. Hence, it is desired not only to reduce the first but the third, fourth and fifth side lobe levels for which the modified Taylor distribution is best suited.

Modified Taylor Distribution

This distribution is based on a continuous function and can be used to calculate the element excitations according to their distance from the center element in the array. In this distribution, the side lobe reduction ratio refers to the first side lobe level and the rest of the side lobes recede in a similar level to that in uniform distribution. Based on the literature presented in Chapter 2, two separate Matlab® codes are developed to calculate the array weights. The first set of Matlab® codes calculates the array weights for single parameter Taylor distribution and generates the array weights based on element spacing, beam angle, number of elements and relative side lobe level. The second set of Matlab® codes calculates the array weights for $\bar{n}$ -Taylor distribution and generates the array weights for $\bar{n}$ number of near side lobe levels that need to be controlled in addition to element spacing, beam angle, number of elements and relative side lobe level.

For a linear array of 22 elements spaced 0.75λ with the main beam at broadside and 30dB relative side lobe level, the modified Taylor single parameter array weights are as given in Table 3-5.

.

Table 3-5: Taylor single parameter array weights for 22 element linear array spaced 0.75λ with 30dB SLL

Taylor Single Parameter Array Weights			
Calculated weights a_m	**Maximum value max(a_m)**	**Normalized weights a_{mnorm}= a_m/ max(a_m)**	**Calculated HPBW Degrees**
0.0293	0.3288	0.089	4.1682
0.0535		0.162	
0.0832		0.253	
0.1172		0.356	
0.1541		0.468	
0.1922		0.584	
0.2294		0.697	
0.2635		0.801	
0.2926		0.889	
0.3149		0.957	
0.3288		1	
0.3288		1	
0.3149		0.957	
0.2926		0.889	
0.2635		0.801	
0.2294		0.697	
0.1922		0.584	
0.1541		0.468	
0.1172		0.356	
0.0832		0.253	
0.0535		0.162	
0.0293		0.089	

Similarly, for a linear array of 22 elements spaced 0.75λ with the main beam at broadside and 30dB relative side lobe level and first five side lobe levels reduced ($\bar{n} = 5$), the $\bar{n}$ -Taylor array weights are as given in Table 3-6.

Table 3-6: Array weights for 22 element linear array spaced 0.75λ with 30dB SLL for Taylor $\bar{n} = 5$ distribution

	Modified $\bar{n}$-Taylor Array Weights			
$\bar{n}$	Calculated weights a_m	Maximum value max(a_m)	Normalized weights $a_{mnorm} = a_m / \max(a_m)$	Calculated HPBW Degrees
5	1	3.9526	0.253	3.9129
	1.1423		0.289	
	1.4127		0.357	
	1.7808		0.451	
	2.2027		0.557	
	2.6312		0.666	
	3.0286		0.766	
	3.3722		0.853	
	3.6494		0.923	
	3.8478		0.973	
	3.9526		1.000	
	3.9526		1.000	
	3.8478		0.973	
	3.6494		0.923	
	3.3722		0.853	
	3.0286		0.766	
	2.6312		0.666	
	2.2027		0.557	
	1.7808		0.451	
	1.4127		0.357	
	1.1423		0.289	
	1		0.253	

The array weights obtained for Dolph Tschebycheff distribution are applied to the initial linear array of 22 elements and each model is simulated and the obtained results are analyzed for occurrence of grating lobes, side lobe levels and beamwidth. The analysis is covered in the next chapter.

3.1.1.2.4 Active Impedance Calculation

The mutual coupling between the elements in an array has a significant effect on the impedance of the element (in this case the sub array). Figure 3-44 shows how mutual coupling affects the impedance of

an element in an array environment. As shown in the figure, in addition to voltage V1, the electric fields of other elements in the array induce currents in element 1. The total field in element1 is the vector sum of all the fields. Hence, the current induced in element 1 not only depends on the phase and amplitude of other elements but also the physical location of other elements.

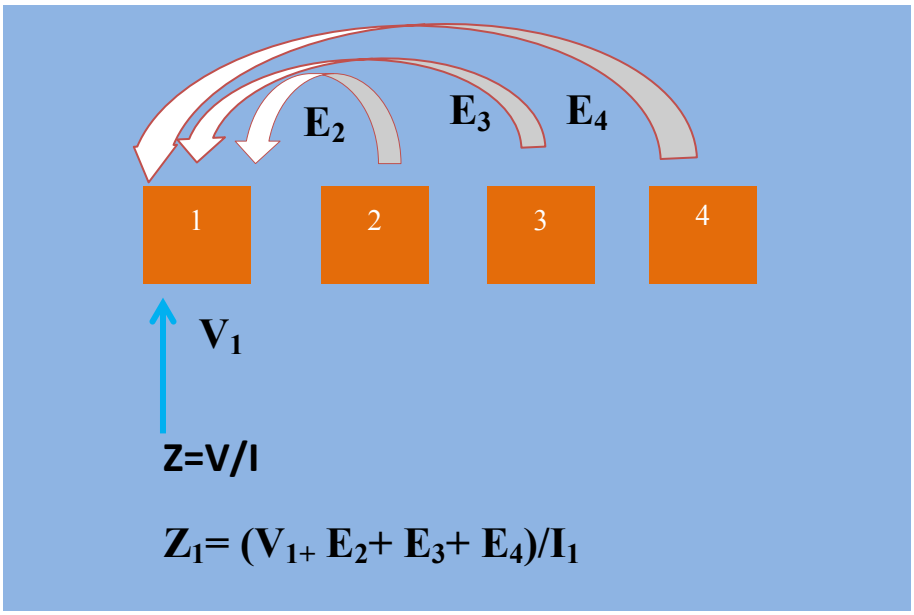

Figure 3-44: Mutual coupling paths for element 1 in the array

The active input impedance which is the impedance of an element due to mutual coupling between other elements in an array environment can be calculated by directly applying the required amplitudes and phases to elements and examining the resulting input impedance. This is achieved by solving the array using Ansoft Designer®.

Once the array has been simulated to obtain necessary Smith Chart plots containing active impedance values, the active impedances at each port are matched to 50Ω (or any other desired value) using quarter wave transformer sections by using equation (44).

$$Z_{match} = \sqrt{Re(Z_{active}) * Z_0} \tag{44}$$

This transformation takes care of the real part of the active impedance. The imaginary parts of Z_{active} are balanced either by stubs/baluns or by tuning of the sub array itself. After introducing matching impedance sections at each port, the array assembly now appears to be an n-port network with $Z_0 = 50\Omega$ as shown in Figure 3-45.

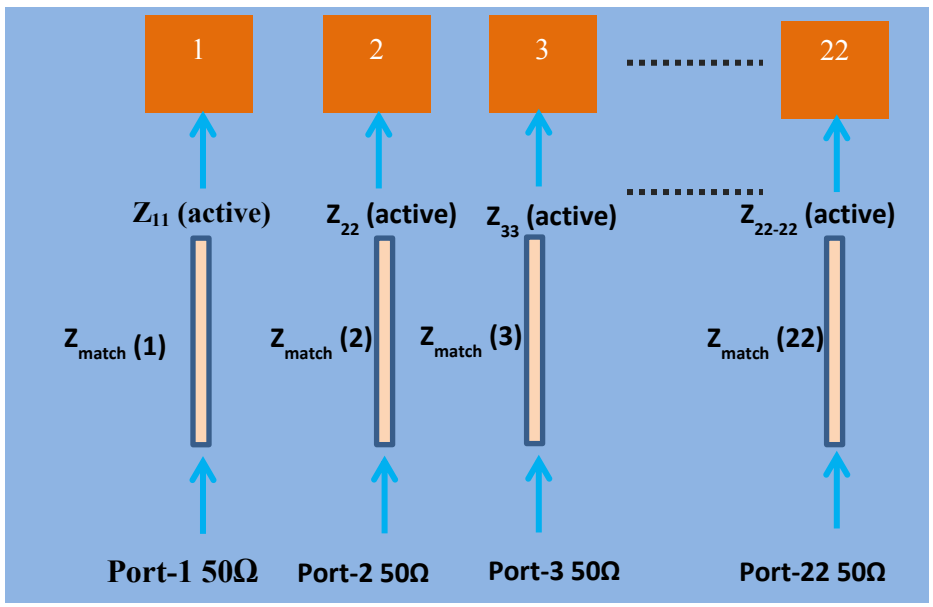

Figure 3-45: Active impedance correction to match port impedance of 50Ω

3.1.1.2.5 Final Array Modeling using Ansoft Designer®

The normalized array coefficients of Table 3-4,

Table 3-5 and Table 3-6 represent the values of RF power(linear) that needs to be applied at each element. This power is then normalized to the total power in the array by using

$$P_{norm} = \frac{P_{linear}}{\sum P_{linear}} \tag{38}$$

The normalized power at each element for Dolph Tschebycheff array of are given in Table 3-7

Table 3-7: Normalized power for each element in the array

Dolph Tschebycheff Normalized Power Calculation		
$P_{linear} = \mathrm{a_{mnorm}}$	$\sum \mathrm{P_{linear}}$	$\mathrm{P_{norm}}$
0.344	14.49	0.024
0.274		0.019
0.368		0.025
0.470		0.032
0.575		0.040
0.678		0.047
0.774		0.053
0.859		0.059
0.927		0.064
0.975		0.067
1		0.069
1		0.069
0.975		0.067
0.927		0.064
0.859		0.059
0.774		0.053
0.678		0.047
0.575		0.040
0.470		0.032
0.368		0.025
0.274		0.019
0.344		0.024

Based on the power split ratios and depending upon the real estate available, either series or corporate type of feed network is designed. Once the feed topology has been determined and junction

impedances calculated, the sub array elements are connected together and the array is analyzed using Designer®.

3.2 Prototype Fabrication

Based on the methodology mentioned in the preceding sections, several designs for sub array were obtained using Designer® by Ansoft. The initial single layer sub array design was fabricated using the milling machine in the Applied Electromagnetics Laboratory at UPRM. Subsequent multilayer designs were fabricated at Prototron Circuits in Tucson, AZ. All measurements for S-parameters were made using network analyzer and pattern measurements were made at the anechoic chamber at Radiation Laboratory in UPRM.

4 RESULTS AND DISCUSSION

4.1 Overview

Based on the requirements of the CASA Student Led Test Bed (STB) Off-The-Grid (OTG) X band radar network, a dual polarized antenna array was designed. The antenna array was designed to have low cross polarization (<-30 dB) and low return loss (<20 dB). The antenna array was simulated using Ansoft Designer®. The prototypes for sub arrays were fabricated at Prototron Circuits. This chapter presents the results of simulation and measured results of the 2X2 sub arrays and linear arrays. All the plots presented are all for 9.4 GHz except for return loss and VSWR plots which are presented as a frequency sweep.

4.2 Sub Array Design

As a building block of the antenna array and based on the methodology as discussed in the previous chapter, a 2 X 2 sub array is designed for operating at 9.4 GHz. The 2 X 2 sub array was then inspected for conforming to requirements of low return loss, low cross polarization and good port isolation. This section presents the results of simulation for two different multilayered designs for the antenna sub array.

4.2.1 Three layer 2 X 2 Sub Array

4.2.1.1 Simulation

Based on the design of [25], a 2 X 2 sub array was designed on a single layered substrate for operation at 9.4 GHz in the X band. The layout is as discussed in the previous chapter in Figure 3-21.

Since the monolithic structure was not compact enough and presented the problem of crossing of feed lines when integrated into an array, the design was modified to move the feed network in a different layer (as discussed in the previous chapter). The results of the multilayered antenna structures are discussed in the following sections.

First, a three layered antenna structure was designed with each layer having $\epsilon_r = 2.33$ and all three ers of same thickness of h = 0.787 mm as shown in Figure 4-1. Since Rogers RT Duroid® 5880 substrate having $\epsilon_r = 2.2$ has a greater thermal expansion coefficient in the direction perpendicular to the patch which makes it unsuitable for drilling vias and thru holes, RT Duroid® 5870 is used as a substitution. In order to minimize the coupling between the transmission lines, the feed network was separated into two different layers as shown in Figure 4-2. The feed network was then connected to the patch layer with the help of vias.

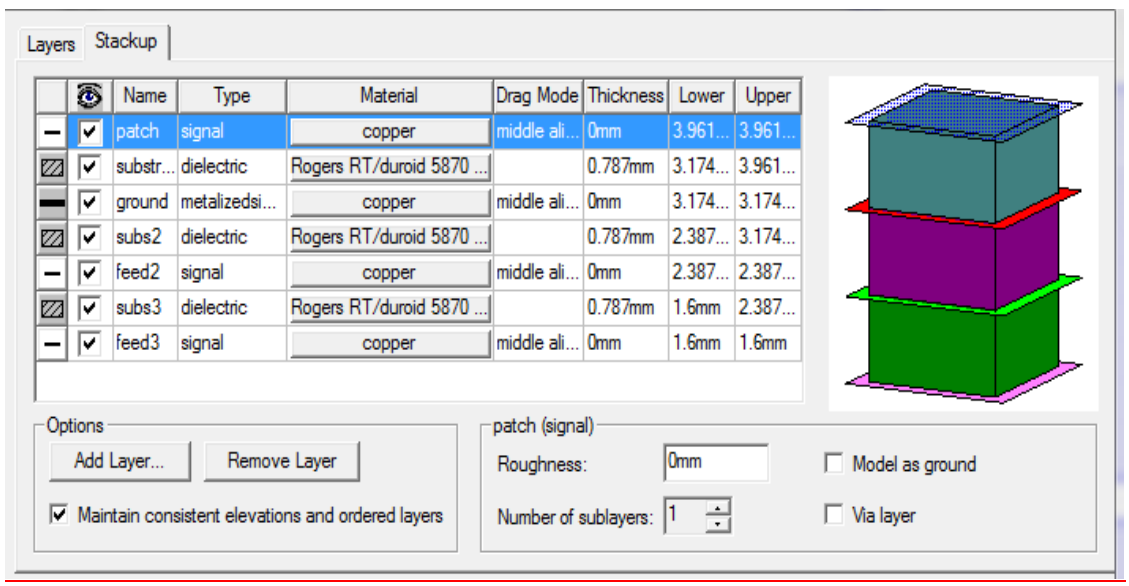

Figure 4-1: Three layered antenna: layer stack up

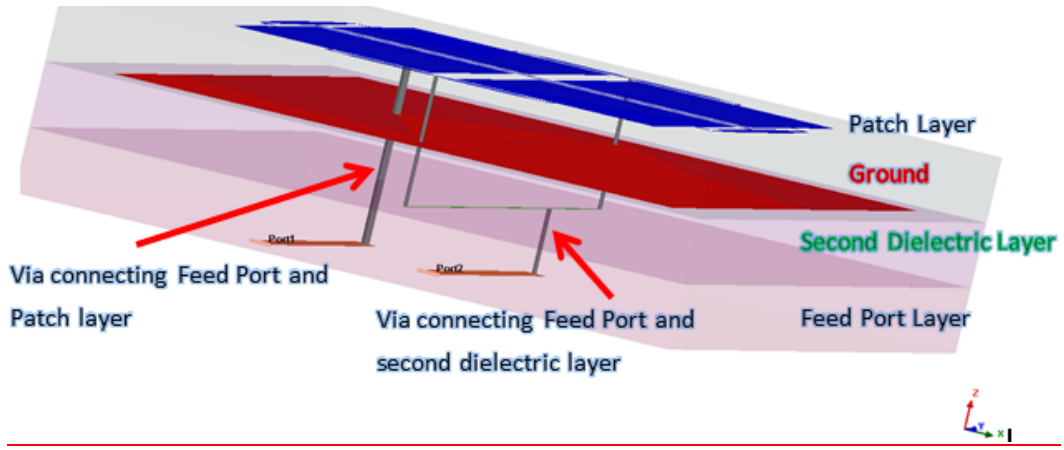

Figure 4-2: Three layered antenna structure using RT Duroid® 5870

Each patch radiator in the sub array assembly has L = 9.59 mm (0.3 λ_0) and the spacing between the sub array elements is 0.342 λ_0 resulting in overall sub array dimension of 23 mm X 23 mm (0.72 λ_0 each side). The simulation results for the return loss of the three layered antenna are shown in Figure 4-3. The antenna was found to have isolation between the ports of < -30 dB throughout the entire frequency sweep from 9 GHz to 10 GHz. The impedance bandwidths for both ports were around 8% and low values of return loss were noticed for both ports at 9.4 GHz.

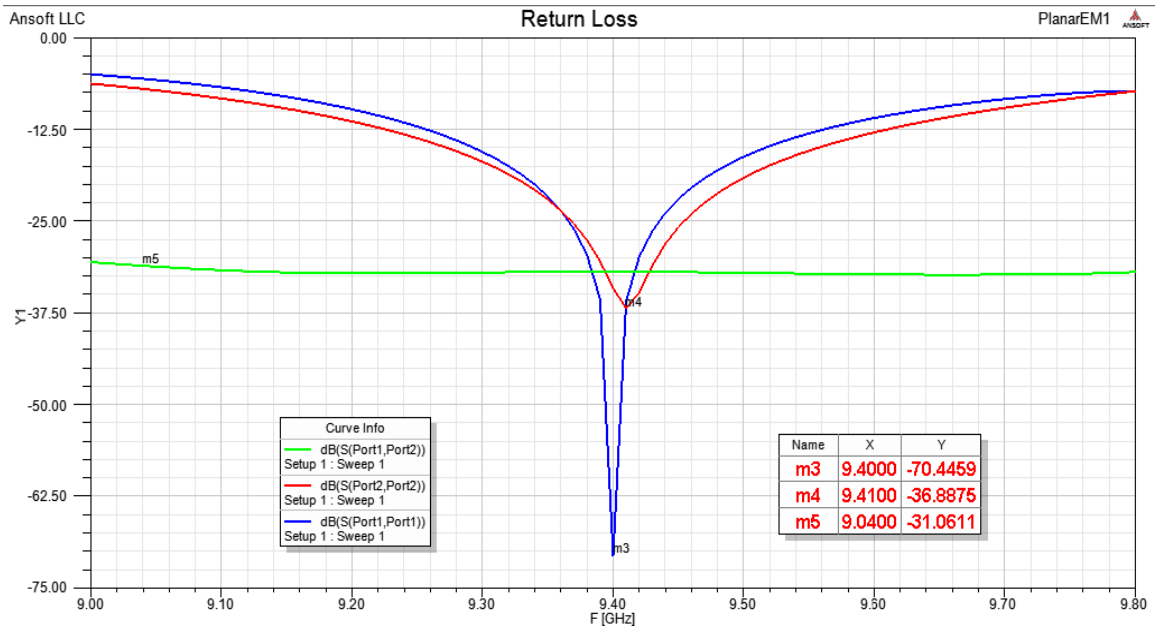

Figure 4-3: Three layered sub array: Return Loss

The plots of VSWR for ports 1 and 2 are shown in Figure 4-4 and Figure 4-5. The plots show that for bandwidth of 250 MHz around the desired frequency of 9.4 GHz, VSWR for both ports are less than 2. The VSWR <2 bandwidth for the ports is 440 MHz

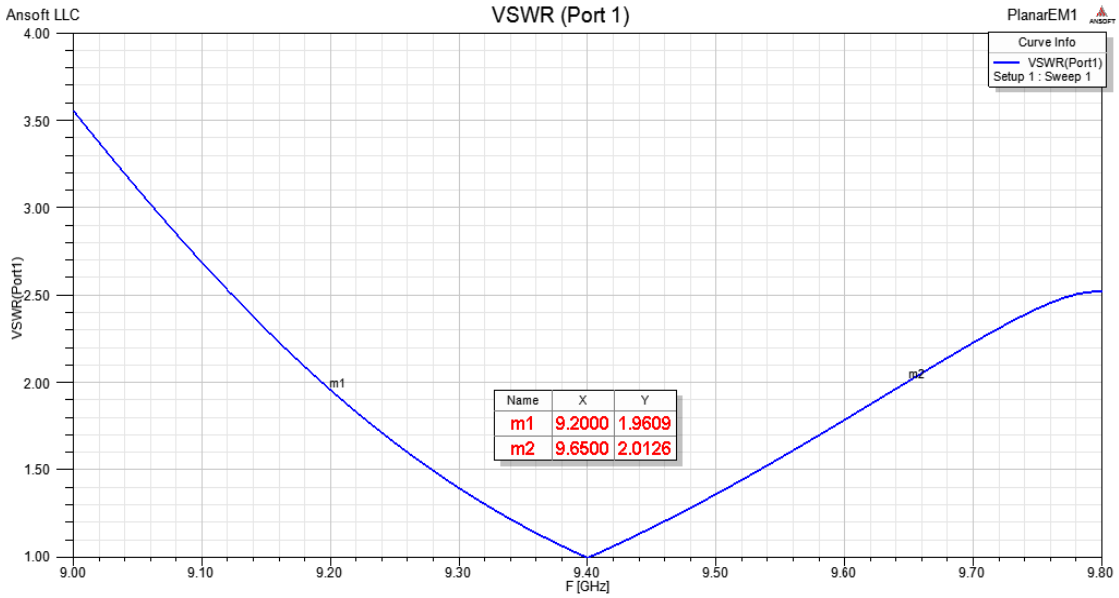

Figure 4-4: Three layered sub array: VSWR for Port 1

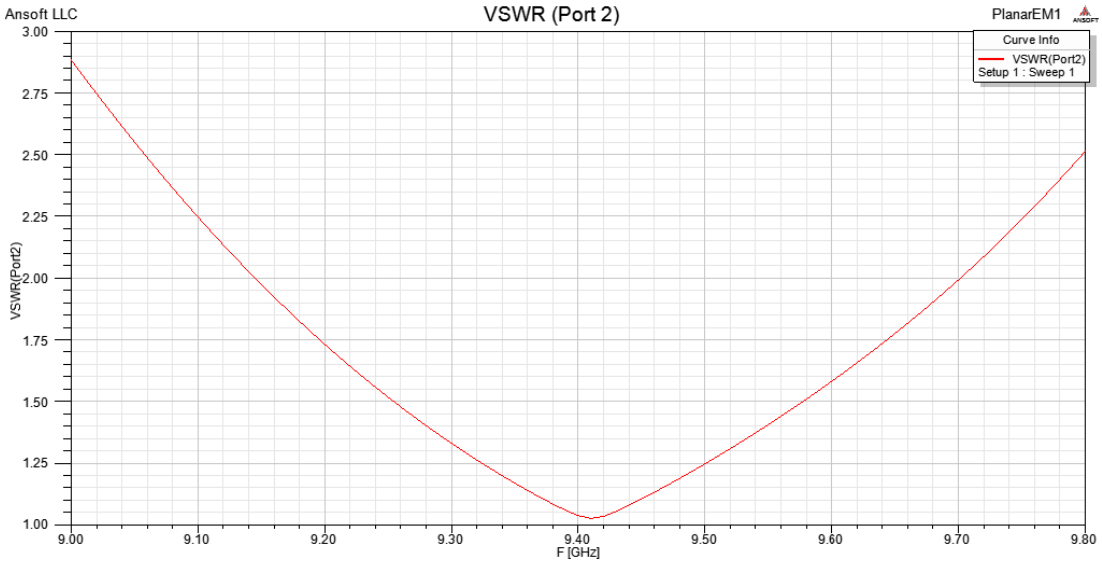

Figure 4-5: Three layered sub array: VSWR for Port 2

Impedance plots for both ports are shown in Figure 4-6 and Figure 4-7. The input impedance at Port 1 and Port 2 are close to 50 Ohm at 9. 4 GHz. As shown in Figure 4-8, the three layered array was found to have a gain of around 9 dB at 9.4 GHz and Front-to-Back Ratio of 15 dB. Next, the radiation in the E plane and H plane were examined to determine the cross polarization levels. As shown in Figure 4-9 and Figure 4-10, the antenna was found to exhibit low cross polarization levels (-45 dB) at broadside.

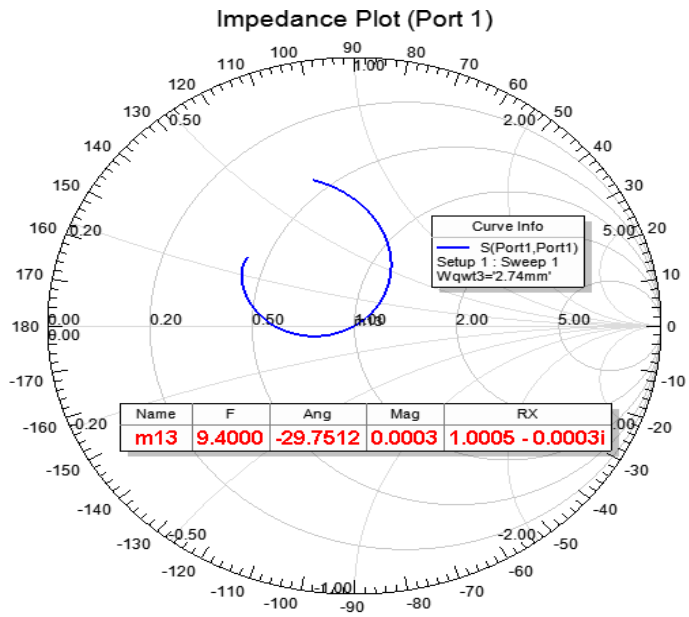

Figure 4-6: Three layered sub array: Impedance Plot for Port 1

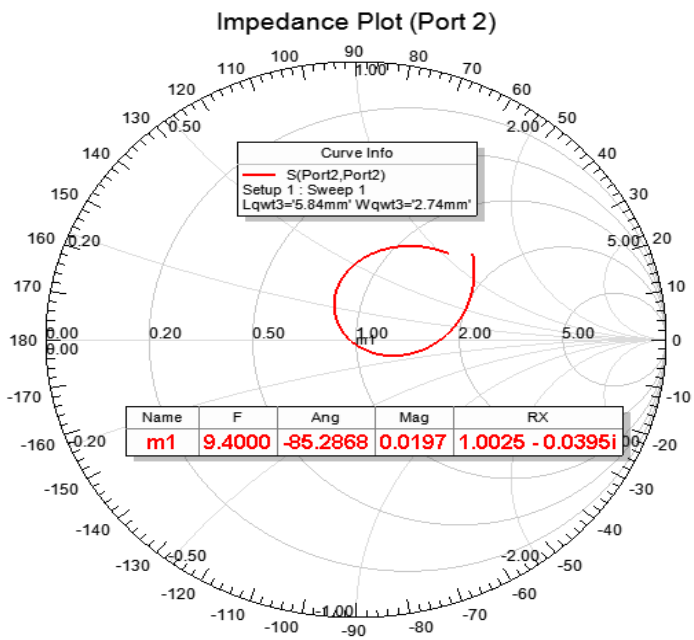

Figure 4-7: Three layered sub array: Impedance Plot for Port 2

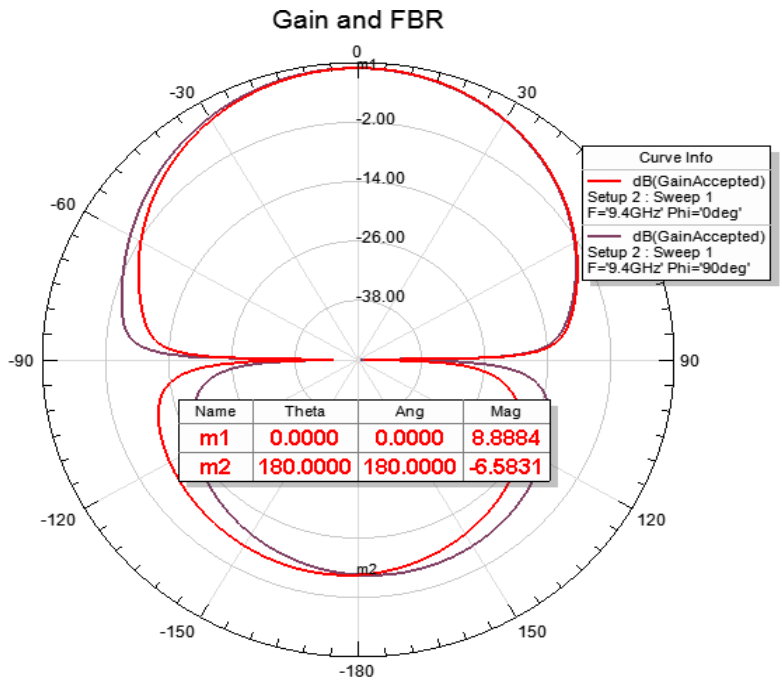

Figure 4-8: Three layered sub array: Gain Plot

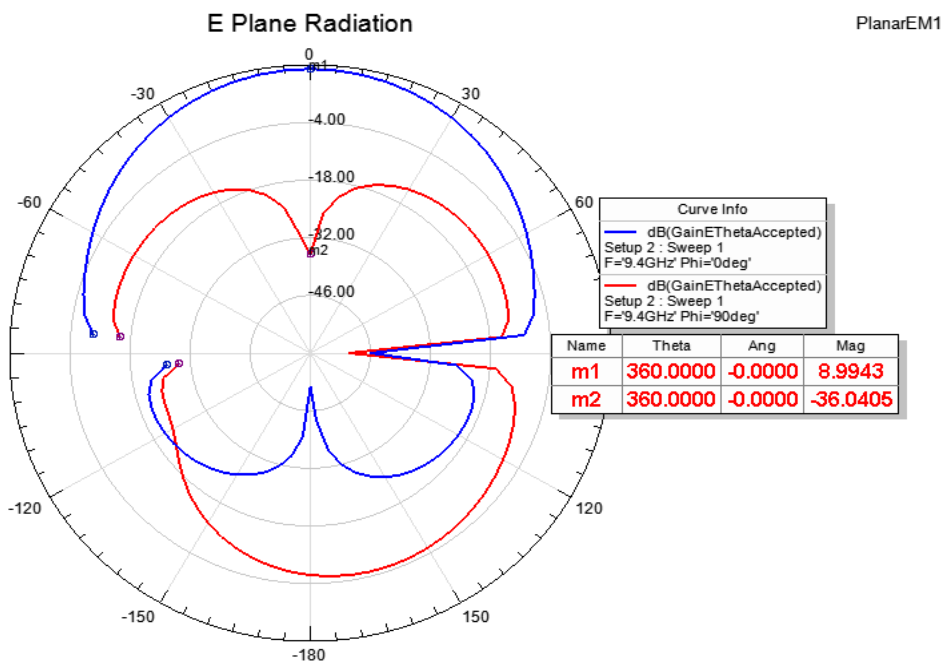

Figure 4-9: Three layered sub array: E-Plane Radiation

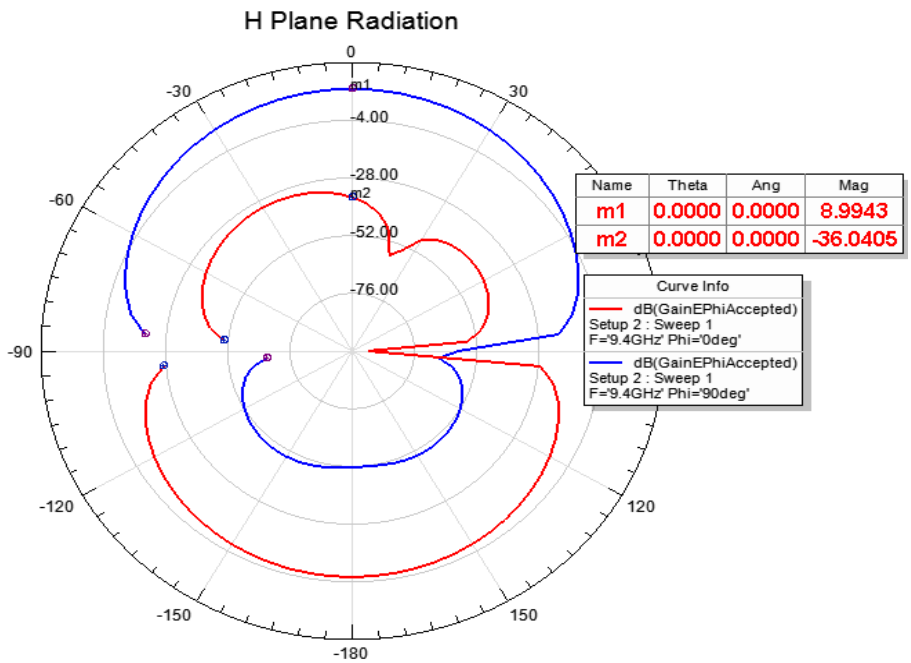

Figure 4-10: Three layered sub array: H-Plane Radiation

4.2.1.2 Prototype Measurements and Discussion of Results

A prototype of the three layered sub array was fabricated in order to test the results of simulation. Owing to traces in three different substrate layers and via diameters less than 0.5 mm, the prototypes could not be fabricated in the radiation laboratory. The prototype was fabricated at Prototron Circuits without the connector assembly. Connectors for both ports were added to the fabricated prototype at the radiation laboratory at UPRM. The measurements for S-parameters were taken using a network analyzer and radiation pattern measurements were taken at the radiation laboratory at UPRM. The prototype of the three layered antenna is as shown in Figure 4-11.

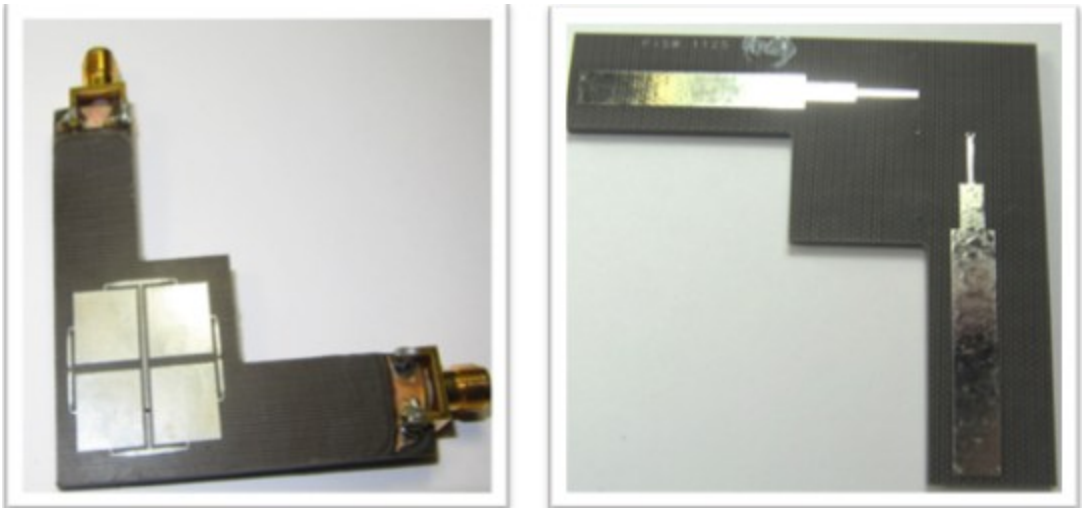

Figure 4-11: Three layered antenna sub array prototype

The comparison for the values of S11 between the simulated and the measured results are shown in Figure 4-12 . The co and cross polarization values at 9.4 GHz for simulation and prototype are shown in Figure 4-13. The overall thickness of the antenna for simulation was 2.38 mm including two separate bonding layers (0.0258 mm each) placed between the substrate layers. The finished thickness of the prototype was 2.56 mm. The increase in the overall thickness was due to the addition of more than two separate and non-uniform thicknesses of the bonding layers between the substrate layers. As a direct result of the increase in the overall thickness, the prototype was found to be resonating at 9.32 GHz instead of 9.4 GHz as shown in Figure 4-12. Also, there was an error in registration of the via holes causing an open circuit in the prototype for Port 2. This meant that the prototype could not be used for measuring S22 and S12 (isolation between the ports). Figure 4-13 shows the co and cross polarization levels for simulation and the prototype for Port 1. While simulation results indicated -32 dB of cross polarization level at broadside, the measured pattern exhibited -27 dB. The measured pattern was also found to exhibit multiple lobes. This was due to the fact that the ground plane size for the prototype was very small.

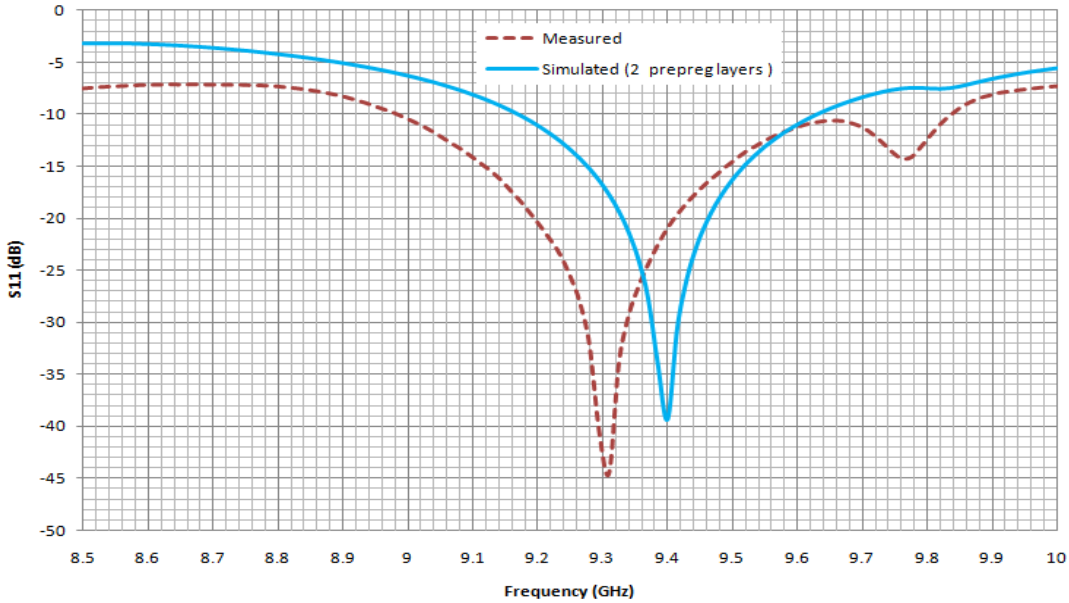

Figure 4-12: Three layered sub array: S11 simulated and measured

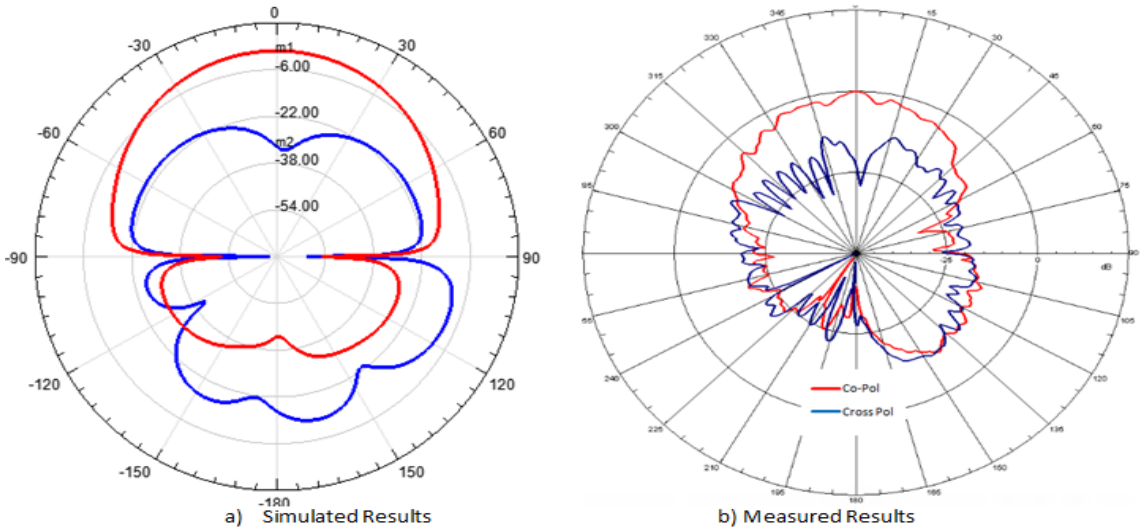

Figure 4-13: Three layered sub array: Co- and Cross Polarization Levels at 9.4 GHz (S11 active)

Due to the discrepancies in the overall thickness and the finite size of the ground plane, the measured results did not concur with the simulation results. The finished thickness of 2.56 mm indicated that there were more than two layers of pre-preg material (FR-26) each 0.0257 mm and reflected thickness

equivalent to having seven pre-preg material layers. In order to test the accuracy of the model, another set of simulation was done with thickness of pre-preg material equal to that in the prototype and the values of S11 were observed. The results from the model accuracy test shown in Figure 4-14 indicate that the simulation model was accurate and the results from both the simulation and measurements concur at 9.32 GHz. Also, radiation pattern measurements were taken at 9.32 GHz as shown in Figure 4-15. Although, the measured pattern had more nulls than in the simulation results, the cross polarization level in the measured pattern was shown to be lower than that in simulation results with Port 1 active.

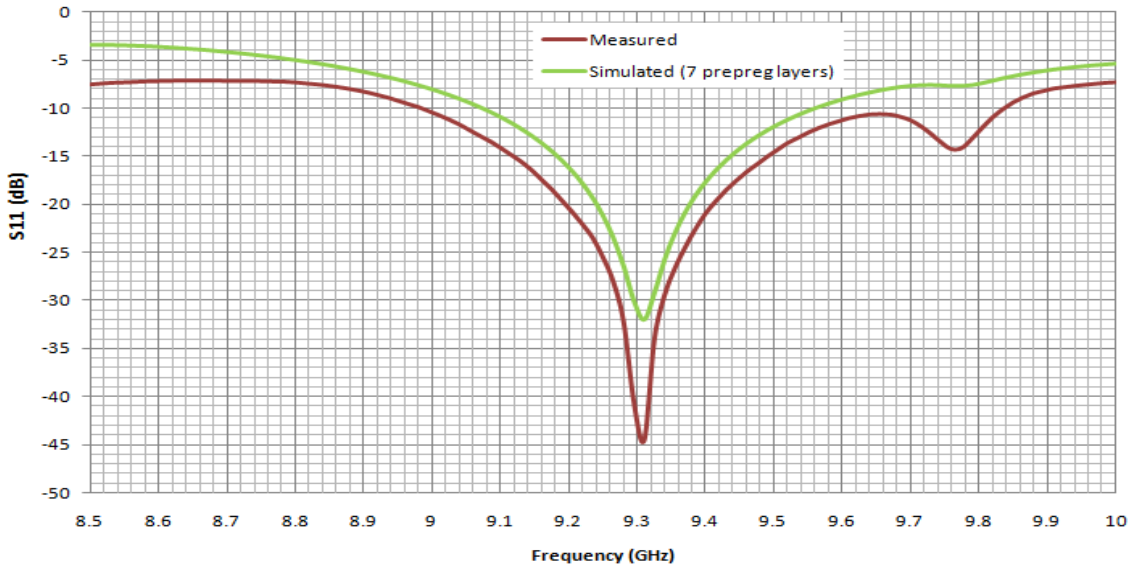

Figure 4-14: Three layered sub array: model accuracy test

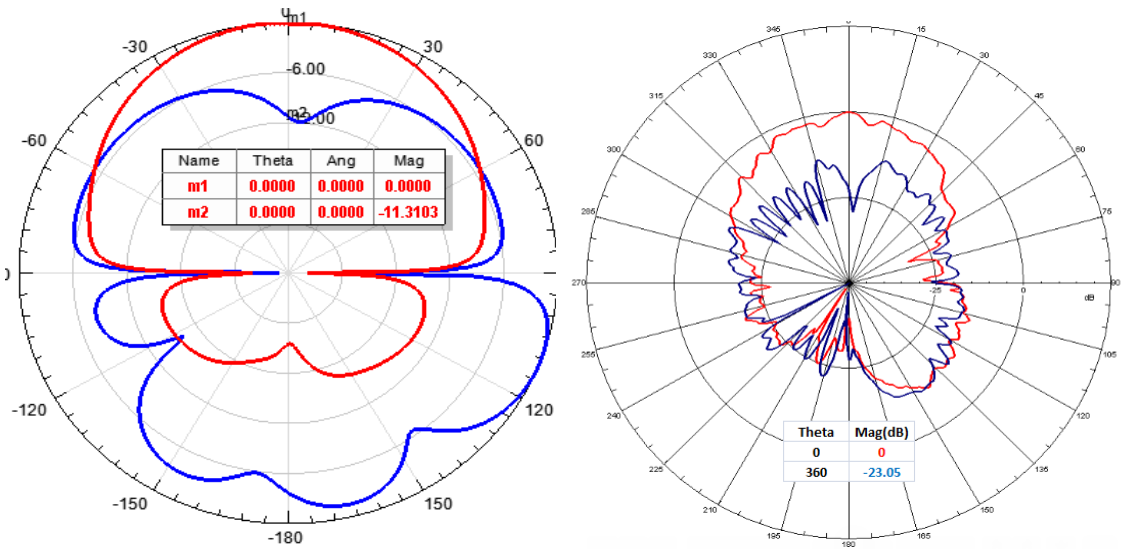

a) Simulated Results b) Measured Results

Figure 4-15: Three layered sub array: Co- and Cross Polarization Levels at 9.32 GHz

4.2.2 Two layer 2X2 Sub Array

4.2.2.1 Simulation

From the prototype of the three layered sub array, it was noticed that although it is advantageous to separate the feed network into two different layers, it necessitates additional bonding material between the layers which can adversely affect the performance by contributing to the increase in overall thickness. The additional feed layer necessitates the use of blind vias between the patch layer and one of the feed layers and an additional via from the feed layer to the other feed layer as shown in Figure 4-2. Blind vias are more expensive than fabricating with simple plated thru holes. A single blind via can contribute to around 20%-30% increase in the fabrication cost and since the design contained three blind vias, the overall fabrication cost was inflated.

In order to eliminate the use of blind vias and make the design cost effective and more reliable, the additional feed layer was removed and the sub array was redesigned with only two substrate layers.

For the new design, two different dielectric layers are used for the radiator and feed layers. The patch substrate (Duroid 5870) has $\epsilon_r = 2.33$ and h = 0.787vmm while the feed layer (TSM-DS3) has $\epsilon_r = 3$ and h = 0.254 mm. Also, a layer of bonding material compatible with the TSM-DS3 is used as shown in the layer stackup in Figure 4-16. The FR-26 pre-preg bonding material has $\epsilon_r = 2.6$ and finished thickness of 0.07 mm. The layout of the sub array is the same as before while the resulting structure sans the additional feed layer was as shown in Figure 4-17 and Figure 4-18. The design contains three thru holes and eliminated the use of blind vias completely.

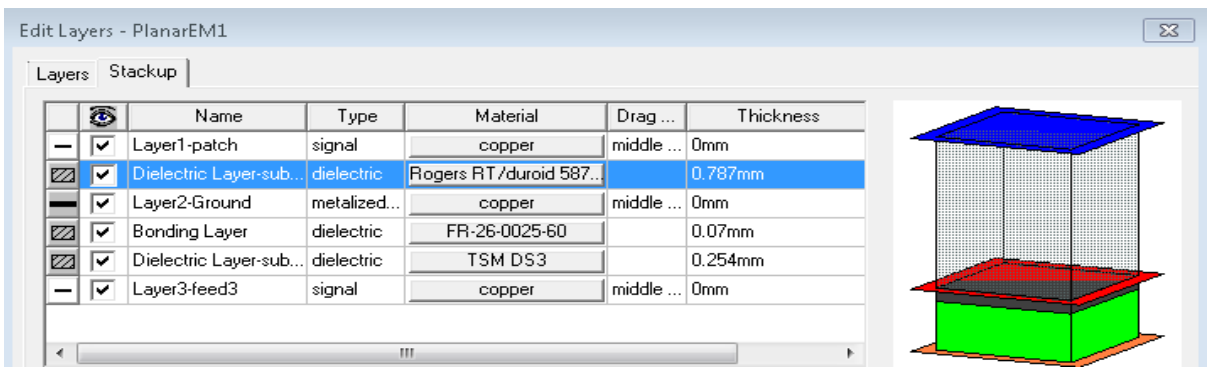

Figure 4-16: Two layered sub array: layer stackup

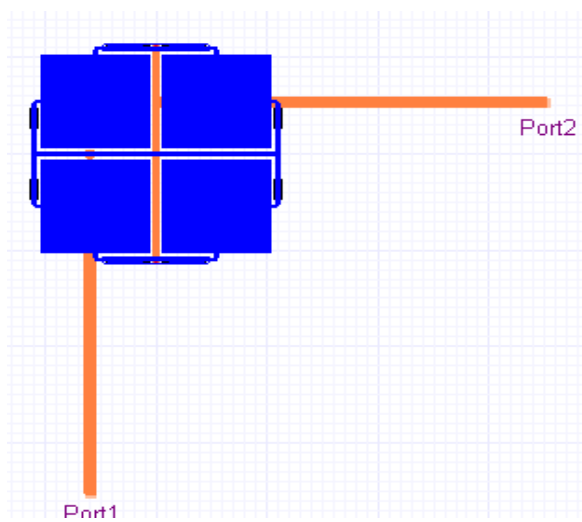

Figure 4-17: Two layered sub array layout (top view)

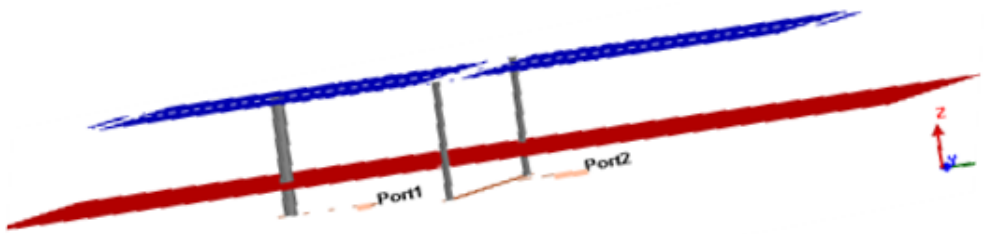

Figure 4-18: Two layered sub array layout (cross-sectional view)

The return loss plots for the two layered sub array are shown in Figure 4-19. The impedance plots are presented in Figure 4-20 and Figure 4-21. The VSWR plots for the ports are shown in Figure 4-22 and Figure 4-23. The results show that the 10 dB bandwidth is 400 MHz for both ports and the port isolation is less than -40 dB for the entire bandwidth. The input impedance seen at both ports is close to 50 Ω at 9.4 GHz. The VSWR plots show that for a bandwidth of 200 MHz around 9.4 GHz the VSWR values are less than 1.5 as desired for most radar applications.

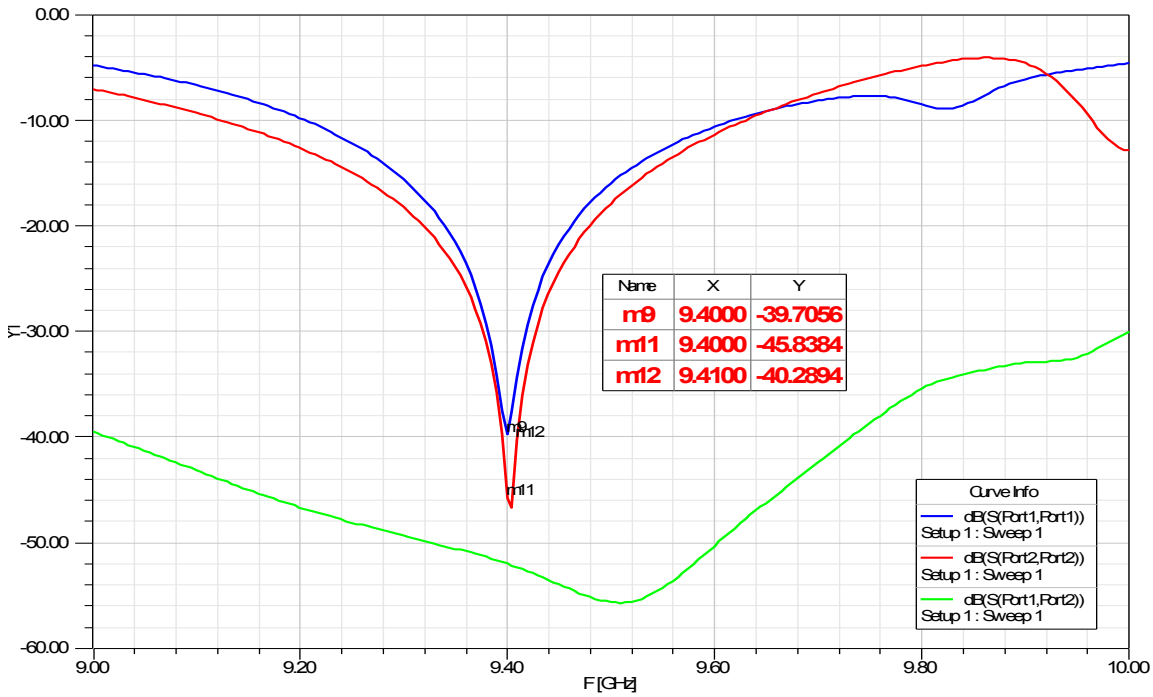

Figure 4-19: Two layered sub array: Return Loss

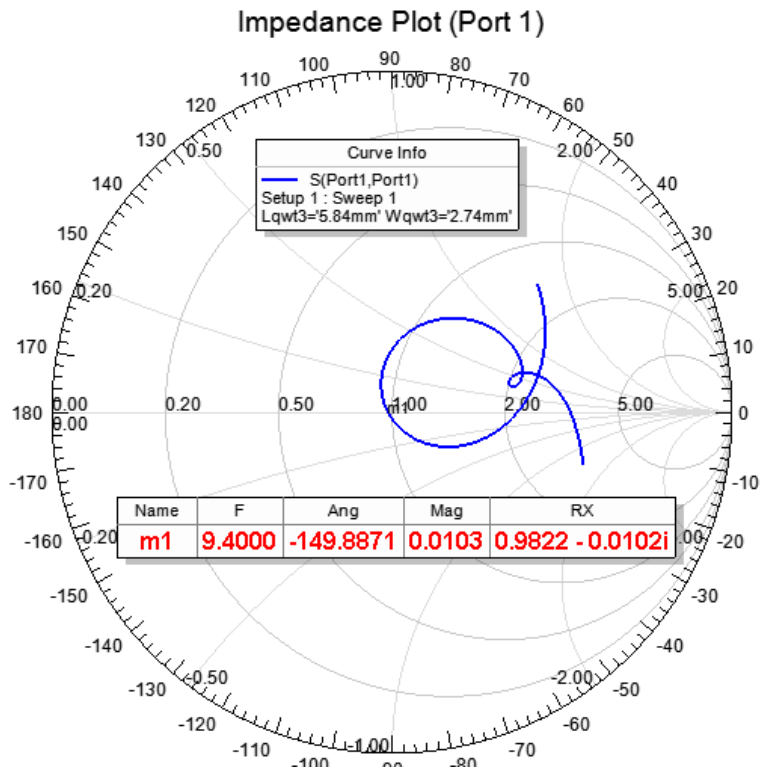

Figure 4-20: Two layered sub array: Impedance Plot for Port 1

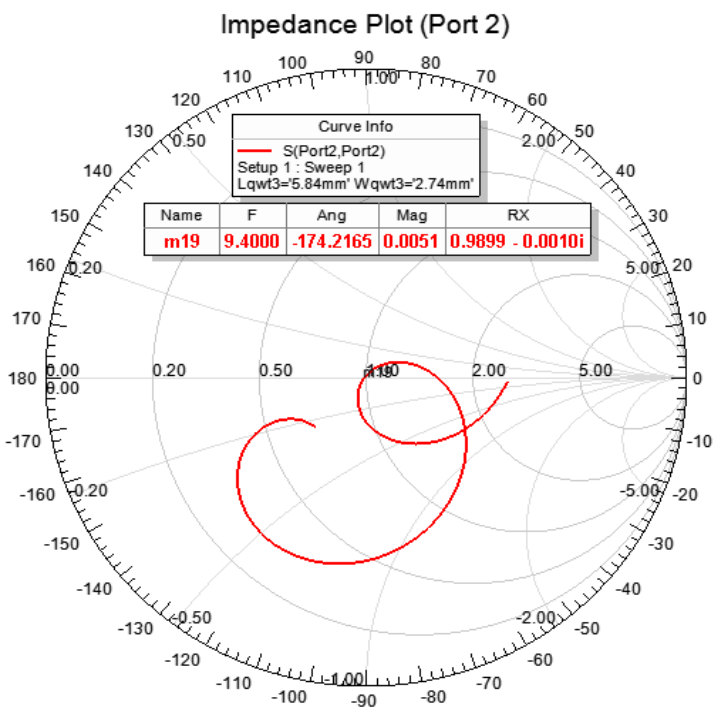

Figure 4-21: Two layered sub array: Impedance Plot for Port 2

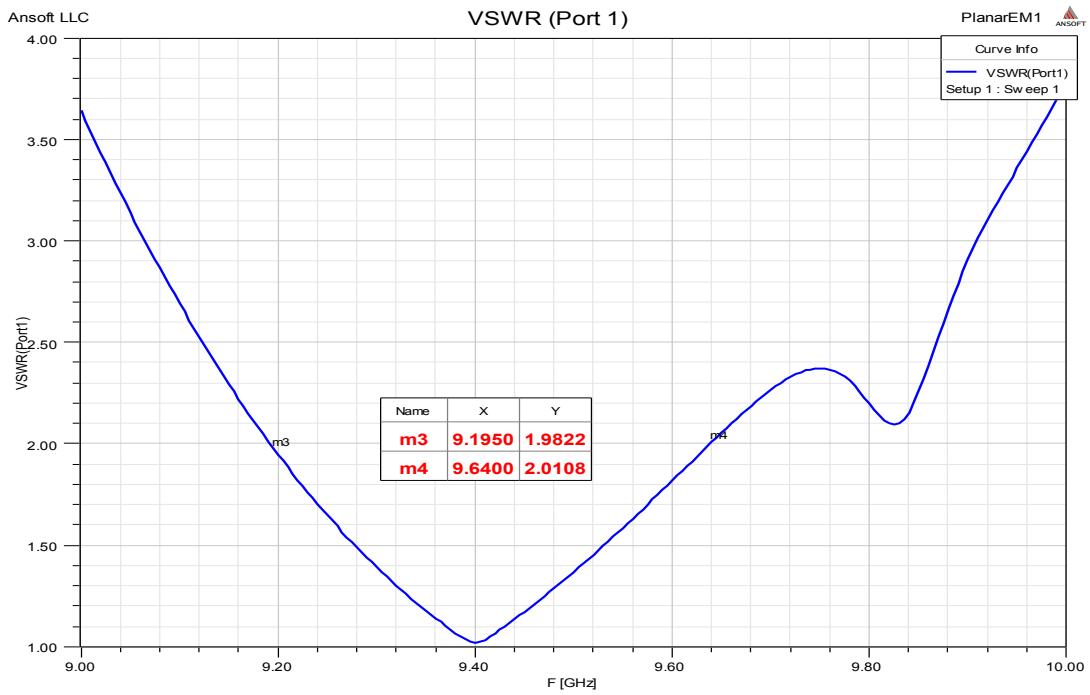

Figure 4-22: Two layered sub array: VSWR for Port 1

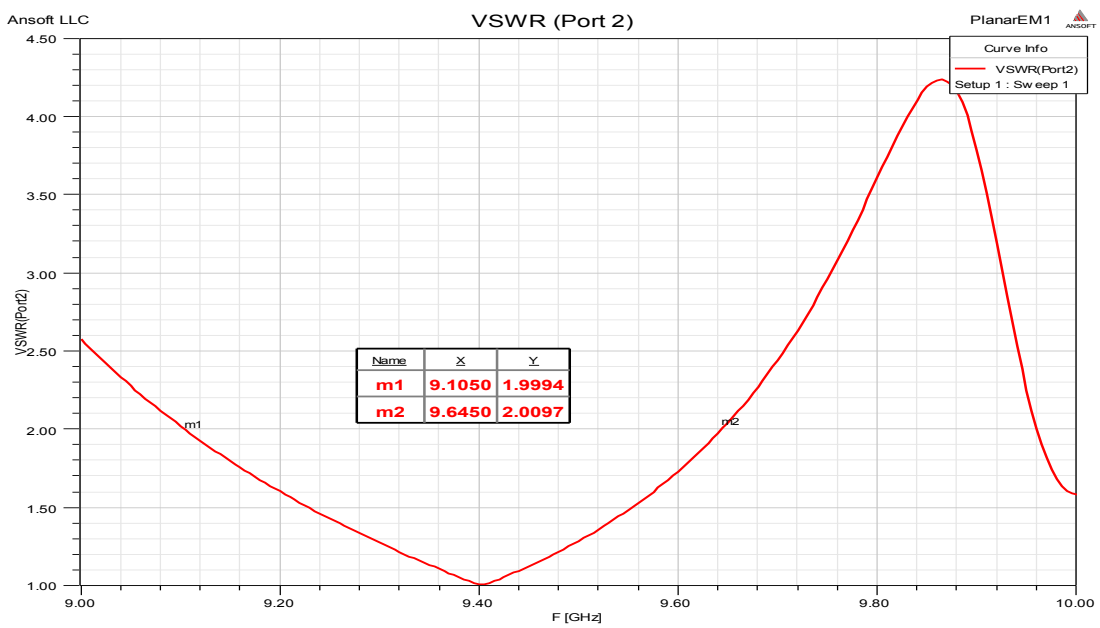

Figure 4-23: Two layered sub array: VSWR for Port 2

The two layered antenna has a gain of 9 dB at broadside and Front-to-Back Ratio of 30 dB as shown in Figure 4-24 .This means that there is very less radiation from the feed network. The directivity is close to 10 dB while the efficiency is 88% as shown in Figure 4-25 and Figure 4-26. In addition to exhibiting low loss, the antenna also has low cross polarization levels of the order of -46 dB at broadside for both E and H plane radiation as shown in Figure 4-27 and Figure 4-28.

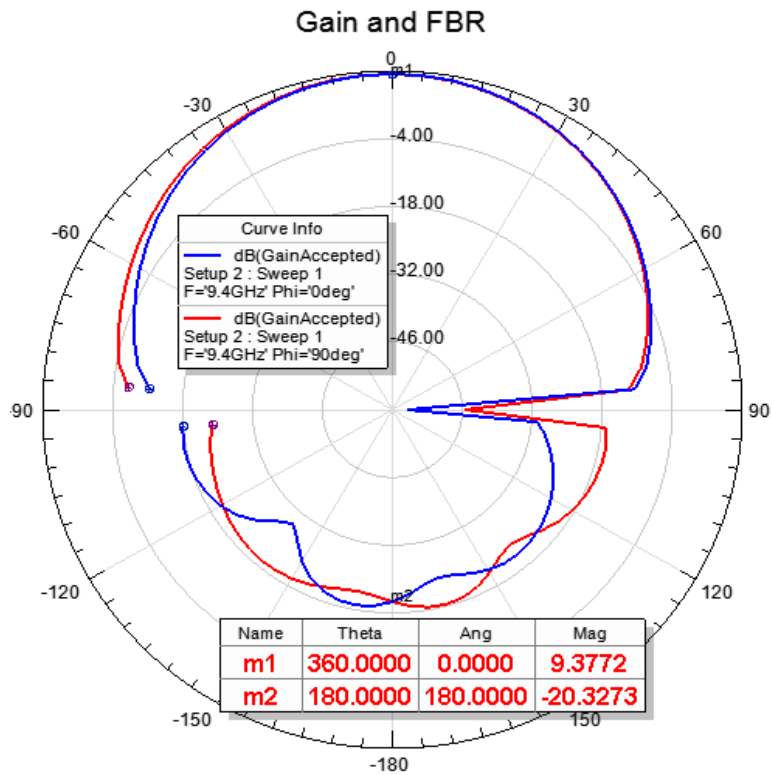

Figure 4-24: Two layered sub array: Gain Plot

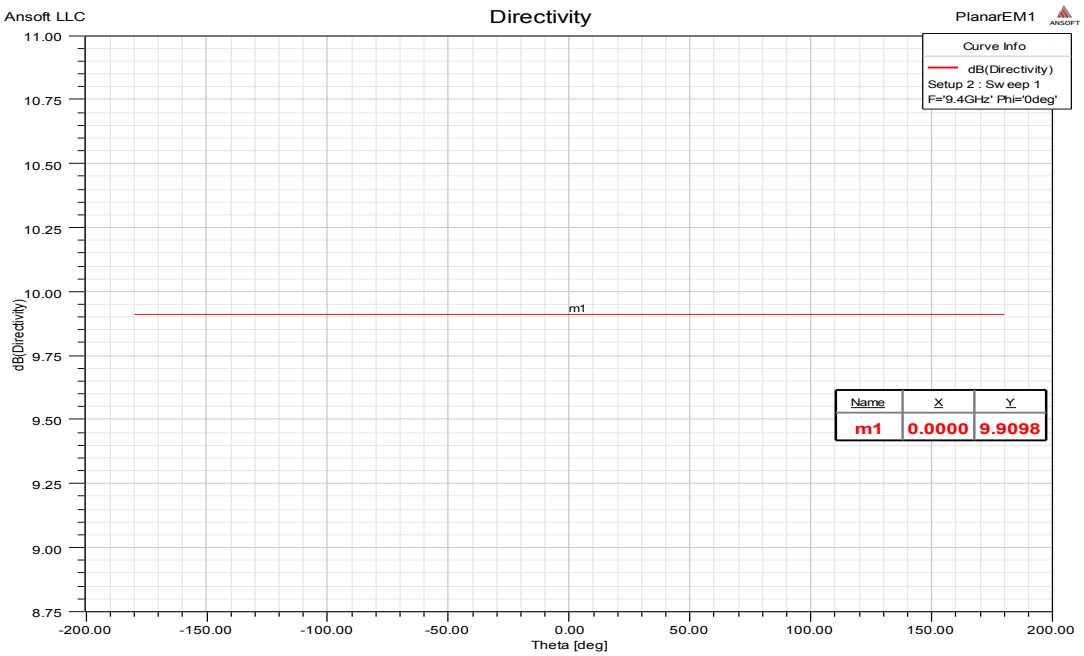

Figure 4-25: Three layered sub array: Directivity Plot

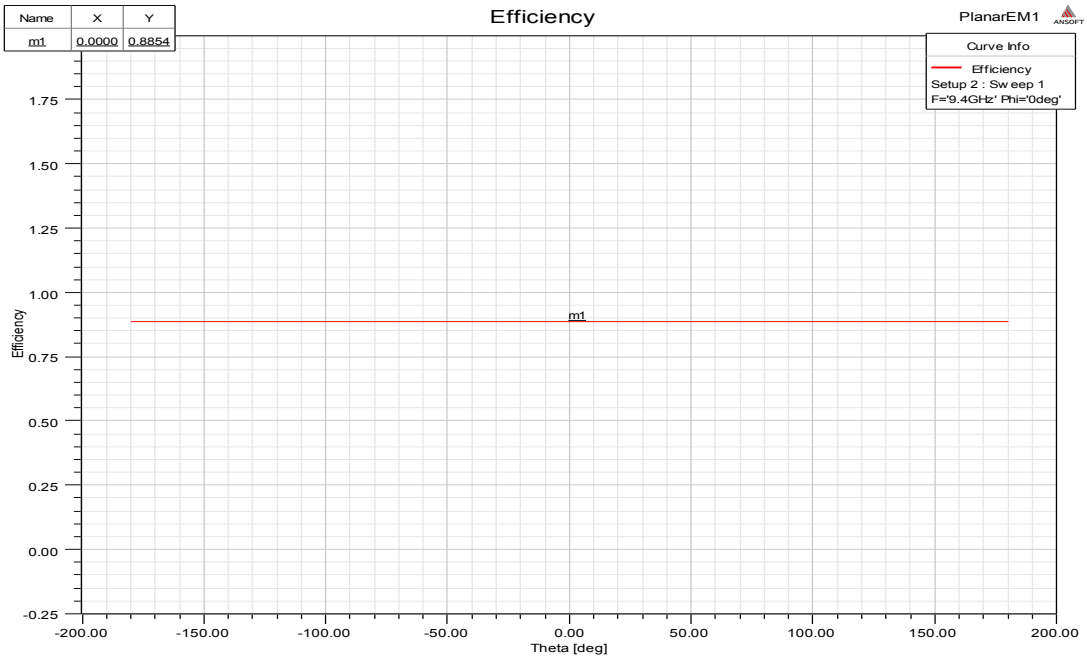

Figure 4-26: Two layered sub array: Efficiency

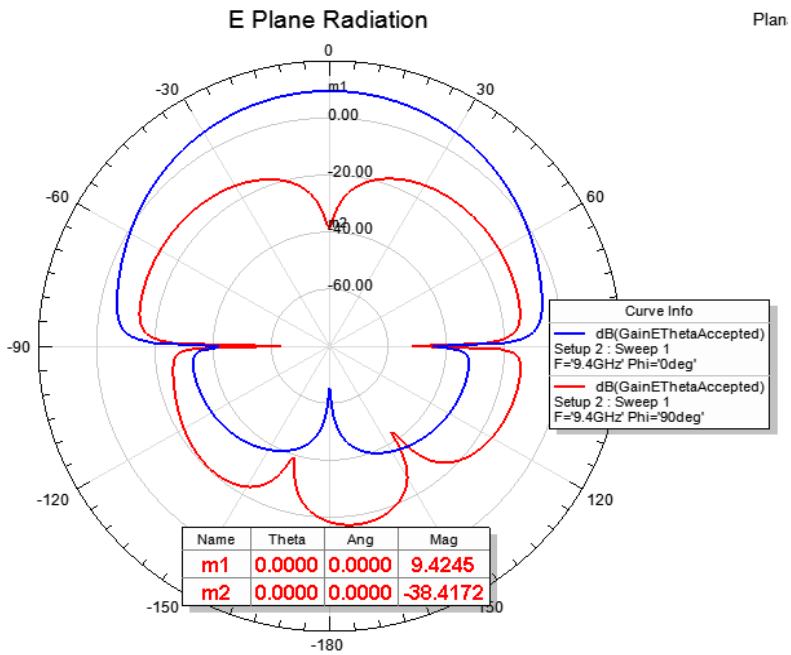

Figure 4-27: Two layered sub array: E-Plane Radiation

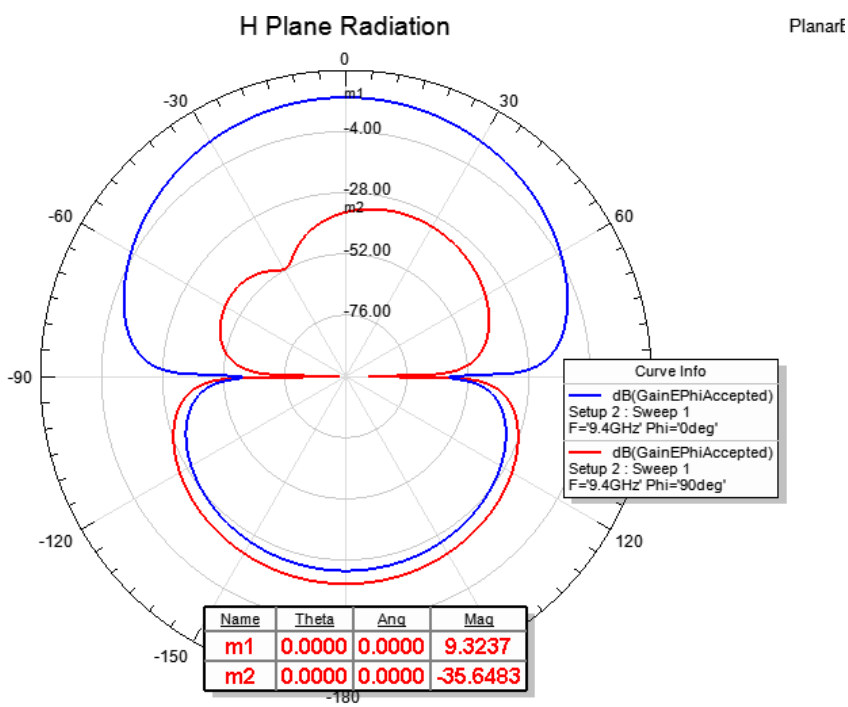

Figure 4-28: Two layered sub array: H-Plane Radiation

4.2.2.2 Prototype Measurements and Discussion of Results

Based on the simulation results as discussed in the preceding section, a prototype of the two layered array was fabricated. Due to extremely small via diameters and the multilayer structure, the antenna could not be fabricated at UPRM premises. As with the three layered prototype, the two layered antenna was fabricated at Prototron Circuits. The results from the prototype are discussed in this section.

The comparison of S-parameters of the fabricated and simulated antenna is presented in Figure 4-29, Figure 4-30 and Figure 4-31. The measured results for S11 show agreement with the simulated result with in the vicinity of 9.4 GHz with improved measured results for some frequencies within the impedance bandwidth. Although there is a difference if around 10 dB between the simulated and measured values at 9.4 GHz, the linear values are so small that the difference is negligible. For higher frequencies, there is deviation between the simulated and measured values of S11. Similarly, for S22, within the vicinity of design frequency the measured results are in close agreement with the simulated results but for frequencies further away from 9.4 GHz there are marked variations. Although the measured results show a wide variation between the simulated and measured results for the isolation between the ports (S12), the isolation remains well below -30 dB from 9 GHz to 9.8 GHz. Within the vicinity of 9.4 GHz, the port isolation is of the order of -38 dB.

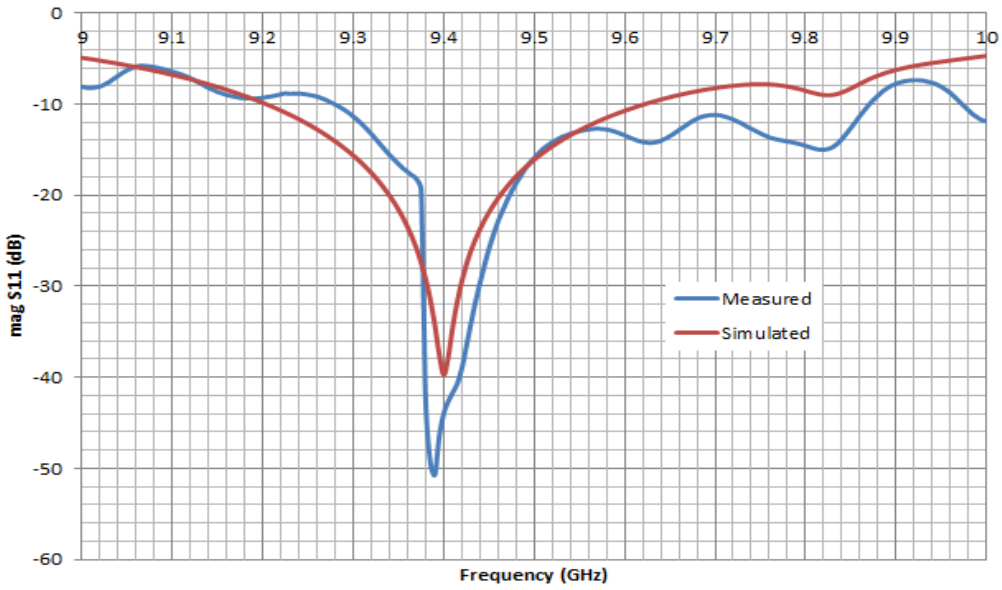

Figure 4-29: Two layered sub array: S11 simulated and measured

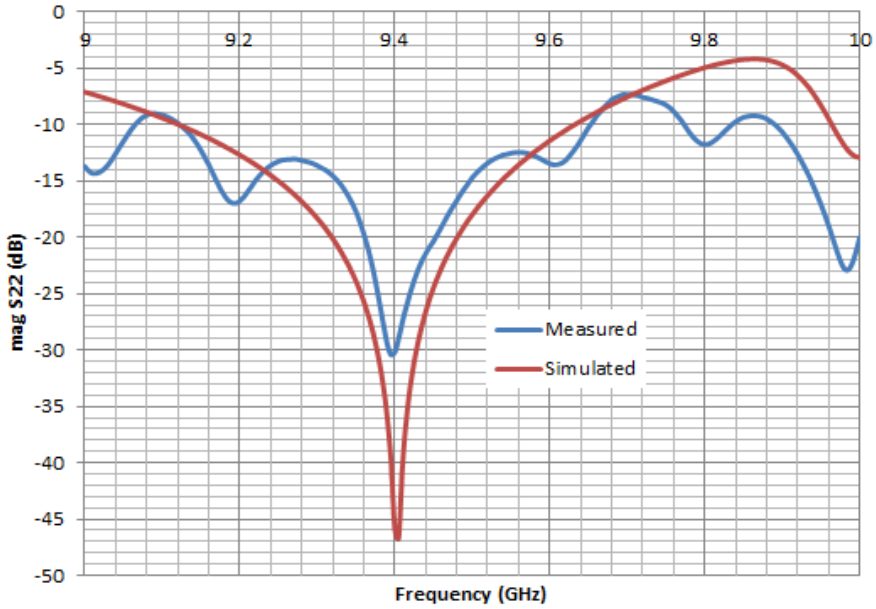

Figure 4-30: Two layered sub array: S22 simulated and measured

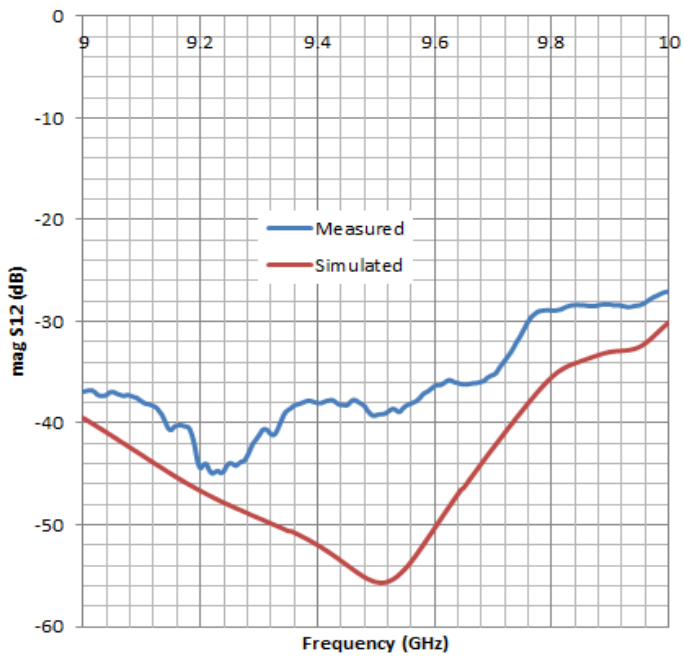

Figure 4-31: Two layered sub array: S12 simulated and measured

4.3 Linear Array Design

After finalizing the design for the sub array a linear array of sub arrays was designed. The design procedure is as discussed section 3.1.1.2. Based on the calculations of the array aperture, for a separation of 0.75λ between the sub array elements it was determined that a total of 11 sub array elements were needed to achieve a beamwidth of 3 degrees in broadside. Hence, a linear array of 11 sub arrays separated 0.75λ was simulated. The results as shown in Figure 4-32 showed that a beamwidth of ° could only be achieved with 11 elements and more elements were needed to achieve the desired beamwidth of 6°. The results of subsequent simulations are discussed in the following sections.

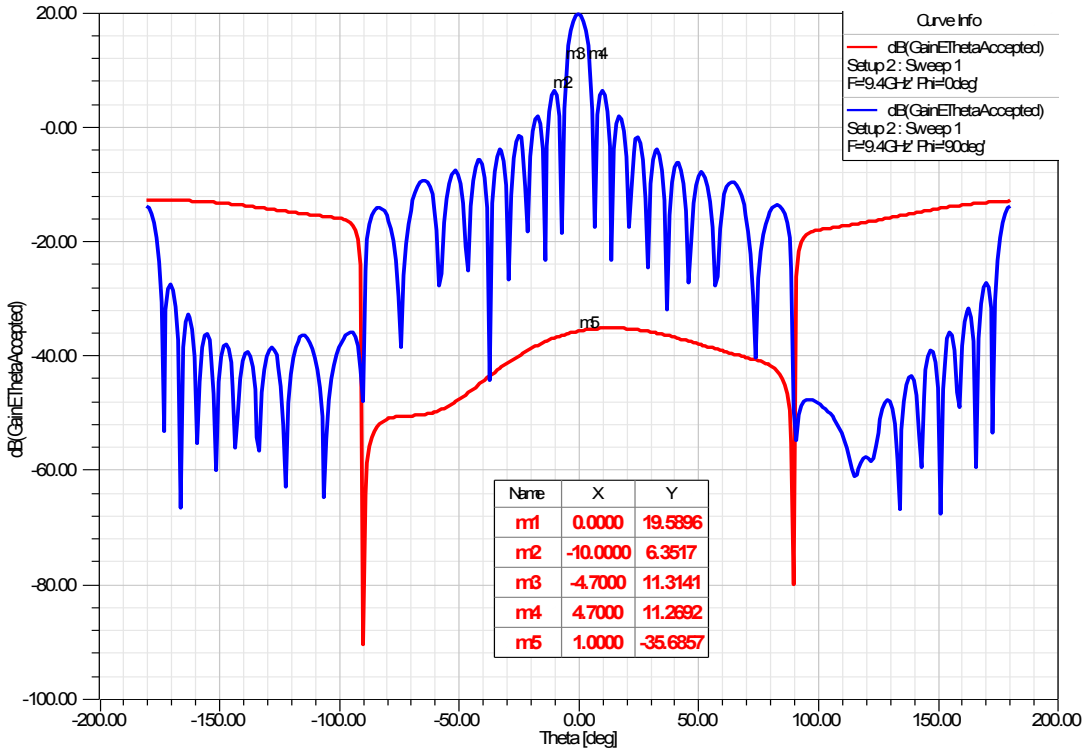

Figure 4-32: 11 element linear array radiation pattern

4.3.1 Linear Array without Feed Network

In order to estimate the best configuration and amplitude distribution for the antenna array, several simulations were done for the basic configuration as shown in Figure 4-33. The basic configuration was used to test for the active input impedance at each sub array, beamwidth and SLL levels and do not comprise of the microstrip feed network. Initially, uniform amplitude distribution was applied to the linear array elements (in this case sub arrays) and beamwidth and SLL were observed for increasing number of elements. Next, amplitude taper was considered and simulations were performed to estimate the bandwidth and SLL for different array configurations as discussed in this section.

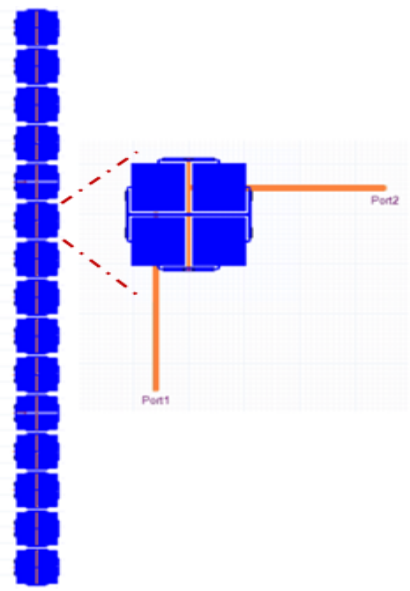

Figure 4-33: Basic configuration of linear array of sub arrays

4.3.1.1 Uniform Amplitude Distribution

As an initial estimate for beamwidth, a linear array of sub arrays was designed with uniform amplitude distribution among the elements (sub arrays). The simulation result of indicated that 11 element linear array does not fulfill the requirement of half power beamwidth(HPBW) of 6°. The number of elements was then increased to 15 and the simulation results are as shown in Figure 4-34. The results are for Port 1 active and show that the beamwidth of 4.6° can be achieved by the 15 element linear array. The SLL was 13 dB below the main beam as expected for uniform amplitude distribution. The cross polarization was below -60 dB at broadside.

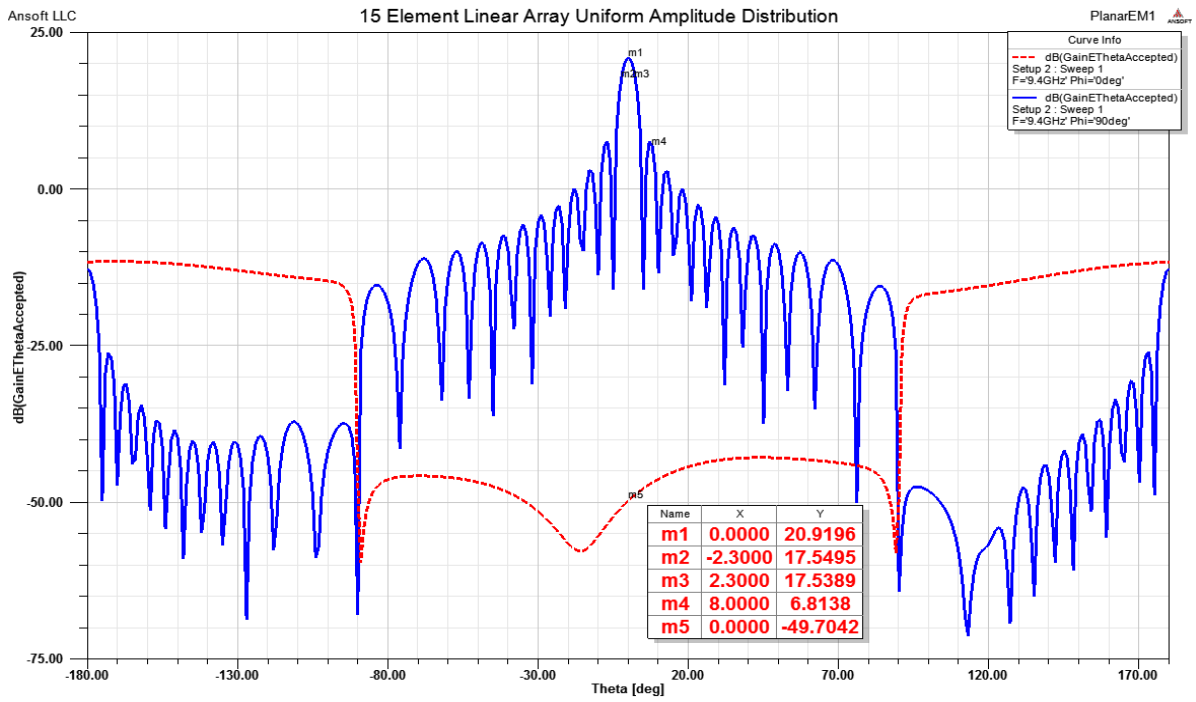

Figure 4-34: 15 element linear array radiation pattern for uniform distribution

Considering possible beam broadening after addition of the feed network, the number of elements was increased. The number of elements in the linear array was increased up to 22 and the simulation results as shown in Figure 4-35 demonstrated that the array could achieve HPBW of 3°. The first SLL was 13 dB below the main lobe and the cross polarization level was less than -60 dB and the FBR was greater than 30 dB.

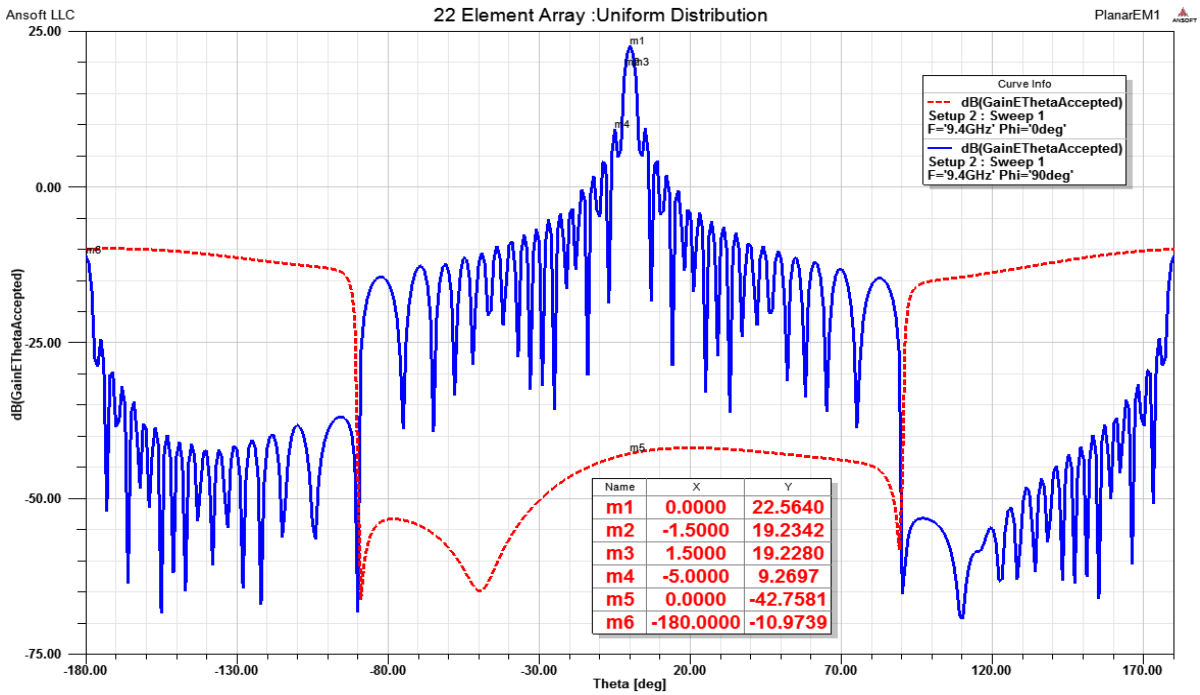

Figure 4-35: 22 element linear array radiation pattern for uniform distribution

4.3.1.2 Amplitude Tapering

The uniform amplitude distribution demonstrated that a beamwidth as narrow as 3° could be achieved for the 22 element array which satisfied one of the requirements. Also, the design of the feed network for the uniform distribution would be simple and the SLL was 13 dB below the main lobe. Despite the simplicity, uniform distribution was not considered a suitable choice for the antenna array to be used in the OTG radar node due to two reasons. First, although the first side lobe is at 13 dB below the main lobe, due to phase distortions after the addition of the feed network, this value could rise significantly. Secondly, in a scanning array environment such as that in the OTG radar one of the side lobe levels could increase to cause a grating lobe to appear in the pattern. This grating lobe in the pattern would lead to false target detection. Hence, amplitude tapering was considered to reduce the SLL below the 13 dB achieved by uniform distribution.

Although there are techniques such as Dolph Tschebycheff, Elliot and Villeneuve that are used for amplitude synthesis in an array, Taylor distribution was chosen as it is more widely used in antenna arrays. The coefficients for Taylor distribution were calculated using Matlab. Both Taylor 1-p and Taylor $\bar{n}$ distributions were taken into consideration.

4.3.1.2.1 Taylor 1-P Distribution

Taylor single parameter (1-p) distribution allows maintaining the first side lobe level at the desired level below the main lobe. The coefficients generated by the Matlab program for a 15 element linear array with the first SLL at 35 dB below the main lobe are as shown in Table 4-1. The results of simulation are shown in Figure 4-36. The results show that HPBW of 6.4° can be achieved. Also the HPBW was greater than that of the uniformly distributed array. This was expected as amplitude tapering contributes to broadening of the antenna beam. The first SLL was at approximately 34 dB below the main lobe which was close to the desired value of 35 dB. The cross polarization level achieved by the distribution was greater than -60 dB at broadside.

Since the HPBW was higher than the desired value, the number of elements was increased to 22. Table 4-2 shows the coefficients for 22 element linear array with Taylor 1-P distribution as calculated by a Matlab program for SLL = -35 dB for the first side lobe. Figure 4-37 shows the simulation result for the 22 element array with only one of the ports activated. The results showed that SLL = 36 dB was achieved which was greater than the designed level for the first side lobe. HPBW of 4.2° was obtained which was close to the Matlab calculated value but and greater than that of the uniform distributed array with the same number of elements. Beam broadening was expected as compared to the value of uniformly distributed array. The cross polarization level achieved by the array was -62 dB at broadside.

Table 4-1: Matlab generated array weights for 15 Element linear array.

Calculated weights a_m	Maximum value $\max(a_m)$	Normalized weights $a_{mnorm} = a_m / \max(a_m)$
0.255	9.622	0.0265
0.331		0.0344
0.465		0.0483
0.624		0.0648
0.773		0.0803
0.892		0.0927
0.971		0.1009
1		0.1039
0.971		0.1009
0.892		0.0927
0.773		0.0803
0.624		0.0648
0.465		0.0483
0.331		0.0344
0.255		0.0265

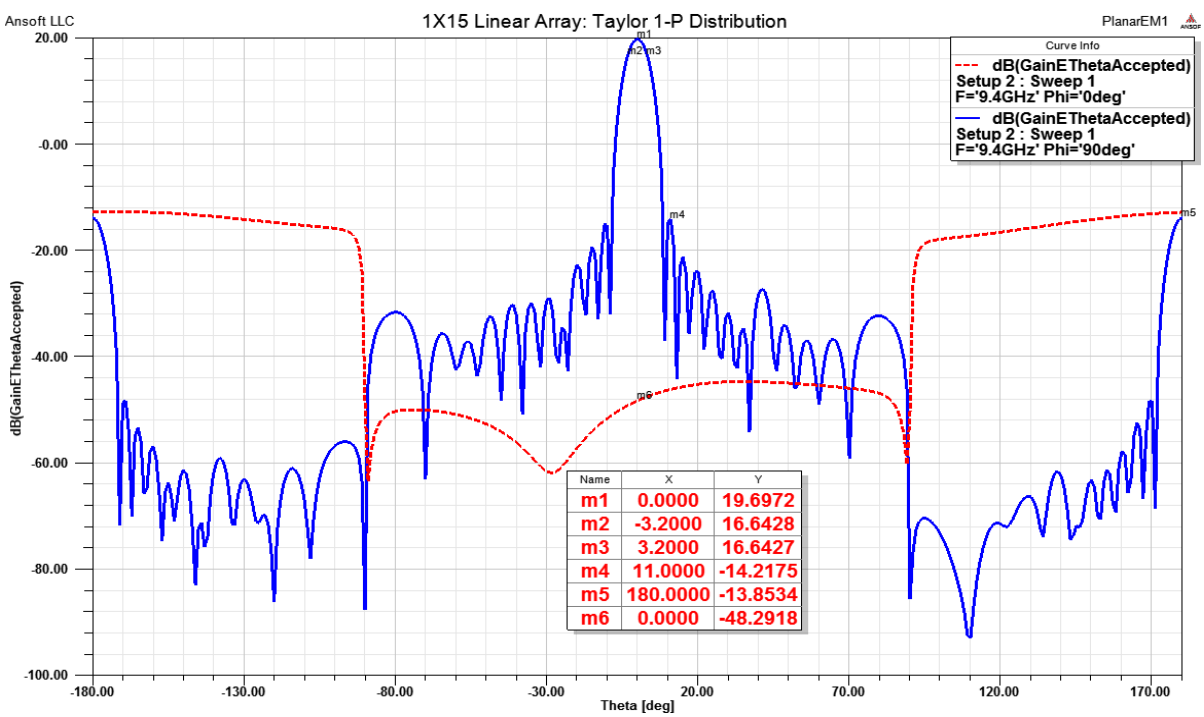

Figure 4-36: Radiation pattern for 15 element linear array with Taylor 1-P distribution (Port 1 active)

Table 4-2: Matlab generated array weights for 22 Element linear array with SLL= -40 dB for Taylor 1-P distribution

Taylor Single Parameter Array Weights			
Calculated weights am	Total value Sum(am)	Normalized weights amnorm= am/ Sum(am)	Calculated HPBW Degrees
0.0293	9.6224	0.007116	4.1682
0.0535		0.012994	
0.0832		0.020207	
0.1172		0.028465	
0.1541		0.037427	
0.1922		0.04668	
0.2294		0.055715	
0.2635		0.063997	
0.2926		0.071064	
0.3149		0.07648	
0.3288		0.079856	
0.3288		0.079856	
0.3149		0.07648	
0.2926		0.071064	
0.2635		0.063997	
0.2294		0.055715	
0.1922		0.04668	
0.1541		0.037427	
0.1172		0.028465	
0.0832		0.020207	
0.0535		0.012994	
0.0293		0.007116	

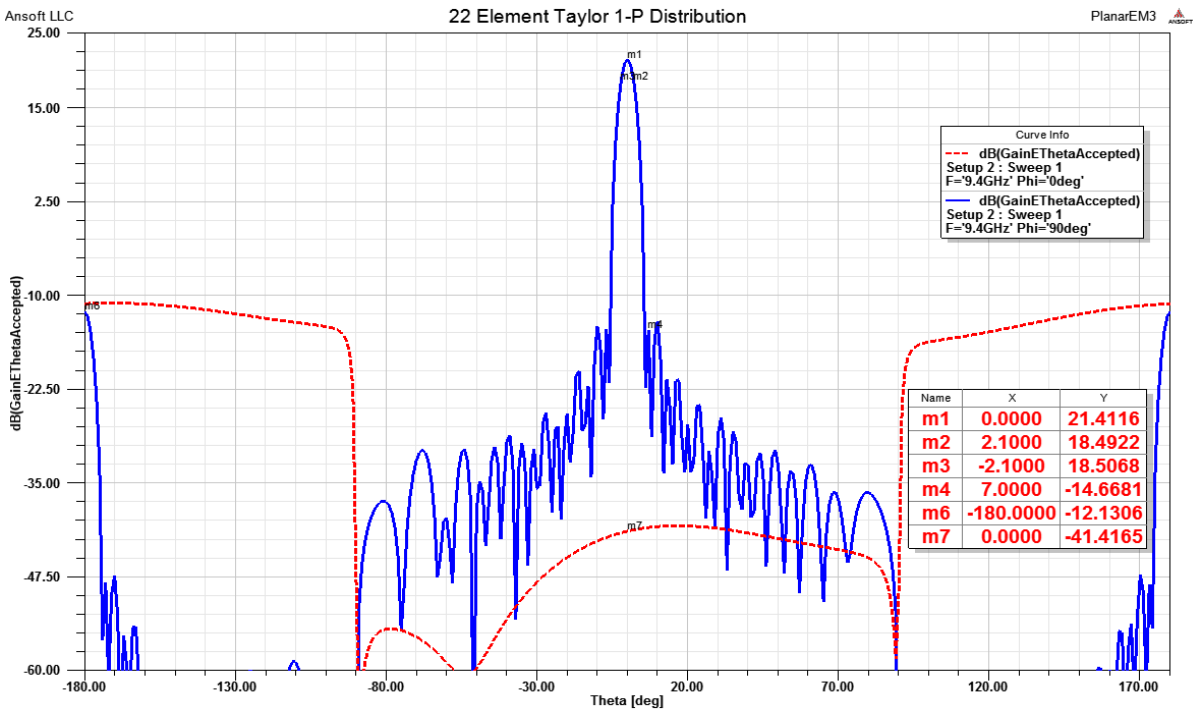

Figure 4-37: Radiation pattern for 22 element linear array with Taylor 1-P distribution (Port 1 active)

4.3.1.2.2 Taylor n̄ Distribution

The results from Figure 4-36 and Figure 4-37 show that Taylor 1-p distribution can be used to achieve desired values for the first SLL. However when the antenna array is used for scanning, it is desired to maintain several other adjacent side lobes at the lowest possible levels. This is done to reduce the chances of one of the near side lobes reaching levels greater than the first side lobe and acting like a grating lobe. A grating lobe within the scan range means false target detection. A better way to ensure that none of the near lobes in the vicinity of the main lobe achieve higher levels is to use Taylor n̄ distribution where n̄ represents the nth side lobe from the main lobe that can be reduced to the desired level and all other side lobe levels decrease monotonically in value from the value at the nth level. For the array design, the first five side lobe levels were selected for SLL suppression. Therefore, Taylor n̄ distribution with n̄=5 was used. Similar to the Taylor 1-P case, a Matlab program was used

to generate the values for the distribution based on the number of elements, SLL value and the desired number of side lobes under the specified level and separation between the array elements.

Table 4-3 shows the array coefficients for Taylor $\bar{n}$ distribution with $\bar{n}$ = 5, SLL = -30 dB and separation d = 0.75λ between the sub arrays for a 15 element array. The coefficients were applied at the sub array amplitude inputs and the results that were obtained are shown in Figure 4-38. The results show that HPBW of 5.6° could be achieved. This value was lower than the calculated value. Also the HPBW was greater than that of the uniformly distributed array but was less than that of the Taylor 1-P distribution for the same number of elements. The first SLL was at approximately 30 dB below the main lobe which was close to the desired value of -30 dB and the first five side lobes were also held at values lower than 30 dB from the main lobe. The cross polarization level achieved by the distribution was greater than -68 dB at broadside.

Table 4-3: Taylor n̄ distribution coefficients for 15 element array with n̄ = 5, d = 0.75λ and SLL = -30 dB

	Modified $\bar{n}$ -Taylor Array Weights			
n̄	**Calculated weights a_m**	**Total value Sum(a_m)**	**Normalized weights a_{mnorm}= a_m/ Sum(a_m)**	**Calculated HPBW Degrees**
5	0.26	**9.62**	0.027027	**7.2532**
	0.33		0.034304	
	0.47		0.048857	
	0.62		0.064449	
	0.77		0.080042	
	0.89		0.092516	
	0.97		0.100832	
	1.00		0.10395	
	0.97		0.100832	
	0.89		0.092516	
	0.77		0.080042	
	0.62		0.064449	
	0.47		0.048857	
	0.33		0.034304	
	0.26		0.027027	

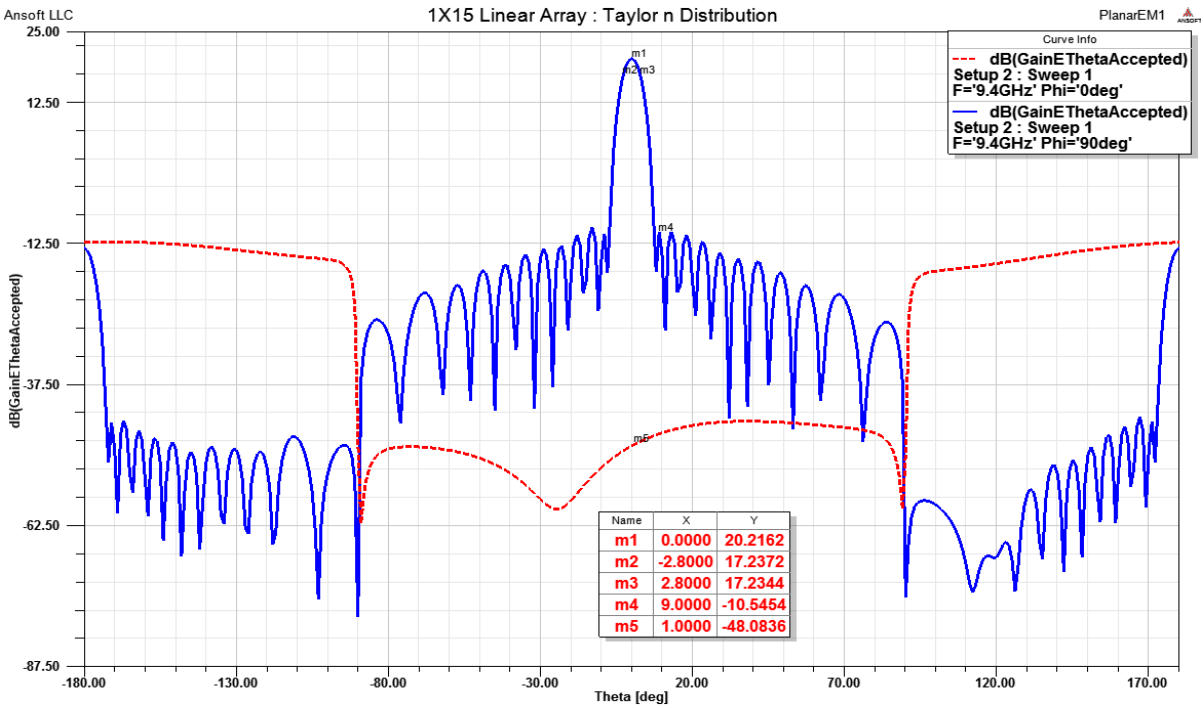

Figure 4-38: Radiation pattern for 15 element array with Taylor $\bar{\mathbf{n}}$ = 5 distribution

Although after applying Taylor $\bar{n}$ distribution, the HPBW for the 15 element array decreased as compared to the uniformly distributed array of 15 elements, HPBW was still greater than the desired HPBW of 6°. Therefore, in order to achieve a narrower beam, the number of elements in the array was increased to 22. Table 4-4 shows the array weights for a 22 element array for Taylor $\bar{n}$ distribution for SLL = -30 dB, N = 22 and d = 0.75λ. Figure 4-39 shows the simulation result for the distribution. By using such distribution in a 22 element array, HPBW of 4° was achieved which was less than that for Taylor 1-P distribution and greater than that for uniform amplitude distribution. Also SLL for the first five lobes were well below 30 dB from the main lobe as desired and cross polarization levels were around -62 dB at broadside.

Table 4-4: Taylor $\bar{n}$ distribution coefficients for 22 element array with

$\bar{n}$ = 5, d = 0.75λ and SLL = -30 dB

	Modified $\bar{n}$ -Taylor Array Weights			
$\bar{n}$	Calculated weights a_m	Total value Sum(a_m)	Normalized weights a_{mnorm}= a_m/ Sum(a_m)	Calculated HPBW Degrees
5	1	56.0406	0.0178	3.9129
	1.1423		0.0204	
	1.4127		0.0252	
	1.7808		0.0318	
	2.2027		0.0393	
	2.6312		0.0470	
	3.0286		0.0540	
	3.3722		0.0602	
	3.6494		0.0651	
	3.8478		0.0687	
	3.9526		0.0705	
	3.9526		0.0705	
	3.8478		0.0687	
	3.6494		0.0651	
	3.3722		0.0602	
	3.0286		0.0540	
	2.6312		0.0470	
	2.2027		0.0393	
	1.7808		0.0318	
	1.4127		0.0252	
	1.1423		0.0204	
	1		0.0178	

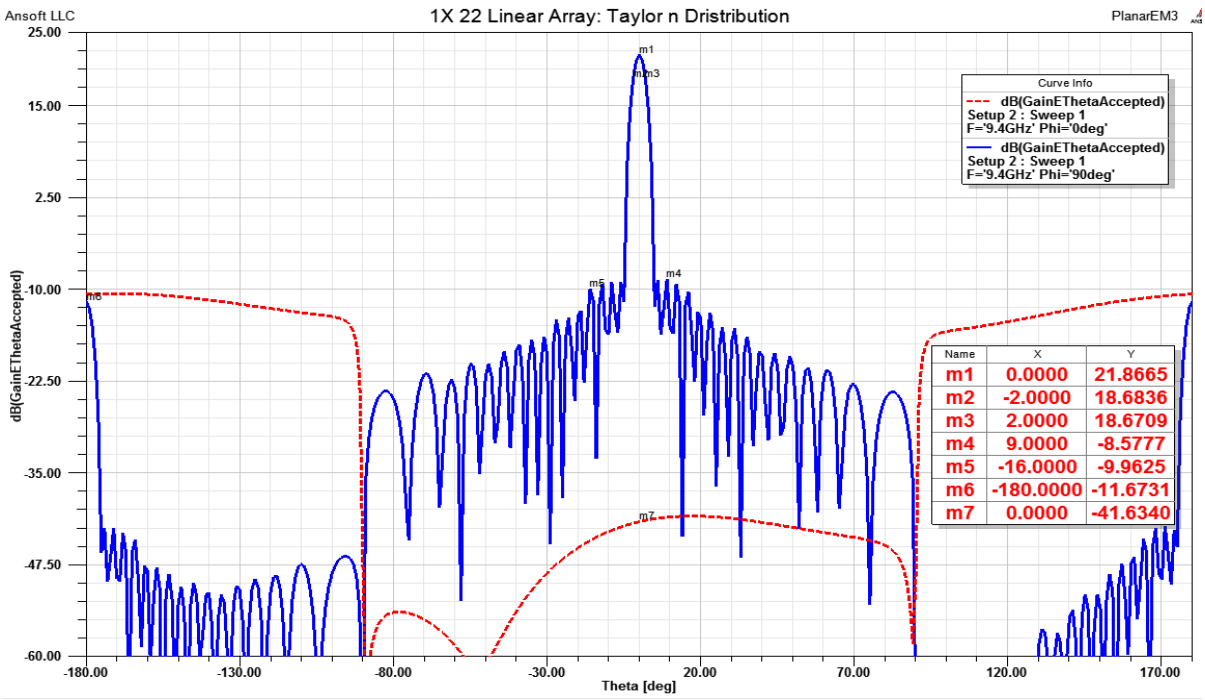

Figure 4-39: Radiation pattern for 22 element array with Taylor $\bar{n}$ = 5 distribution

4.3.1.3 Linear Array with Feed Network

The next step in the array design was the design of the feed network. Although the 22 element configuration having Taylor $\bar{n}$ =5 distribution exhibited values of HPBW, SLL and cross polarization levels closer to the desired values, the array was not suitable for fabrication purposes. Although custom-made boards could be fabricated, most manufacturers including Prototron Circuits were found to use 18 in X 24 in as the largest board size for fabrication. Fabricating boards beyond the dimensions would significantly increase the overall cost of fabrication. Hence, a trade-off was necessary between the antenna parameters and the cost.

The linear array was designed with each sub array measuring 0.74λ and the lowest separation between the elements of the linear array was 0.75λ. Since there was no room for reducing the

separation between the elements in the linear array, the number of elements was reduced to 17 in order to fit in a sheet of 18 in x 24 in.

Table 4-5 shows the calculated coefficients for the 17 element array having Taylor $\bar{n}$ = 5 distribution with SLL = -30 dB and separation between the patches d = 0.75λ. Figure 4-40 shows the results of simulation for the 17 element array. The results obtained showed that HPBW of 5° could still be achieved by using 17 elements. SLL for the first five lobes were below -30 dB and cross polarization level was -60 dB at broadside. Although, HPBW needed to be sacrificed in order to fit the linear array in an 18 in X 24 in board, good SLL and cross polarization values were retained. Also, a linear array of 17 X 17 sub array elements could fit in an 18 in X 24 in board completely.

Table 4-5: Taylor $\bar{n}$ distribution coefficients for 17 element array with

$\bar{n}$ = 5, d = 0.75λ and SLL = -30 dB

$\bar{n}$	Calculated weights a_m	Total value Sum(a_m)	Normalized weights a_{mnorm}= a_m/ Sum(a_m)
5	1.0000	42.9466	0.0233
	1.2337		0.0287
	1.6605		0.0387
	2.1971		0.0512
	2.7429		0.0639
	3.2229		0.0750
	3.6000		0.0838
	3.8481		0.0896
	3.9362		0.0917
	3.8481		0.0896
	3.6000		0.0838
	3.2229		0.0750
	2.7429		0.0639
	2.1971		0.0512
	1.6605		0.0387
	1.2337		0.0287
	1.0000		0.0233

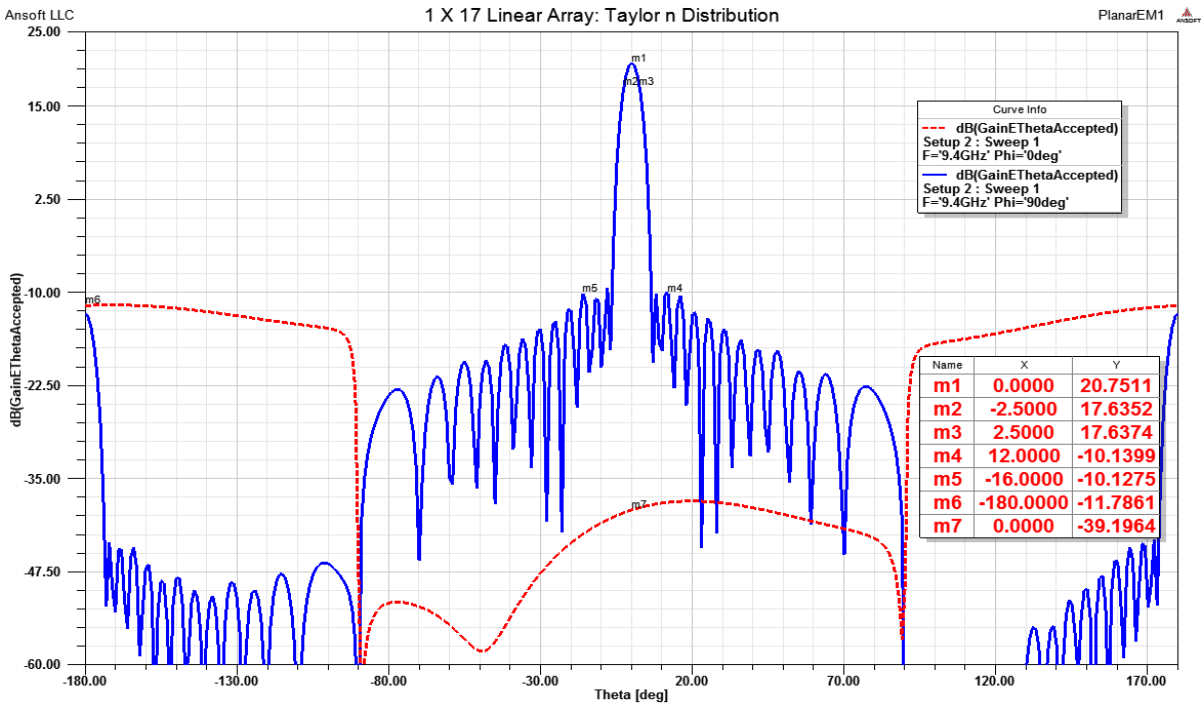

Figure 4-40: Radiation pattern for 17 element array with Taylor $\bar{n}$ = 5 distribution

After the calculation of the normalized array weights as shown in Table 4-5, the feed network was designed. First the active input impedance values were obtained for the 17 element array as shown in Table 4-6 . Based on the active input impedance values and the array weights at each port, matching network were designed as shown in Figure 4-41 for the first two elements in the array. Figure 4-42 shows the return loss plot for the array. The results show that the 10 dB bandwidth for both the H and V ports are around 8.5% at 9.4GHz. The isolation between the ports is below -40 dB for the frequency sweep from 9 GHz to 9.8 GHz. Figure 4-43 shows the radiation pattern of the array. Addition of phase network adds phase distortions to the array causing beam squinting. The array beam was found to be steered at -12 degrees as opposed to being directed along broadside. Also, there were side lobe levels which are not at -30 dB as designed. However, the side lobes were still at levels

below 13 dB from the main lobe. The cross polarization level was -45 dB along the direction of the main lobe at -12° and -36dB along broadside. Beam broadening was also observed and the new HPBW is around 16°.

Table 4-6: Active impedance values for the 17 element array at V and H ports

Active Impedance for 17 element Taylor array	
V Port	H Port
46.789962802143 - 9.01088425306994i	49.304412401177 - 15.5407238352203i
45.0666712432407 - 11.1143990318043i	49.376125406106 - 15.5848260727606i
45.3639565887645 - 10.7448620482461i	49.3766285592176 - 15.5089141829381i
45.4889832191288 - 10.4059595201544i	49.0303572083066 - 16.0053966598471i
45.3294291589774 - 11.4647215608973i	49.5142804671469 - 15.2418570942042i
45.3536301127517 - 10.5650614297024i	49.5966649931325 - 15.2208551653574i
45.2981406571868 - 10.631570699566i	49.3328449217765 - 15.5266654453605i
45.2942774628408 - 10.0234210491723i	49.3356699432343 - 15.5912410814275i
45.3641825507733 - 10.2378128648768i	49.239659352475 - 15.8336736229435i
45.542687948948 - 9.95139624514066i	49.0339612012618 - 16.0368502933114i
45.3251198395279 - 10.9154749409697i	49.4052022181108 - 15.3830392598933i
45.1942297500203 - 10.4427847426966i	49.3350802799571 - 15.6913454321639i
45.526156155217 - 10.9455765565793i	49.4435725511888 - 15.457476192702i
45.2183052683046 - 10.1425796045508i	49.4629533285007 - 15.3651498944122i
45.2268672460722 - 10.8945228493077i	49.516901902532 - 15.3097550911378i
44.9169362989059 - 11.0505023921272i	49.4337993137783 - 15.4720039436952i
47.1999191682798 - 7.77044680155462i	48.8277531697693 - 16.1651593211946i

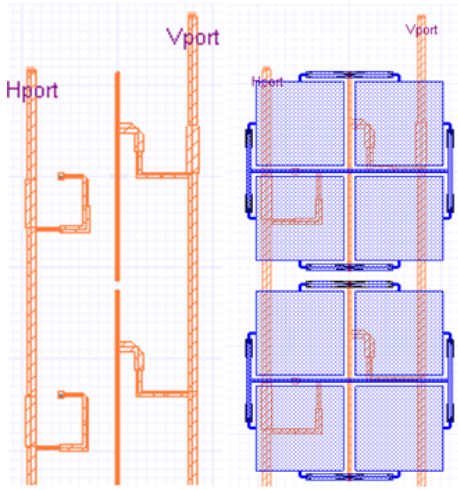

Figure 4-41: A section of the feed network for the 17 element array

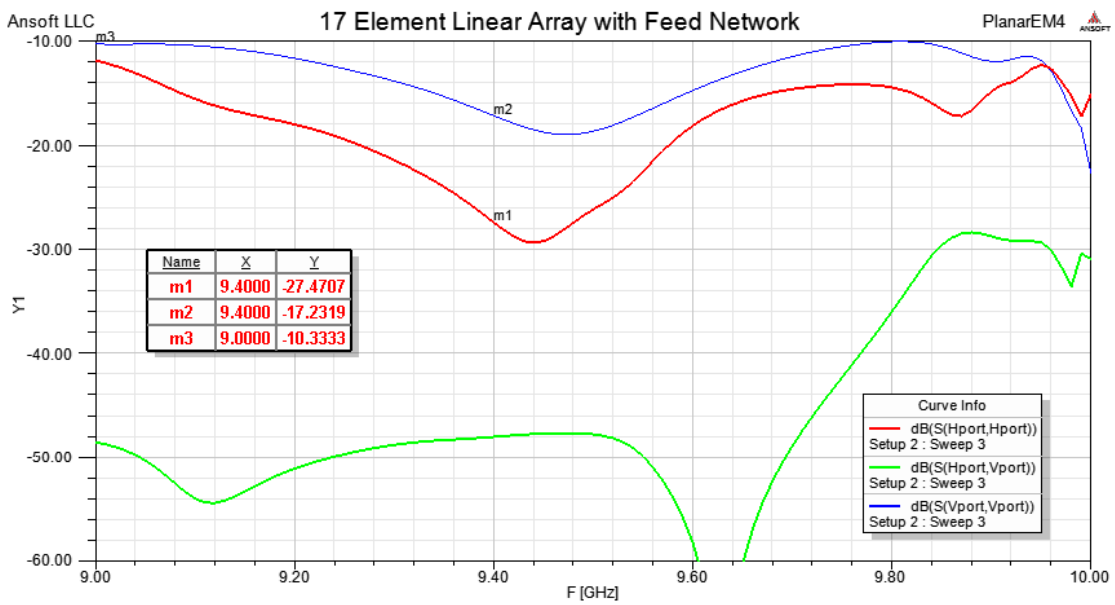

Figure 4-42: Return Loss plot for the 17 element array with feed network

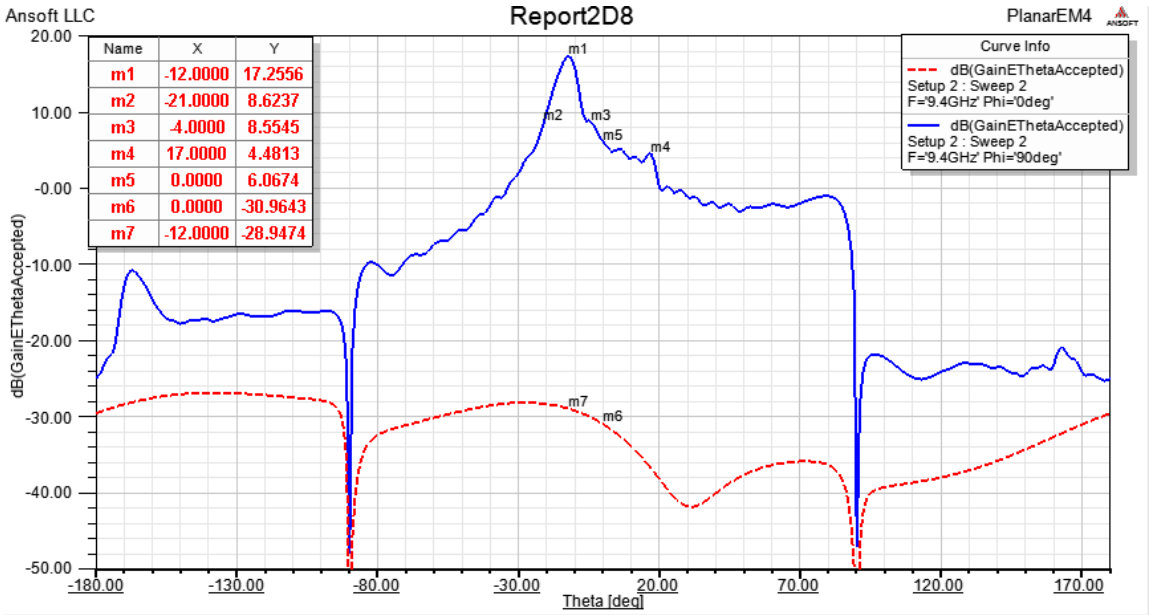

Figure 4-43: Radiation pattern of 17 element array with feed network

4.4 Planar Array

After the simulation for a linear array was completed, a planar array was constructed by arranging linear arrays in separate columns. The planar array was then simulated and the results observed. a 17 X 17 planar array was created as shown in Figure 4-44. However, for computing purposes in order to reduce simulation time a 17 X 9 planar array was simulated and the results are shown in Figure 4-45 and Figure 4-46. The results show that although the beam is steered towards -12° in the elevation plane, the planar array can still be used to scan the beam electronically in the azimuth plane.

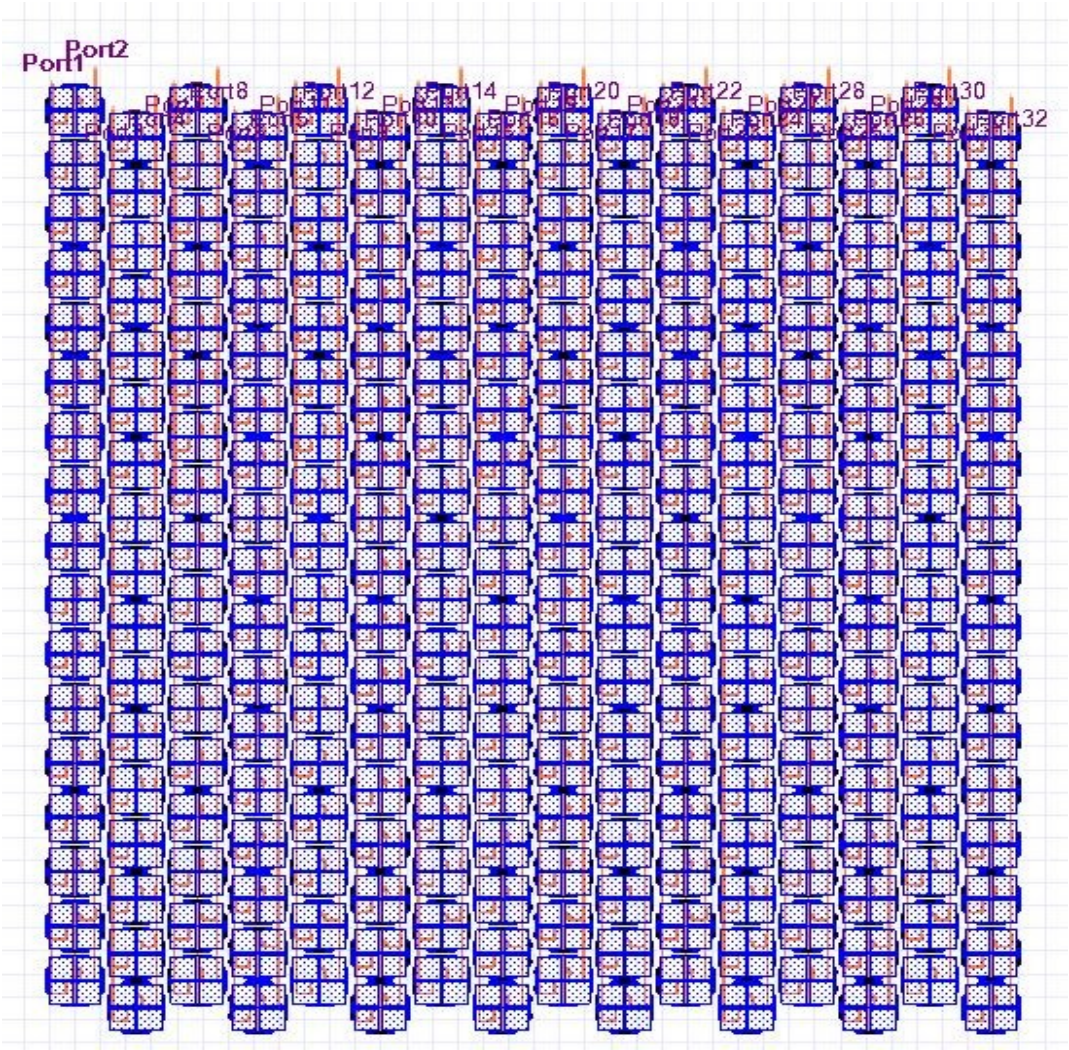

Figure 4-44: 17 X 17 Planar Array having nested configuration

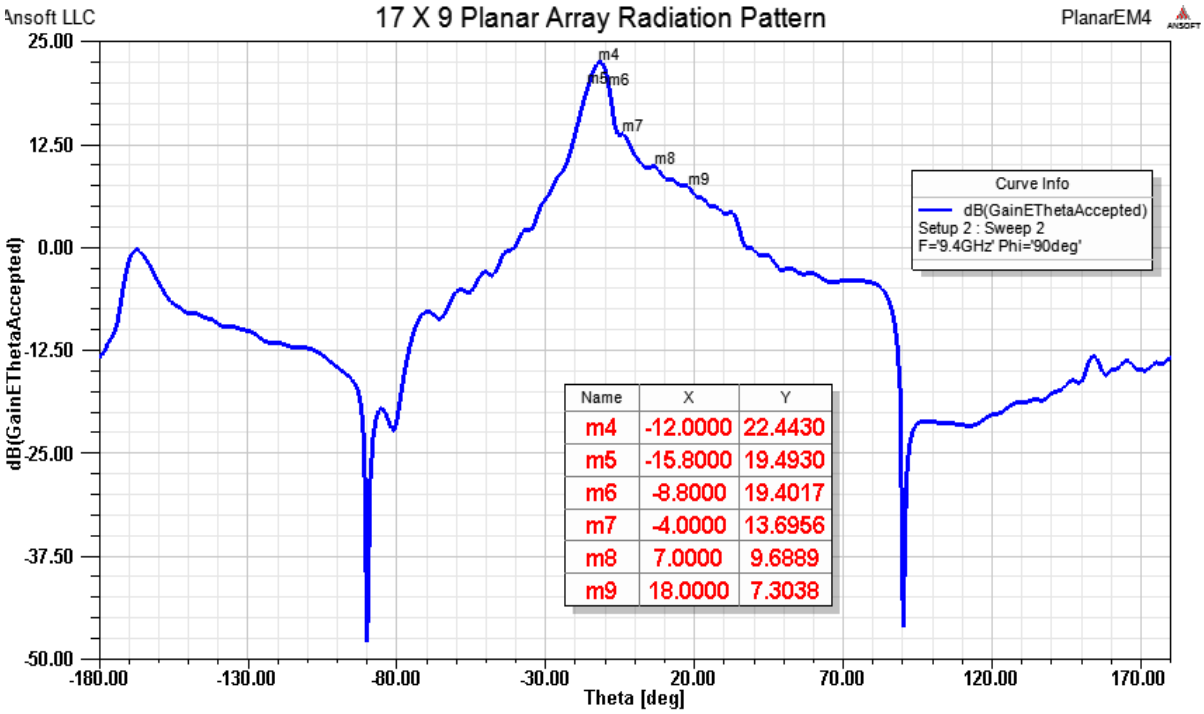

Figure 4-45: Radiation Pattern of 17 X 9 Planar Array in the Elevation Plane

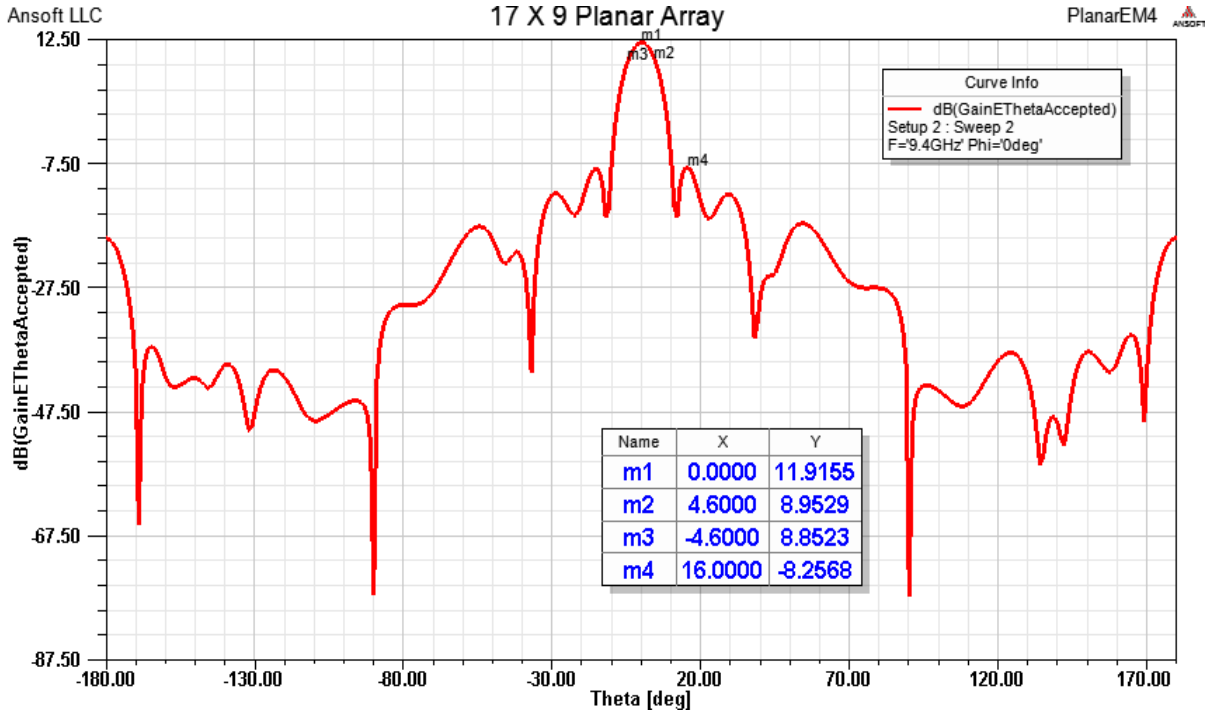

Figure 4-46: Radiation Pattern of 17 X 9 Planar Array in the Azimuth Plane

5 CONCLUSIONS AND FUTURE WORK

5.1 CONCLUSIONS

The design of a dual polarized antenna array operating in the X band at 9.4GHz was presented and discussed. First a 2 X 2 dual polarized antenna sub array was designed. The dual polarized radiator assembly was then used as elements in a linear array. Columns of such linear arrays were used to form a planar array structure.

Several configurations were studied for dual polarization. Based on the design of [25] a dual polarized 2 X 2 microstrip sub array was designed. A different substrate material than the one used in [25] was used to design the 2 X 2 sub array. Two different multilayer architectures were considered for the design of the sub array and each was first and studied for bandwidth, cross polarization levels and isolation between the ports.

A three layered structure of the 2 X 2 sub array was designed using RT Duroid 5870 substrate having permittivity 2.33 and height 0.787mm for the patch layer and the two feed network layers. Simulation results showed VSWR < 2 bandwidth of 440 MHz, port isolation less than -30 dB for the entire frequency range from 9 GHz to 10 GHz and cross polarization levels up to -45 dB. However, fabricated prototype results did not fully agree with the simulated results. The disagreement was attributed to increase in the overall thickness of the antenna by the use of pre preg bonding material between the layers. The more the number of layers, the more unpredictable the finished thickness of the pre preg bonding layers and hence the overall thickness of the antenna.

A two layered structure of the 2 X 2 sub array was designed using different substrate material for the patch and the feed network. RT Duroid 5870 substrate having permittivity 2.33 and height 0.787mm

was used for the patch layer and TSM DS3 substrate having permittivity 3 and thickness of 0.254mm was used feed network layer. Simulation result showed VSWR < 2 bandwidth of 400 MHz, good port isolation (-40 dB) and high polarization purity (-47 dB).Measured results from the fabricated prototype was in close agreement with the simulation results. The sub array structure measured 0.74λ on either side.

A linear array was designed using the 2X2 sub array as elements. Different number of elements and several amplitude distributions were considered and evaluated. It was desired to obtain HPBW of 6°, low side lobe level (SLL) and low cross polarization level.

A 15 element linear array of 2X2 sub arrays was created with a center-to-center spacing of 0.75λ and having uniform amplitude distribution. Such linear array exhibited HPBW of 4.6° and low cross polarization level (-60 dB at broadside). In order to obtain a narrow beam the number of elements was increased to 22. The 22 element uniformly distributed array exhibited HPBW of 3° and cross polarization level of -60 dB at broadside. Both uniformly distributed arrays had SLL of -13 dB relative to the main lobe and did not exhibit any grating lobes.

To reduce the SLL below -13 dB, amplitude tapering was applied to the antenna arrays. Taylor 1-P and Taylor $\bar{n}$ distribution were considered. The array coefficients were generated using Matlab. The 15 element Taylor 1-P distributed array exhibited HPBW of 6.4°, first SLL of -34 dB and cross polarization level of -60 dB at broadside. For the 22 element array, Taylor 1-P distribution yielded 4.2° HPBW first side lobe level of -36 dB and cross polarization level of -62dB at broadside.

Considering possible occurrence of grating lobes during scanning, Taylor $\bar{n}$ distribution was considered for the linear array. It was desired to maintain the first five side lobe levels at -30 dB below the main lobe. Hence, Taylor $\bar{n}$ distribution with $\bar{n}$ =5 was applied at the array inputs at each port. The array coefficients were generated using Matlab. The 15 element Taylor $\bar{n} = 5$ distributed

array exhibited HPBW of 5.6°, SLL of -30 dB for the first five side lobes and cross polarization level of -68 dB at broadside. For the 22 element array, Taylor $\bar{n} = 5$ distribution yielded 4° HPBW, SLL of -30 dB for the first five side lobes and cross polarization level of -62dB at broadside.

For fabrication purposes, the standard board size of 18 in X 24 in was considered. Due to limitation of real estate, the number of elements in the linear array was reduced to. A 17-element array was designed in order to fit into the standard board size. The results obtained showed that HPBW of 5° could be achieved by using 17 elements. SLL for the first five lobes were below -30 dB and cross polarization level was -60 dB at broadside. Although, HPBW needed to be sacrificed in order to fit the linear array in an 18 in X 24 in board, good SLL and cross polarization values were retained. The active impedance values for individual sub array elements were calculated in the array environment and feed network designed accordingly.

Addition of feed network contributes to phase distortions in the linear array thereby giving rise to beam squinting. For the 17 element array, after the addition of the feed network, the main beam is steered at -12° from broadside. Although, cross polarization levels were well below -30 dB for the entire scan range, the beam was considerably broader. The beam shift can be fixed by making changes to the feed network by introducing stub lines to eliminate reactive components at each junction and matching the real impedance values using quarter wave transformer sections.

A planar array was constructed from the linear arrays using nested configuration. Although, in the elevation plane the beam is steered towards -12° in the elevation plane, the antenna array is capable of scanning in the elevation plane without significant grating lobes.

Hence, using a modular approach, a planar array made up of linear array of sub arrays can be fabricated as presented in this thesis to satisfy requirements for the OTG radar network.

5.2 FUTURE WORK

This thesis presents a modular approach in designing a planar array. The simulation results need to be verified by fabricating prototypes for both linear and planar arrays. Once the prototypes have been fabricated, the scan range of the planar array in the azimuth can be determined. Prototype fabrication of linear and planar arrays is left as future work.

6 REFERENCES

[1] G.A. Pablos-Vega, J.G. Colom-Ustáriz, S. Cruz-Pol, J.M Trabal, V. Chandrasekar, J. George, F. Junyent, "*Development Of An Off-The-Grid X-Band Radar For Weather Applications*" Proceedings of IGARSS, July 2010, pp. 1077-1080

[2] D. S. Zrnic and A. V. Ryzhkov, ""*Advantages of rain measurements using specific differential phase*" J. Atmos. Oceanic Technol., vol. 13, pp. 454-464, 1996.

[3] S. Y. Matrosov, et al., "*X-Band Polarimetric Radar Measurements of Rainfall*" J. Appl. Meteorol., vol. 41, pp. 941-952, 2002

[4] G. A. Deschamps "*Microstrip Microwave Antennas*" presented at the third USAF Symposium on Antennas, 1953

[5] H. Gutton and G. Baissinot, "*Flat Aerial for Ultra High Frequencies*" French Patent No 703 113, 1955

[6] E. V. Byron, "*A new flush-mounted antenna element for phased array application*", proceedings of Phased-Array Antenna Symposium, 1970 pp. 187-192

[7] R.E. Munson, "*Single slot cavity antennas assembly*" U.S. Patent No. 3713162, Jan. 23, 1973

[8] R.E.Munson, "*Conformal microstrip antennas and microstrip phased arrays*" IEEE Transactions on Antennas and Propagation, vol AP-22, pp. 74-77, Jan 1974

[9] A.G. Derneryd, " *Linear microstrip array antennas*" Chalmer Univ. Tech. Memo., Nov. 29, 1976

[10] Y. T. Lo, D.D. Harrison, D. Solomon, G.A.Deschamps, and F.R.Ore, "*Study of microstrip antennas, microstrip phased arrays, and microstrip feed networks*" Rome Air Development Center, Tech. Reo. TR-77-406, Oct. 21,1977

[11] Girish Kumar and K.P. Ray, "*Broadband Microstrip Antennas*", Artech House, 2003

[12] K. R. Carver, "*Microstrip antenna technology*" IEEE Transactions on Antennas and Propagation, vol AP-29, Jan 1981

[13] Chad E. Patterson et al. "*A Lightweight Organic X-Band Active Receiving Phased Array with Integrated SiGe Amplifiers and Phase Shifters*" IEEE Transactions on Antennas and Propagation,51, January 2011, pp 100-109

[14] Shih-Hsun Hsu et al. "*A Dual-Polarized Planar-Array Antenna for S-Band and X-Band Airborne Applications*." IEEE Antennas and Wireless Propagation Magazine, 51, 2009, pp. 71-78.

[15] Qu X et al. "*Dual-band dual-polarised microstrip antenna array for SAR applications*." IET Electronics Letters Microwaves, Antennas & Propagation, 1, April 2007

[16] Fedir F. Dubrovka, Sergiy Y. Martynyuk, "*Wideband Dual Polarized Planar Antenna Arrays*" Proceedings of International Conference on Antenna Theory and Techniques, September, 2003, Ukraine

[17] Juan S. Skora, Aurelio Sanz and Ruben D. Moran Fabbra "*Dual Polarized Phased Array Antenna for Airborne L-band SAR*" IEEE Antennas and Wireless Propagation Letters, 2005, pp. 192-196

[18] Kuo-Lun Hung and Hsi-Tseng Chou, "*A Design of Slotted Waveguide Antenna Array Operated at X-band*" IEEE Antennas and Wireless Propagation Letters, 2010

[19] Ye Qian, et al. "*Design of a dual-feed orthogonal polarized patch antenna array*." Proceedings of the International Conference on Microwave and Millimeter Wave Technology (ICMMT), August 2010

[20] D. Krishna, M. Gopikrishna, C. Aanandan, P. Mohanan, and K. Vasudevan, "*Compact Dual-Polarized Square Microstrip Antenna with Triangular Slots for Wireless Communication*," lEE Electronics Letters, 42,16, August 2006, pp. 894-895.

[21] R. Caso, A.A. Serra,M. et al, "*A Square Ring Slot Feeding Technique for Dual-Polarized Patch Antennas*" IEEE Antennas and Wireless Propagation Letters, 2010

[22] Marrero-Fontanez V.J., Rodriguez-Solis, R.A. "*Dual polarized aperture coupled microstrip patch antenna for X-band series-fed array*." IEEE Antennas and Wireless Propagation Letters, 2007,pp.

[23] Shun-Shi Zhong et al "*Corner-Fed Microstrip Antenna Element and Arrays for Dual-Polarization Operation*", IEEE Transactions On Antennas And Propagation, 2002

[24] ShiChang Gao and ShunShi Zheng, "*A Dual-Polarized Microstrip Antenna Array with High Isolation Fed by Coplanar Network*" Proceedings of RAWCON, 1998.

[25] J. Huang, "*Dual-Polarized Microstrip Array with High Isolation and Low Cross-Pol*," Microwave Optic. Tech. Letters, 1991

[26] Mohsen Kaboli, Seyed Abdollah Mirtaheri, and Mohammad Sadegh Abrishamian ."*High-Isolation X-Polar Antenna.*" IEEE Antennas and Wireless Propagation Letters, 9, 2010, pp 401-404

[27] Andrea Vallecchi, Guido Biffi Gentili ."*A Shaped-Beam Hybrid Coupling Microstrip Planar Array Antenna for X-band Dual Polarization Airport Surveillance Radars.*" Proceedings of EuCAP,November 2007, pp. 1-7

[28] C.R White, G.M Rebeiz ."*A dual-polarized slot-ring antenna with independent tuning*.", IEEE AP-S Symposium Digest, June 2007

[29] K. Mak, H. Wong, and M. Luk, "*A Shorted Bowtie Patch Antenna with a Cross Dipole for Dual Polarization*," IEEE Antennas and Wireless Propagation Letters, 6, 2007, pp. 126-129.

[30] R.J. Mailloux "*Microstrip Array Technology",* IEEE Transactions On Antennas And Propagation, January 1981

[31] D.M. Pozar "*Considerations for Millimeter Wave Printed Antennas",* IEEE Transactions On Antennas And Propagation, vol AP-31, September 1983

[32] D.M. Pozar "*Microstrip Antennas",* IEEE Transactions On Antennas And Propagation, vol 80, January 1992

[33] C. Balanis, "*Modern Antenna Handbook*", 3rd ed., Wiley & Sons Publication, 2008

[34] R.J. Mailloux "*Phased Array Antenna Handbook"*, 2nd ed., Artech House, 2005

[35] F.S. Johansson, L. Rexberg, R.N. Petersson "*Theoretical and Experimental Investigation of Large Microstrip Array Antenna Design"*, Saab Ericcson Space AB, S-405 15, Gothenburg

[36] Ely Levien , David Treves, Gabi Malamund and Shmuel Shtrikman; "*A Study of Microstrip Array Antennas with the Feed Network*", IEEE Trans. Antennas and Propagation, Vol. 37, No. 4, pp 426-434, April 1989

[37] R.J. Mailloux "*Grating Lobe Characteristics of Arrays with Uniformly Illuminated Contiguous Subarrays",* IEEE Transactions On Antennas And Propagation, 1984

[38] D.M. Pozar "*Scanning Characteristics of Infinite Arrays of Printed Antenna Subarrays",* IEEE Transactions On Antennas And Propagation, 1992

[39] D.M. Pozar and D.H. Schaubert "*Microstrip Antennas",* IEEE Press, January 1995

7 INDEX OF TERMS

OTG	Off-the-Grid
CASA	Center for Adaptive Sensing of the Atmosphere
MSA	Microstrip Antenna
MMIC	Monolithic Microwave Integrated Circuit
RMSA	Rectangular Microstrip Antenna
SMSA	Square Microstrip Antenna
VSWR	Voltage Standing Wave Ratio
HPBW	Half Power Beam Width
SLL	Side Lobe Level
FBR	Front-to-Back Ratio
QWT	Quarter Wave Transformer